THE ASSIGNMENT OF GAS PHASE ION STRUCTURES AND FRAGMENTATION MECHANISMS BY MASS SPECTROMETRY

A Thesis Submitted to the

School of Graduate Studies and Research

In Partial Fulfillment of the Requirements

for the Degree of

Doctor of Philosophy

In the Ottawa-Carleton Chemistry Institute

Department of Chemistry

University of Ottawa

Ottawa, Ontario

Canada

November 1992

Candidate

Martin Sirois

Supervisor

Professor John L. Holmes

A

Maman, Papa

Claude Anne, Catherine et Bébé

REMERCIEMENTS

Après avoir rédigé cette thèse dans la langue de Shakespeare, je prends la liberté et le plaisir d'adresser mes remerciements dans ma langue maternelle, le français.

Je désire tout d'abord remercier mon superviseur, Prof. John L. Holmes, pour son enthousiasme, sa patience, sa disponibilité et sa générosité. Grâce à lui, mon intérêt pour la spectrométrie de masse n'a cessé de grandir ces quatres dernières années. Merci également de m'avoir donné l'opportunité d'assister a des conférences internationales, notamment l'ASMS (Tucson et Washington) et l'IMC (Amsterdam).

Mon séjour à l'Université d'Ottawa, n'aurait pas été aussi agréable sans la compagnie de mes collègues étudiants et Post-Doc. Tout D'abord, un merci bien spécial à Dr. George Mathai sans qui la synthèse de composés isotopiquement marqués se serait avérée cauchemardesque. Merci aussi à Martine Bissonnette, Marcia Blanchette, Dr. Marcel Hop, Dr. Jian-Ru Cao, David Harnish, Hongwen Chen, Paul Mayer, Christiane Aubry, Yan Ann, Dr. Dmitri Zagorevskii et Dr. Yu-Ran Luo pour vos encouragements et votre support continuel.

Je tiens également à remercier Dr. Fred P. Lossing pour les mesures thermochimiques ainsi que Dr. Clem Kazakoff pour les analyses de GC/MS. Merci à Dr. Sander Mommers, celui qu'on appelle au secours lorsque des problèmes techniques

surgissent. Je ne voudrais surtout pas oublier Dr. John Krause qui m'a donné la chance de participer à des séances de "Kiddie-Chem" organisées pour des élèves du secondaire. Merci John, j'en garde des souvenirs impérissables (surtout la crème glacée du vendredi après-midi!).

Finalement, j'aimerais exprimer toute ma grattitude à ma mère, mon père, Claude Anne, Catherine et tous les gens qui m'entourent, pour leur support, leur compréhension et leurs encouragements continuels.

A vous tous mille fois MERCI!!

Novembre 1992

ABSTRACT

The interpretation of mass spectra has made great progress over the past decade, as experimental methods have been developed for assigning structures to organic ions in the gas phase. This thesis describes the important experiments in gas phase ion chemistry whose correct interpretation can lead to the assignment of structures, and the elucidation of fragmentation mechanisms of organic positive ions.

THE LOW ENERGY FRAGMENTATIONS OF FIVE ISOMERIC $[H_3,C,N,O_2]^{+\bullet}$ IONS

The low energy fragmentation characteristics of the $[H_3,C,N,O_2]^{+\bullet}$ isomers, $H_3CNO_2^{+\bullet}$, **1**, $H_2C{=}N(O)OH^{+\bullet}$, **2**, $H_3CONO^{+\bullet}$, **3**, $HC(O)NHOH^{+\bullet}$, **4**, and $HC(OH){=}NOH^{+\bullet}$, **5**, were studied in detail by metastable ion mass spectrometry. Appearance energy measurements established the potential energy surface of the isomers **1**, **2** and **3** showing the intricate interrelation between them. For isomers **4** and **5**, it was concluded that they do not intercommunicate with ions **1**, **2** and **3** prior to fragmentation. Neutralization-reionization mass spectrometry indicated that the enol form of formohydroxamic acid structures as well as the keto analogue are stable in the gas phase.

THE NEUTRAL COUNTERPARTS OF THE $C_2H_7O^+$ ISOMERS

The neutral counterparts of the $C_2H_7O^+$ isomers, $CH_3O^+(H)CH_3$, $CH_3CH_2OH_2^+$ and C_2H_4•••H-OH_2^+ have been studied by means of neutralization-reionization mass spectrometry. It was observed that the internal energy of protonated dimethyl ether ions is directly related to the stability of the neutrals generated by electron transfer, and on their dissociation. With regard to $CH_3CH_2OH_2^+$ and C_2H_4•••H-OH_2^+, it was concluded that the former ion can be obtained as a neutral species in the gas phase, whereas the latter isomer could not be produced as a neutral species.

CLASSICAL AND NON-CLASSICAL FORMS OF THE ETHYL CATION AND THEIR PARTICIPATION IN THE IONS $RO^+(C_2H_5)R'$

Oxonium ions formed via ion/molecule reactions between several oxygen centered molecules and the ethyl cation were studied. Significant H/D mixing in these oxonium ions was observed only when a labeled ethyl cation was reacted with a non-labeled ROR′ molecule. The degree of H/D mixing depends only on the size of R and R′, being independent of the observational timeframe from 1-30 μs. When non-labeled ethyl cations were reacted with labeled ROR′ molecules, H/D mixing was not observed. The results were interpreted as arising from the classical and non-classical forms of the ethyl cation having different reactivities with ethers of different sizes.

HOMOLOGOUS HYDROGEN-BRIDGED INTERMEDIATES $R_1R_2O\bullet\bullet\bullet H\bullet\bullet\bullet C(O)R_3$ FROM IONIZED β-HYDROXYETHERS

The unimolecular dissociations of several β-hydroxyethers and some of their isotopomers were studied by metastable ion and collision induced dissociation mass spectrometry. It was found that molecular ions of the form $R_1OCH(R_2)CH(OH)R_3$ yield protonated ethers, $R_1O^+(H)R_2$, via intermediates of the type $R_1R_2O\bullet\bullet\bullet H\bullet\bullet\bullet C(O)R_3^{+\bullet}$.

TABLE OF CONTENTS

CHAPTER 8

HOMOLOGOUS HYDROGEN BRIDGED INTERMEDIATES

LIST OF FIGURES

LIST OF TABLES

CHAPTER 1

INTRODUCTION

1.1 What is Mass Spectrometry?

Mass Spectrometry (MS) is a powerful analytical technique that is used to identify unknown compounds, and to elucidate the structural and fragmentation mechanism of molecules.

The basis of mass spectrometry is the production of positive and negative ions from neutral compounds in the gas phase and the examination of the subsequent decomposition of these ions. As its name implies, a mass spectrometer measures mass (or strictly mass-to-charge ratio) and gives no direct information on ion structures. In mass spectrometric terms, structure is defined as the arrangement of atoms only, i.e. how they are bonded together in the ion or neutral, and not to the bond lengths and angles between atoms. Without further analysis of mass selected ions, little more than their elemental composition is available. For ions containing more than a very few atoms the number of possible corresponding isomeric structures makes their sure structure assignment less than straightforward, and further analysis is required.

However, on the basis of a variety of mass spectrometric observations, combined with ab initio molecular orbital theory calculations and thermochemical data, one can often

confidently assign structures to ions and neutral species in the gas phase.

1.2 What is a Mass Spectrometer?

The instrument ranges in size from a small box about the size of a home microwave oven to large research instruments that fill an entire laboratory. The different functions of a mass spectrometer are represented in the following block diagram.

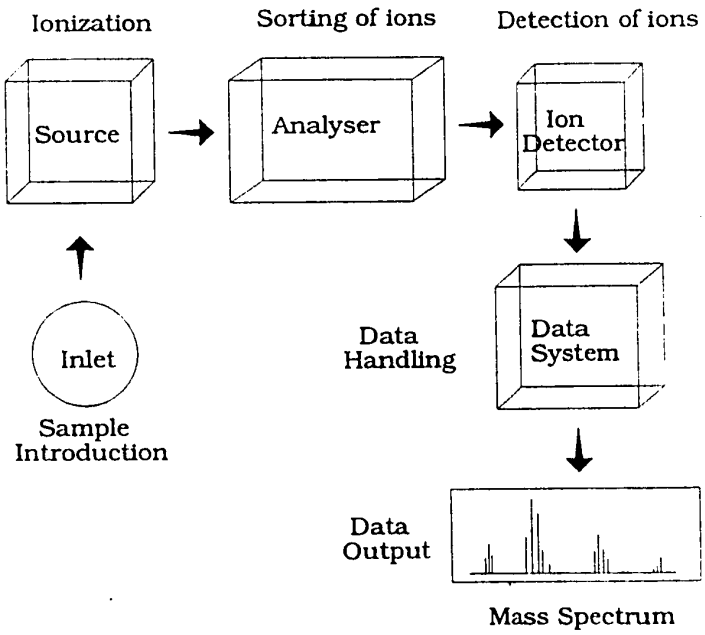

Figure 1.1 The components of a mass spectrometer.

The gaseous sample, which may initially be a solid, liquid or vapor, is introduced into a vacuum chamber through an inlet and ionized (by means of an electron beam) in the ion source. The ions, which are in the gas phase, are sorted in the mass analyser according to their mass-to-charge (m/z) ratios, and then they are collected by a detector. In the detector, the ions generate an electrical signal that is proportional to the number of ions. The data system records these electrical signals and then converts them into a mass spectrum. Some mass spectrometers are much more complex than that described above but generally speaking, the processes that occur in a mass spectrometer are: 1) ionization, 2) mass sorting and 3) detection.

1.3 What this Thesis is All About!

This thesis focuses on two major fundamental aspects of gas phase ion chemistry. The first is the production and characterization of novel ion and neutral species using the wide variety of dissociative mass spectrometric techniques now available. The second deals with the elucidation of fragmentation mechanisms of ionic species via mass spectrometric techniques, in concert with thermochemical data and isotopic labeling experiments. The experimental Chapters 5, 6, 7 and 8 are preceded by three chapters which describe the instruments used to perform the different mass spectrometric experiments. The theory and basic aspects governing these experiments are also discussed.

Chapter 2 gives a description of the mass spectrometers used in this work, the VG ZAB-2F and the Kratos AEI MS-902S. Also described is the electron energy selector mass spectrometer, with which a number of appearance energies have been measured.

In Chapter 3 a list of the types of ions formed in a mass spectrometer is drawn up. The basics of ion fragmentation are also discussed.

The purpose of Chapter 4 is to describe the important experiments in gas phase ion chemistry whose correct interpretation can lead to the assigment of structures to organic positive ions. The methodology may be divided into two main categories, (i) the determination of ion enthalpies and transition state energies for their fragmentation and (ii) the detailed examination of the unimolecular and collision induced dissociation of ions. Hence, Chapter 4 introduces the concepts and principles of appearance (AE) and ionization (IE) energy measurements, as well as those of dissociative techniques such as metastable ion (MI), collision induced dissociation (CID), collision induced dissociative ionization (CIDI), and neutralization-reionization (NR) mass spectrometry.

Chapter 5 describes the low-energy fragmentations of five isomeric $H_3,C,N,O_2^{\cdot+}$ isomers which were studied in detail, chiefly by metastable ion mass spectrometry. Appearance energy measurements established the potential energy surface for these isomers and neutralization-reionization mass spectrometry indicated that the enol form of formohydroxamic acid structures as well as the keto analogue are stable in the gas phase.

Chapter 6 deals with the generation of hypervalent radicals formed upon neutralization of protonated ethanol and protonated dimethyl ether. The dissociative ion chemistry of these two species is also discussed and especially that of protonated ethanol, for which two isomeric forms are now known to coexist in the gas phase.

Chapter 7 concerns the study of oxonium ions formed via ion-molecule reactions between several oxygen centered molecules and the ethyl cation. The participation of the classical and non-classical forms of the ethyl cation in the formation of these oxonium ions is discussed in detail. We propose that when the oxygen centered molecules are relatively small, they react preferentially with the more stable isomer of the ethyl cation, namely the non-classical form. When the reacting oxygen centered molecules are increased in size they react to a greater extent with the classical form of the ethyl cation.

In Chapter 8 a study of the unimolecular dissociations of several β-hydroxyethers and some of their isotopomers are presented. It is proposed that the latter dissociate via homologous hydrogen bridged intermediates.

CHAPTER 2

INSTRUMENTATION: THE MASS SPECTROMETERS

2.1 Introduction

To accomplish the work performed in this thesis three mass spectrometers were used: 1) the VG (Vacuum Generators) Analytical ZAB-2F, 2) the Kratos AEI MS-902S and 3) the electron energy selector mass spectrometer. A brief description of all three is given in this chapter but the emphasis will be on the VG ZAB-2F since the latter was used to generate the great majority of the results described in the forthcoming chapters. Note however that the function of the various parts of a mass spectrometer has been described in great detail **[1-6]**, and thus only the more important features of these components will be accounted for below.

2.2 The VG ZAB-2F

Figure 2.1 shows a schematic diagram of the original VG ZAB-2F mass spectrometer **[2]**. The VG ZAB-2F is a tandem mass spectrometer **[4, 7]** which is said to be of reversed geometry, because opposite to an instrument of forward geometry, the magnetic analyser, B, is placed before the electrostatic analyser, E. The advantage of the BE instruments over the EB geometries is the ability for the former to mass-select any given ion prior to performing an experiment on it in the post magnet region (see Chapter

4). The BE geometry was first described by Beynon et al **[8]** and instruments of such geometry were mainly designed to study and elucidate reaction mechanisms and ion structures via observation of metastable and collision induced dissociations occuring in the second field free region (2FFR) of the instrument.

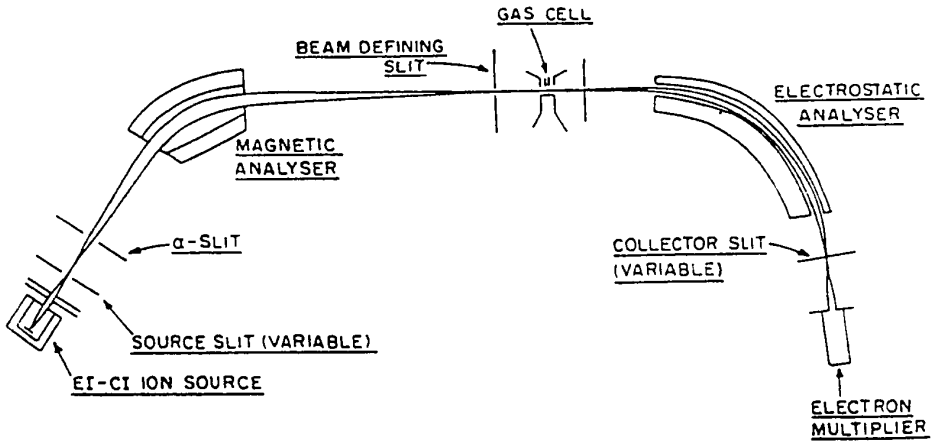

Figure 2.1 The VG Analytical ZAB-2F double focussing mass spectrometer of reversed geometry

2.2.1 The Ion Source

The ion source (Figure 2.2) is the device in which the sample is ionized. Samples can be introduced via four different inlets:

i) Liquid samples may be introduced through a septum-injection inlet which allows vapours to diffuse slowly from the heated reservoir into the source through a

capillary tube.

ii) For solid compounds, a direct probe inlet is used. This can be heated to obtain the necessary sample pressure.

iii) Gases may be introduced directly via gas lines.

iv) When studying volatile compounds (gases, liquids or solids) a variable leak inlet and capillary glass line may be used to introduce the sample into the ion source.

After entering the ion source, the sample is ionized by means of electrons emitted from a tungsten filament. The electron beam is interacting with the outer shell electrons of the sample molecule giving rise to the formation of a radical cation:

$$M + e \rightarrow M^{+\bullet} + 2e \qquad (2.1)$$

Because such an ionization process is very fast ($< 10^{-16}$ s **[9]**) compared to vibrational periods ($> 10^{-14}$ s), electron impact (EI) ionization is normally considered to be a vertical process. Although the energy of the electrons is variable, it is usually set at ~70 eV since near this value an electron energy invariant ion flux is obtained **[10]**.

Since the electron beam has an energy of 70 eV, a value much larger than the ionization energy of organic molecules (typically 10 eV **[11]**), the molecular ions can be generated with a large amount of excess internal energy. Therefore this can give rise to

the fragmentation of the molecular ions in the ion source:

$$M^{+\cdot} \rightarrow A^{+} + B^{\cdot} \qquad (2.2)$$

The repeller (a plate to which a positive voltage is applied) causes the newly formed positive ions to leave the source through the exit slit. The ions then experience a large potential gradient and are accelerated (the standard accelerating voltage (V_{acc}) for the ZAB-2F is 8 kV) towards the first field free region (1FFR). This will result in source generated ions of mass, m, and charge, z, having a translational kinetic energy equal to zV_{acc}.

$$1/2\ mv^2 = zV_{acc} \qquad (2.3)$$

Where v is the velocity of the ions. Therefore, ions having the same charge will have equal translational energies regardless of their masses.

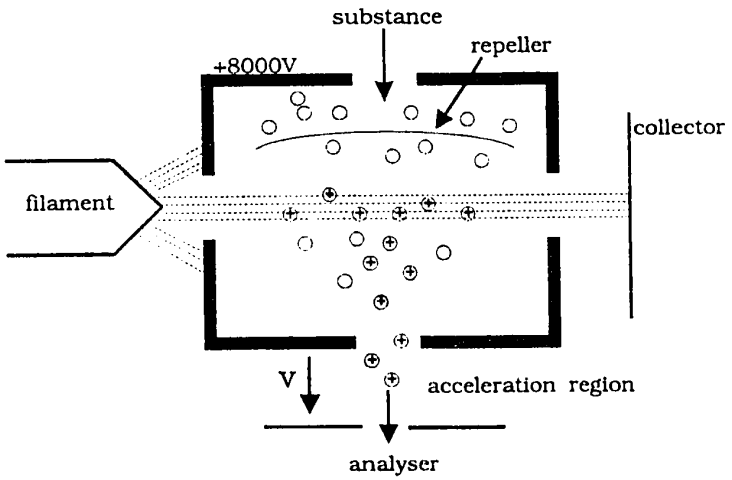

Figure 2.2 Schematic diagram of an electron impact ionization source.

2.2.2 The Magnetic Analyser

After exiting the source and being accelerated, the ions travel through the first field free region and arrive at the magnetic analyser. In the magnetic analyser the ions traverse a magnetic field, B (produced by an electromagnet), which is perpendicular to their motion. Therein the ions will follow a circular path of radius r given by

$$Bzv = mv^2 / r \quad \text{or} \quad r = mv / Bz \tag{2.4}$$

Combining equations (2.3) and (2.4) one obtains:

$$m / z = B^2r^2 / 2\,V_{acc} \tag{2.5}$$

Thus, by varying the strength of the magnetic field, one can "mass" select source ions of desired mass-to-charge (m/z) ratios since V_{acc} and r are constants. By scanning the magnet and detecting the ions right after they exit the magnetic field, one can obtain the single focussing mass spectrum of the source generated ions.

The magnetic sector focusses the ion beam along the r radius in a direction perpendicular to the magnetic field. In Figure 2.3, it is shown that if the ion enters and exits the magnetic field perpendicularly to the field boundaries, the point of origin of the ions, the apex of the field and the point of focus of the ions are colinear (long dashed lines).

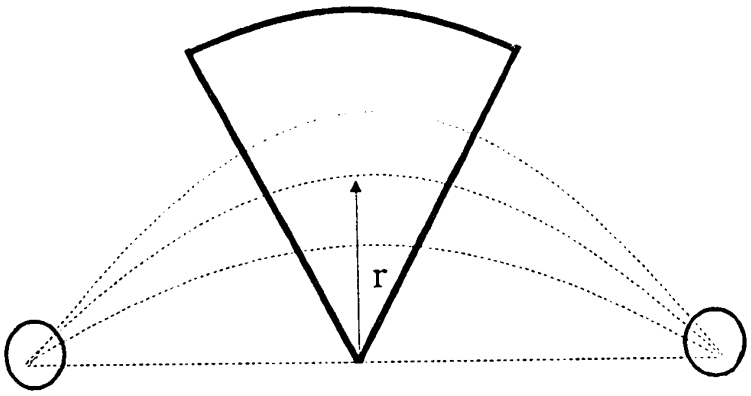

Figure 2.3 *The focussing of ions by the magnetic field.*

2.2.3 Field Free Regions

There are drift regions before and after the magnetic sector called the first and second field free regions respectively. Both of these regions can be exploited for experimental purposes but since the second field free region is the one used in almost all of the experiments, emphasis will be put on the latter.

The second field free region (2FFR) of the ZAB-2F at the University of Ottawa (which originally contained only one collision gas cell, see Fig. 2.1) was subject to several modifications. Figure 2.3 is a schematic diagram of the 2FFR as it stands today. The first modifications **[12]** were to install a second collision gas cell (cell 1) and to insert a beam deflector electrode between the two cells. Collision gases may be leaked independently into both cell 1 and cell 2, each having its own pressure gauge and diffusion pump nearby.

The purpose of the electrode is to deflect all ions from the flight path (by applying a voltage of ca. +500 V to it) so that only fast neutrals, which have been generated in the second field free region prior to the electrode, can enter the second collision cell. Note that the electrode is placed inside a grounded metal cage, in order to prevent field penetration to other regions of the instrument.

A few years later a metal vapor cell was designed and installed in the second field free region **[13]**. The latter was designed in order to perform neutralization-reionization mass spectrometry experiments using metal vapours.

The variety of experiments carried out using the accessories contained in the second field free region are discussed in Chapter 4.

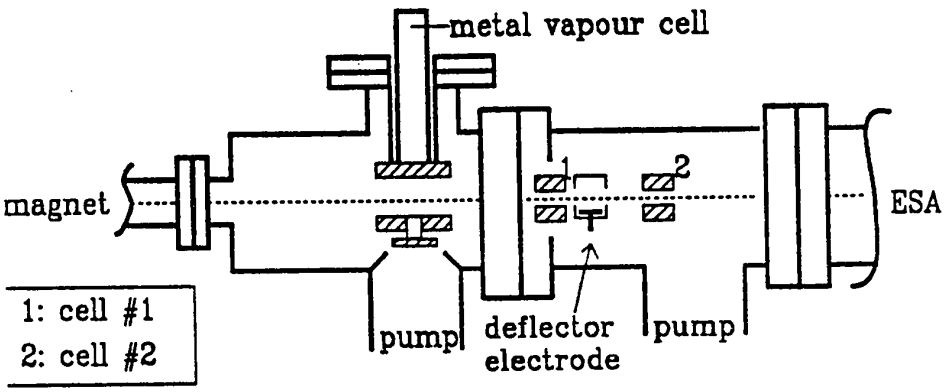

Figure 2.4 *The modified second field free region of the VG ZAB-2F mass spectrometer used at the University of Ottawa.*

2.2.4 The Electrostatic Analyser (ESA)

After the second field free region comes the electrostatic analyser, consisting of two parallel curved metal plates of radius R. A potential is applied to the plates creating an electric field, E, which influences the trajectory of the entering ions. For the ions to reach the detector, their centrifugal force has to be equal to the electric force exerted on them:

$$mv^2 / R = zE \qquad (2.6)$$

Thus with the ESA, ions may be seperated according to their kinetic energy. Since all source generated ions have the same translational energy, $zV_{acc} = 1/2\ mv^2$, equation (2.6) becomes:

$$E = 2\ V_{acc} / R \qquad (2.7)$$

Therefore by setting E to match the voltage given by equation (2.7) it is possible to detect all mass selected ions generated in the source, and by scanning the magnet and setting E to match V_{acc} the double focussing mass spectrum is obtained. The spectrum is called double focussing because the ions are brought to focus at the β-slit by the ESA (see Fig. 2.5). This supplementary focussing device allows for a much greater mass resolution than that obtained in the single focussing mode (by using the magnet only).

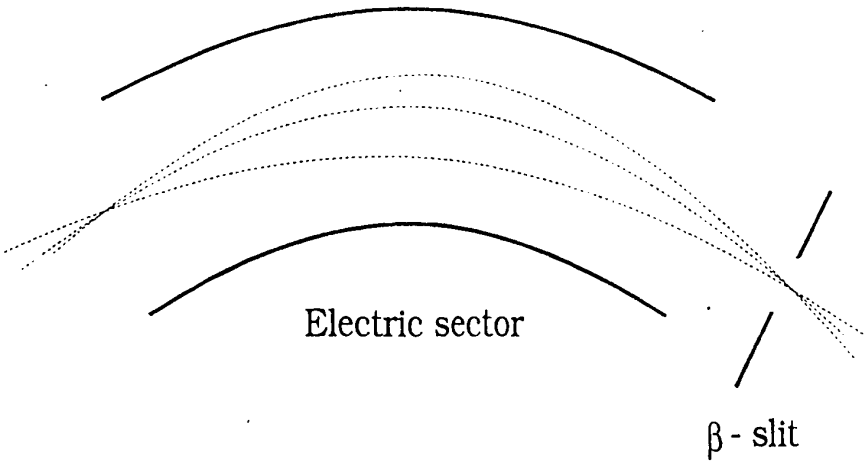

Figure 2.5 *Ion beam focussed at the β-slit by the electric sector.*

2.2.5 The Detector

The detector is an off-axis electron multiplier. The ion beam is deflected onto a negatively charged conversion dynode which emits electrons, which in turn are accelerated and amplified by series of dynodes. The resulting signal is amplified, allowing an initial ion current as low as 10^{-16} A to be detected.

2.3 The Kratos AEI MS-902S Mass Spectrometer

The MS-902S mass spectrometer (Figure 2.5) is a two sector instrument of forward geometry (the ESA precedes the magnetic analyser). Similarly to the ZAB-2F, compounds

may be introduced into the ion source via a variable molecular leak or through a probe. However, as opposed to the ZAB-2F, there is no septum inlet. An important accessory of this instrument is a Daly detector located after the magnetic sector. The advantage of this detector is that metastable ion signals may be enhanced, relative to source generated species. The great utility of the MS-902S is that appearance energy (AE) measurements of metastably generated ions may be performed. A complete description of the method used to measure AE values can be found in reference 14, and a brief description is given in Chapter 4.

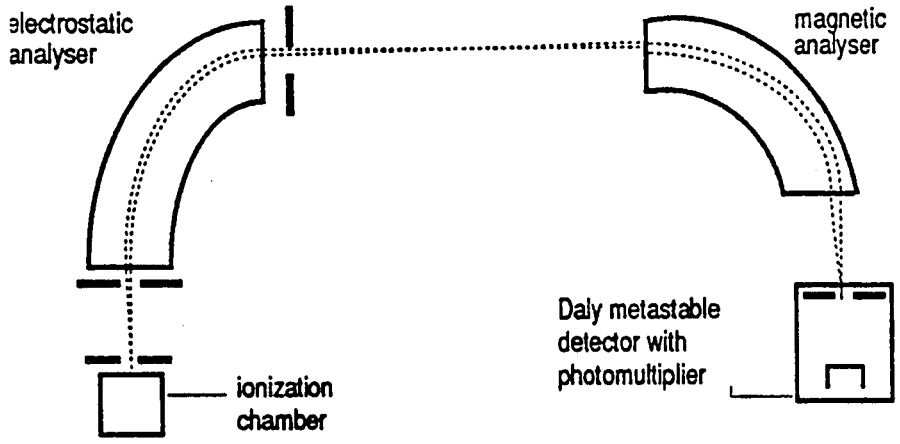

Figure 2.6 The Kratos AEI MS-902S mass spectrometer.

2.4 The Electron Energy Selector Mass Spectrometer

The electrostatic energy selector mass spectrometer was designed and built by F.P. Lossing and co-workers and a complete description of this instrument is given in reference 15. In brief, it consists of an electrostatic energy selector and a quadrupole mass analyser.

This apparatus allows for the accurate (± 0.05 eV) measurements of adiabatic ionization and appearance energy (IE, AE) values.

REFERENCES - CHAPTER 2

1. R.G. Cooks, J.H. Beynon, R.M. Caprioli and G.R. Lester, ***Metastable Ions***, Elsevier Scientific Publishing Co. Amsterdam (1973).
2. R.P. Morgan, J.H. Beynon, R.H. Bateman and B.N. Green, ***Int. J. Mass Spectrom. Ion Phys.*** 28, 171 (1978).
3. J.H. Beynon, F.M. Harris, B.N. Green and R.H. Bateman, ***Org. Mass Spectrom.*** 17, 55 (1982).
4. F.W. McLafferty (Ed), ***Tandem Mass Spectrometry,*** Wiley-Interscience, New-york (1983).
5. J.T. Watson, ***Introduction to Mass Spectrometry,*** 2nd Edn, Raven Press, New-York (1985).
6. J.H. Futrell (Ed), ***Gaseous Ion Chemistry and Mass Spectrometry,*** Wiley-Interscience, New-York (1986).
7. K.L. Bush, G.L. Glish and S.A. McLuckey, ***Mass Spectrometry/Mass Spectrometry Techniques and Apllications of Tandem Mass Spectrometry,*** VCH Publishers Inc. New-York (1988).
8. J.H. Beynon, J.W. Amy and W.E. Baitinger, ***Org. Mass Spectrom.*** 5, 229 (1971).
9. P. Longevialle, ***Principes de la Spectrométrie de Masse des Substances Organiques,*** Masson, Paris (1980).
10. M.E. Rose and R.A.W Johnstone, ***Mass Spectrometry for Chemists and Biochemists,*** Cambridge University Press, Cambridge (1987).

REFERENCES - CHAPTER 2

11. S.G. Lias, J.E. Bartmess, J.F. Liebman, J.L. Holmes, R.D. Levin and W.G. Mallard, ***J. Phys. Chem. Ref. Data,*** 17 (1988).

12. J.L. Holmes, A.A. Mommers, J.K. Terlouw and C.E.C.A. Hop, ***Int. J. Mass Spectrom. Ion Processes,*** 68, 249 (1986).

13. M.C. Blanchette, J. Bordas-Nagy, J.L. Holmes, C.E.C.A. Hop, A.A. Mommers and J.K. Terlouw, ***Org. Mass Spectrom.*** 23, 804 (1988).

14. P.C. Burgers and J.L. Holmes, ***Org. Mass Spectrom.*** 17, 123, (1982).

15. (a) K. Maeda, G.P. Semeluk and F.P. Lossing, ***Int. J. Mass Spectrom. Ion Phys.*** 1, 395 (1968). (b) F.P. Lossing and J.C. Traeger, ***Idem,*** 19, 9 (1976).

CHAPTER 3

BASIC CONCEPTS OF ION FRAGMENTATION

3.1 Introduction

In this Chapter brief definitions of some types of ions formed in a mass spectrometer are given. Also discussed is the behaviour of these ions and the factors which govern their fragmentation in the mass spectrometer.

3.2 Types of Ions Formed in a Mass Spectrometer

The formation of many different kinds of ions can occur in a mass spectrometer **[1]** and those of interest for this thesis are listed below.

3.2.1 Molecular Ions

The term molecular ion designates a positively charged, odd-electron ion, $M^{+\bullet}$, which may be formed upon ionization of a molecule, M, by ejection of an electron:

$$M + e \rightarrow M^{+\bullet} + 2e \qquad (3.1)$$

The ionization process has been described in section 2.2.1.

3.2.2 Stable Ions

A stable ion is one that is formed within the ionization chamber and contains insufficient internal energy to decompose before reaching the detector. The peaks observed in a normal mass spectrum (obtained from the ZAB-2F) are due to stable ions.

3.2.3 Unstable Ions

Unstable ions are those which are formed (in the ion source) with so much internal energy that they decompose before leaving the ionization source. Decomposition will continue until the products contain little excess energy and are stable or metastable (see below).

3.2.4 Metastable Ions

A metastable ion is one that is stable enough to leave the ion source but which decomposes en route to the collector. These types of ions and the experiments performed to study them will be discussed in great detail in Chapter 4.

3.2.5 Fragment Ions

When molecular ions are generated with a large amount of excess internal energy, specific bonds will cleave leading to the formation of fragment ions and neutral fragments. The process can be written as:

$$M^{+\bullet} \rightarrow F^{+\bullet} + N \qquad (3.2)$$

when the fragment is an odd-electron species or by

$$M^{+\bullet} \rightarrow F^{+} + N^{\bullet} \qquad (3.3)$$

when the ion is an even-electron species.

These fragment ions, $F^{+\bullet}$ and F^{+}, are designated as primary ions because they were generated in a single step from the molecular ion. Primary ions may in turn react further and give rise to secondary ions e.g.

$$F^{+\bullet} \rightarrow F_2^{+} + N_2^{\bullet} \qquad (3.4)$$

Obviously, such processes can continue and give further products.

3.3 Ion Reactivity

Electron impact ionization gives rise to the formation of ions having wide ranges of internal energies, and depending on their internal energy ions can be classified as stable, unstable or metastable as described above. Figure 3.1 shows the distribution of energy following electron impact ionization.

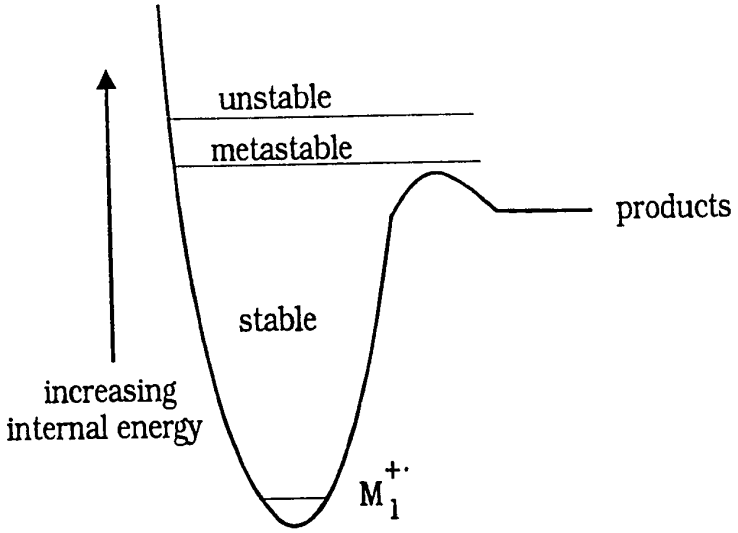

Figure 3.1 *Internal energy distribution indicating the formation of stable, metastable and unstable ions.*

Let us now examine how the ion abundance is affected by the internal energy and the corresponding decomposition rate constant, k. From Figure 3.2 it can be seen that when k increases, the abundance of stable ions is diminishing whereas that of fragment ions

is increasing. Also note that the observation of metastable peaks results from a rather narrow range of ion internal energies and rate constants.

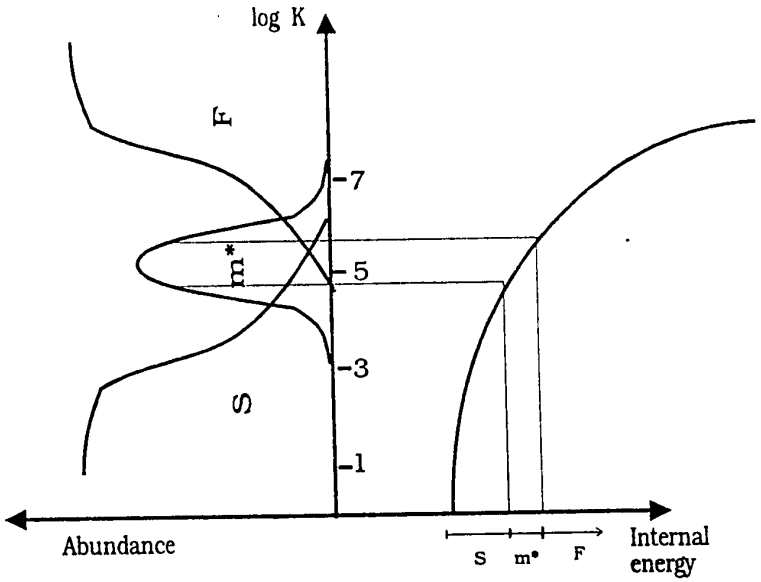

Figure 3.2 *Interrelationship between internal energy, reaction rate and the abundance of stable (S), metastable (m^*), and fragment (F) ions.*

Although the observation of stable, metastable and fragment ions depends on experimental conditions, it is generally accepted **[2]** that stable ions are those for which $k < 10^4\ s^{-1}$, unstable ions have a rate constant $k > 10^6\ s^{-1}$ and metastable ions are those having $10^4\ s^{-1} < k < 10^6\ s^{-1}$. The detailed timeframe of events occuring in the VG ZAB-2F mass spectrometer **[3]** is illustrated by Figure 3.3.

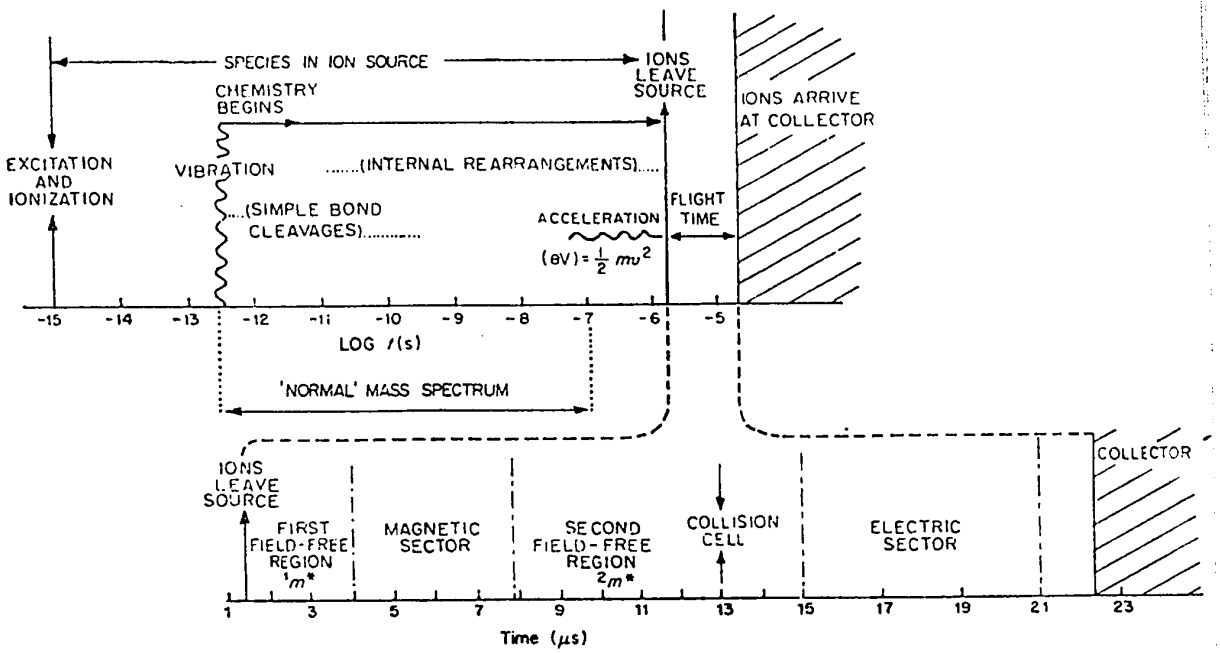

Figure 3.3 Timeframe of events occuring in the VG ZAB-2F mass spectrometer for a typical ion of m/z 100 at an accelerating voltage of 8 kV.

3.3.1 Rearrangement Process

Mass spectrometric studies have shown that a number of compounds yield fragment ions that cannot be formed on the assumption of simple cleavage of bonds in the molecular ion. These ions are formed by rearrangements of atoms (or possibly groups of atoms) during or before breaking bonds in the molecular ion or fragment ions. The stable structure from which a molecular ion finally fragments is called the reacting configuration **[4, 5]**.

The extent to which an ion A^+ will rearrange into isomer B^+ depends on the stability of the product ions and product neutral fragments, together with the relative energy barriers for isomerization as compared with that of the competing normal fragmentation processes. Three general cases illustrating the latter statement may be considered (see Figure 3.4).

(i) The energy barrier for isomerization, E_i, is much larger than that for dissociation, E_d. Therefore, decomposition of A^+ and B^+ will take place much more readily than isomerization.

(ii) The isomerization energy barrier is smaller than either dissociation barrier leading to the products. Thus, the two isomeric structures, A^+ and B^+, will interconvert giving rise to mixture of products from both A^+ and B^+.

(iii) The energy barrier for the rearrangement lies between the two dissociation energy barriers. In such a case, ion B^+ will fragment with no rearrangement, whereas A^+ will isomerize into B^+ prior to fragmenting.

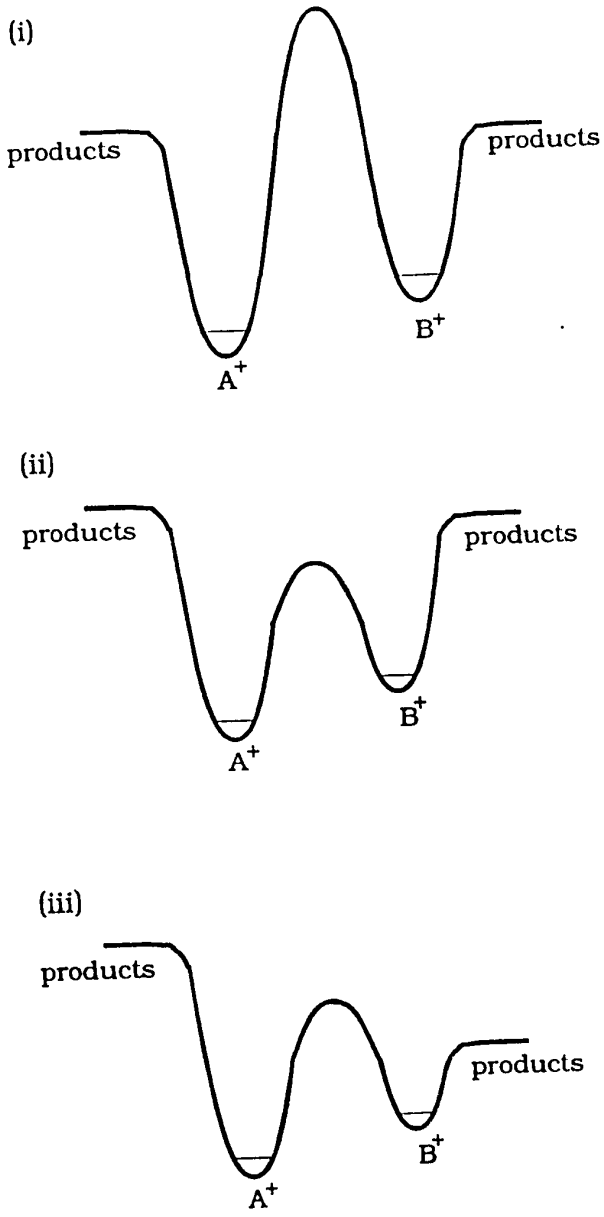

Figure 3.4 *Three potential energy diagrams illustrating the relative energy barriers for isomerization and decomposition processes for two isomeric ions, A' and B'.*

3.3.2 Ion/Molecule Reactions

While most ions in a mass spectrometer are formed in unimolecular reactions, ion/molecule reactions are bimolecular processes which can be studied in the ion source of the mass spectrometer at high pressures (relative to the usual operation mass spectrometer ionization chamber i.e. sample pressure ~ 10^{-6} mbar).

In ordinary mass spectrometry practice, the only kind of ion/molecule reaction that is significant is the transfer of a proton (protonation process) as shown below:

$$M + RH^+ \rightarrow MH^+ + R \qquad (3.5)$$

MH^+ is known as the protonated molecular ion, or (M + 1) ion.

However, in modern tandem mass spectrometry **[6]** a common approach is to react isomeric ions with a common neutral molecule and compare the dissociation characteristics of the ions formed via these ion/molecule reactions. It is presumed that if two ions have different reactivities with a common reagent molecule, their structures are different. This approach has been used for the study carried out in Chapter 7.

3.4 General Remarks Concerning Unconventional Ion Structures

Unconventional ion structures are divided into several classes such as distonic ions, ylid ions, proton-bridged complexes, ion-radical and ion-neutral complexes and destabilized carbenium ions.

Distonic (e.g. $CH_3C^+(OH)O^{\bullet}CH_2$ **[7]**) and ylid ions (e.g. $^{\bullet}CH_2C^+(OH)OCH_3$ **[8]**) are those radical cations which have the formal charge and radical sites on different atoms on the molecule. For ylid ions, the charge and radical are located on adjacent atoms whereas in a distonic ion the charge and radical are further apart **[9]**. Ion-radical ($A^{+\bullet}\bullet\bullet\bullet B^{\bullet}$) and ion-neutral complexes ($A^{+\bullet}\bullet\bullet\bullet B$) may be regarded as ions made of two entities (ion and free radical or ion and neutral molecule) joined together by means of electrostatic bonding **[10]**. Destabilized carbenium ions ($R\text{-}C(O)\text{-}C^+R_2$) are carbocations with an electron withdrawing substituent (e.g. $-CF_3$, -CN, -COR) attached to the positive center **[11]**. Finally, proton-bridged complexes are molecule-radical or molecule-molecule pairs held together by an H^+ ion forming a bridge between the two entities. Because proton-bridged complexes are the basis of the study achieved in Chapter 8, they will be discussed in some detail below.

3.4.1 Proton-Bridged Complexes

Proton-bridged (or H-bridged) ions are unconventional ions which are now generally accepted as playing an important role in some fragmentation mechanisms **[9]**, and they have

been the subject of many recent investigations **[9, 12, 13]**.

Even-electron proton-bound molecule pairs $[M_1 \bullet\bullet\bullet H^+ \bullet\bullet\bullet M_2]$ may be produced via ion/molecule reactions and represent a well studied class of ions. On the other hand, much less is known about odd-electron proton-bound molecule-radical pairs $[M \bullet\bullet\bullet H^+ \bullet\bullet\bullet R^{\cdot}]$, because they are much more difficult to generate via ion/molecule reactions and their production from unimolecular disociation of precursor ions is certainly less than straightforward, necessarily involving complex rearrangements.

It is sometimes difficult to assign a unique structure to H-bridged complexes based only on dissociation characteristics, because isomeric forms are usually involved. Therefore, ab-initio molecular orbital theory calculations, used in concert with experimental data have become a valuable tool in the study of H-bridged species **[12]**. Unfortunately, as the size of the ion increases, so does the cost (i.e. computer time) of such calculations.

However, Larson and McMahon **[14]** have shown that the value of the H-bond strengths, $D(AH^+\text{-}B)$, in a proton bound pair (for which the hetero-atom is oxygen i.e. the proton lies between two O), is related to the proton affinities, PA, of the partners, A and B, according to the following equation:

$$D(AH^+\text{-}B) = 0.46\ [PA(B) - PA(A)] + (30.8 \pm 2\ \text{kcal/mol}) \qquad (3.6)$$

The heat of formation of the H-bridged ion, $\Delta H_f(I^+)$, is therefore:

$$\Delta H_f(I^+) = \Delta H_f(AH^+) + \Delta H_f(B) - D(AH^+-B) \qquad (3.7)$$

Based on the same idea, Mautner **[15]** has derived an equation which can be applied to proton-bond pairs involving nitogen and sulfur atoms:

$$D[AH^+-B] = 0.26\ [PA(B) - PA(A)] + (30 \pm 2\ \text{kcal/mol}) \qquad (3.8)$$

Note that Equations (3.6) and (3.7) were derived for molecular species A and B, but extension to molecule-radical pairs i.e. $A^{\cdot}H^+B$ appears to be possible **[16]**. For example **[16]**, $CH_3C^{\cdot}O\bullet\bullet\bullet H^+\bullet\bullet\bullet OCH_2$ to which the following values are associated: $PA(CH_3C^{\cdot}O)$ = 158 kcal mol^{-1}, $PA(OCH_2)$ = 171.7 kcal mol^{-1}, $\Delta H_f(CH_3COH^+)$ = 203 kcal mol^{-1} and $\Delta H_f(CH_2O)$ = -26 kcal mol^{-1}. Using the above Equations where A = $CH_3C^{\cdot}O$ and B = CH_2O, one obtains $\Delta H_f(I^{+\cdot})$ = 140 kcal mol^{-1} which compares very well with the theoretical ab initio calculation value of 138 kcal mol^{-1}.

REFERENCES - CHAPTER 3

1. R.G. Cooks, J.H. Beynon, R.M. Caprioli and G.R. Lester, ***Metastable Ions,*** Elsevier Scientific Publishing Co. Amsterdam (1973).
2. P. Longevialle, ***Principes de la Spectrométrie de Masse des Substances Organiques,*** Masson, Paris (1980).
3. J.L. Holmes, ***Org. Mass Spectrom.*** 20, 169 (1985).
4. J. Roboz, ***Introduction to Mass Spectrometry: Instrumentation and Techniques,*** John Wiley and Sons Inc. New-York (1968).
5. F.W. McLafferty (Ed), ***Mass Spectrometry of Organic Ions,*** Academic Press Inc. New-York (1963).
6. K.L. Bush, G.L. Glish and S.A. McLuckey, ***Mass Spectrometry/Mass Spectrometry: Techniques and Applications of Tandem Mass Spectrometry,*** VCH Publishers Inc. New-York (1988).
7. P.C. Burgers, J.L. Holmes, C.E.C.A. Hop and J.K. Terlouw, ***Org. Mass Spectrom.*** 21, 549 (1986).
8. J.K. Terlouw, J.L. Holmes and P.C. Burgers, ***Int. J. Mass Spectrom. Ion Processes***, 66, 239 (1985).
9. P.C. Burgers and J.K. Terlouw, ***Specialist Periodical Reports: Mass Spectrometry,*** Ed. M.E. Rose, The Royal Society of Chemistry, London, 10, chapter 2 (1989).
10. (a) S. Hammerum, ***J. Chem. Soc. Chem. Comm.*** 858 (1988). (b) D.J. McAdoo, ***Mass Spectrom. Rev.*** 7, 363 (1988).

REFERENCES - CHAPTER 3

11. (a) A-M. Dommröse and H.F. Grützmacher, ***Org. Mass Spectrom.*** 22, 437 (1987). (b) R. Wolf, A-M. Dommröse and H.F. Grützmacher, ***Org. Mass Spectrom.*** 23, 26 (1988).

12. P.C. Burgers, J.L. Holmes, C.E.C.A. Hop, R. Postma, P.J.A. Ruttink and J.K. Terlouw, ***J. Am. Chem. Soc.*** 109, 7315 (1987).

13. (a) N. Heinrich, J. Schmidt, H. Schwarz and Y.J. Apeloig, ***J. Am. Chem. Soc.*** 109, 1317 (1987).

14. J.W. Larson and T.B. McMahon, ***J. Am. Chem. Soc.*** 104, 6255 (1982).

15. M. Mautner, ***J. Am. Chem. Soc.*** 106, 1257 (1984).

16. J.L. Holmes, ***Adv. Mass Spectrom.*** 11, 53 (1989).

CHAPTER 4

EXPERIMENTAL TECHNIQUES AND MEASUREMENTS

4.1 Introduction

Tandem mass spectrometry is one of the most useful and versatile techniques to gain information on gas phase ion structure. The purpose of this Chapter is to give a general overview of the different experimental methods which are used to aid in the assignment of gas phase ion structures and fragmentation mechanisms. The experimental methods currently available fall into two main categories, (i) ion thermochemistry and (ii) ion dissociation characteristics. It is generally argued that neither of the above methods alone can suffice for ion structure assignment, but used in combination and often in concert with isotopic labeling experiments, these two methods represent a powerful tool for assigning structures to ions in the gas phase.

4.2 Ion Thermochemistry

The heats of formation , ΔH_f, of ions are especially important to establish the structure of gas phase ions, because obtaining identical ΔH_f values for two ions generally implies that they have the same structure.

Heats of formation may be obtained from either ionization energy (IE) or appearance energy (AE) measurements and the data so obtained can be used to firmly establish (by

comparison with literature values) the structure of ionic species. This is particularly useful when a whole system of isomeric species is being studied. Note however, that ΔH_f values are rarely solely used to identify ionic species, but rather they are used in conjunction with ionic dissociation characteristics.

4.2.1 Ionization Energy

The minimum energy required to remove an electron from the highest occupied orbital of a molecule is known as the first ionization energy (IE) **[1]**. Two types of ionization energy are commonly described, the vertical (IE_v) and adiabatic (IE_a) ionization energies. The latter is obtained when a transition from the ground state of the molecule to the ground state of the ion is being measured (Figure 4.1). The IE_v refers to the energy difference between the ground state of the molecule and that of the ion having the same geometry.

The equation which relates the heat of formation of an ion $M_1^{+\bullet}$ and the IE value is shown below.

$$\Delta H_f(M_1^{+\bullet}) = IE(M) + \Delta H_f(M) \qquad (4.1)$$

Therefore the determination of $\Delta H_f(M_1^{+\bullet})$ requires knowledge of the standard enthalpy of formation of the neutral molecule, M. This latter may be found in the literature **[2, 3]** or

may be estimated using the additivity scheme of Benson [4].

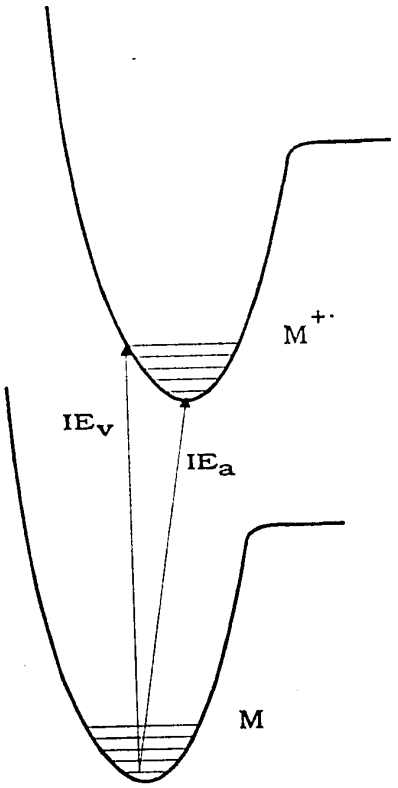

Figure 4.1 *Vertical, IE_v, and adiabatic, IE_a, ionization energies.*

4.2.2 Appearance Energy

The appearance energy (AE) is the minimum energy required to cause the appearance of a fragment ion, $M_2^{+\cdot}$.

$$M_1^{+\bullet} \rightarrow M_2^{+\bullet} + M_3 \qquad (4.2)$$

The heat of formation of the fragment ion, $M_2^{+\bullet}$, is given by

$$\Delta H_f(M_2^{+\bullet}) = AE(M_2^{+\bullet}) - \Delta H_f(M_3) + \Delta H_f(M_1) \qquad (4.3)$$

Hence, provided that $\Delta H_f(M_3)$ and $\Delta H_f(M_1)$ are known, $\Delta H_f(M_2^{+\bullet})$ can be calculated, or alternatively if $\Delta H_f(M_2^{+\bullet})$ and $\Delta H_f(M_1)$ are available then $\Delta H_f(M_3)$ may also be determined from AE measurements.

The ion enthalpy derived from Equation (4.3) will be reliable provided that (i) the fragmentation of $M_1^{+\bullet}$ has no significant kinetic shift (see below) and that (ii) there is no reverse energy barrier (see below) for the reaction

$$M_3 + M_2^{+\bullet} \rightarrow M_1^{+\bullet} \qquad (4.4)$$

Note that simple bond cleavage reactions **[5, 6]** as well as rearrangement reactions **[7]** may display either complication.

(i) Kinetic shift

The kinetic shift, $\varepsilon^{\neq}$, is the energy above the transition state (see Figure 4.2) which is necessary for the observation of $M_2^{+\bullet}$ on the time scale of the experiment. Thus the

kinetic shift is dependent on the internal energy and the rate constant for fragmentation (see Figure 4.3)

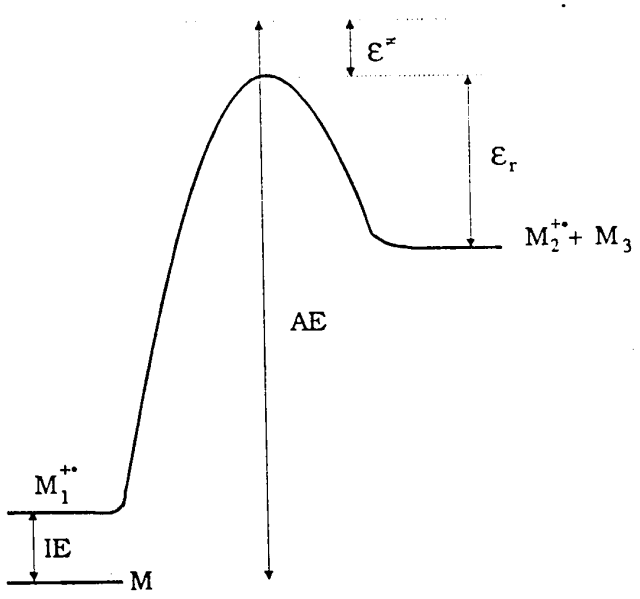

Figure 4.2 *Effect of a kinetic shift, $\epsilon^{\neq}$, and an energy barrier on the measured appearance energy of $M_2^{+\bullet}$.*

A fragmentation reaction will have a significant kinetic shift when its rate constant rises only slowly with increase in internal energy and in such a case, the measured AE values will lead to an upper limit of $\Delta H_f(M_1^{+\bullet})$. When the rate constant rises sharply with

the increase of internal energy, the kinetic shift is less important and the AE values may be used with more confidence [7]. The absence of a metastable peak for the reaction of interest is an indication of such behaviour.

(ii) Energy barrier

From Figure 4.2, one may also see that a too high value of $\Delta H_f(M_1^{+\bullet})$ will be obtained if there is a reverse activation energy, ε_r. For the majority of reactions involving a simple bond cleavage, ε_r will be small or equal to zero since ion-radical recombination reactions (i.e. the reverse of an ion fragmentation) proceed with little or no energy barrier **[7, 8]**. However, rearrangement reactions may often occur with a significant reverse energy **[5, 9]**.

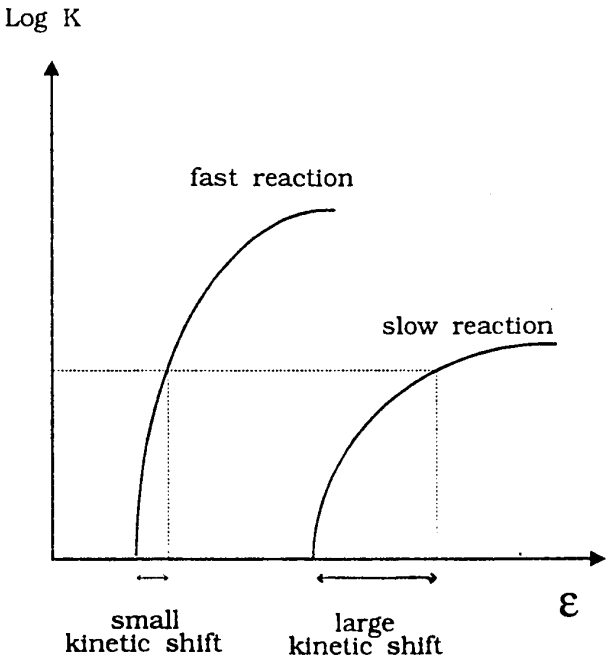

Figure 4.3 *Illustration of the dependence of the kinetic shift upon the internal energy and rate constant for fragmentation.*

4.2.3 Competitive Reactions

The measurement of an AE value can be complicated if there are two or more competing fragmentation channels. Figure 4.4 represents a classical case of the competition between a rearrangement process (R) and a simple bond cleavage (C). In the present case, the activation energy for R is lower than that of C, but the rate constant for the simple bond cleavage rises more sharply than that of the rearrangement process. Therefore process R is dominant at lower internal energies whereas process C takes over at higher energies. In other words, near the threshold for C, the rate of reaction R is much greater. Thus, observation of reaction C will not occur until some energy above its threshold where the rates for both reactions are comparable. As a consequence the observed AE of the simple bond cleavage will be too high.

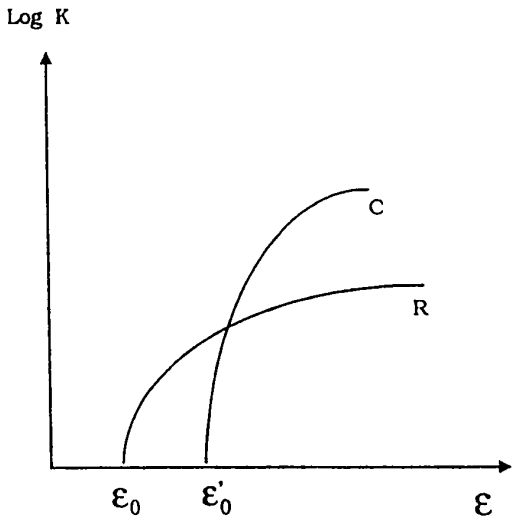

Figure 4.4 *Rate constants as a function of internal energy for two competing reactions R and C.*

4.2.4 Measurements of IE and AE Values

In this thesis, ionization energies of molecules M_1 and appearance energies of fragment ions $M_2^{+\bullet}$ were determined by recording the intensity of the ion signal as a function of the energy of the ionizing electrons. Note that the electron energy scale is first calibrated by a suitable calibrant, e.g. water **[10]**, iodobenzene or diethyl ether **[11]**.

With the energy selector mass spectrometer **[10]**, the IE value for H_2O is usually used as the calibrant and the obtained data are stored in a computer data processing system. The ionization or appearance energy values for molecules or ions of interest are then obtained by taking the electron energy value at the onset of the ion current versus ionizing electron energy curve (Figure 4.5). The uncertainty in ΔH_f values derived from such IE and AE measurements (Eqs. 4.1 and 4.3) is estimated to be not greater than ± 1 kcal mol^{-1}.

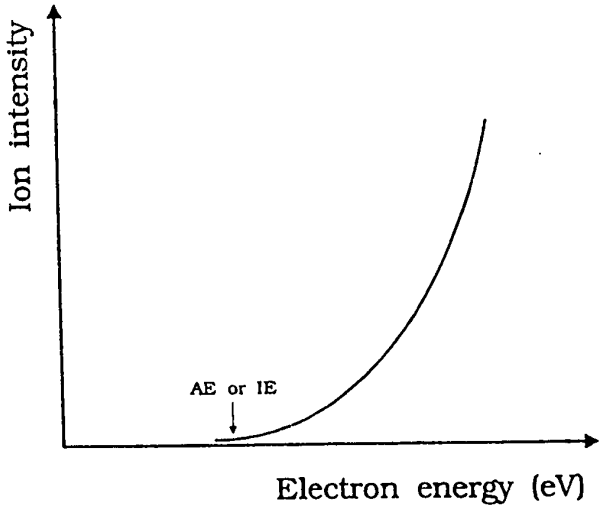

Figure 4.5 *Illustration of an ion abundance vs ionization energy curve. IE and AE values are obtained from the onset of the curve.*

The method used to determine the AE of a metastable peak using the MS-902S mass spectrometer is fully described in reference 11. Briefly it consists in measuring the abundance (peak height) of the metastable peak of interest and one from a calibrant (usually $CH_3CH_2O^+CH_2$ generated from metastable diethyl ether molecular ions) versus electron energy under identical instrumental conditions. The comparison of their threshold energy values will determine the unknown AE value. The uncertainty in ΔH_f values obtained from such AE measurements (Eq. 4.3) is estimated to be not greater than ± 3 kcal mol^{-1}. An example of the utility of AE values to investigate metastable fragmentation pathways of a series of isomers is shown in the next chapter.

4.2.5 Estimation of the Heats of Formation of Ions

Once the ΔH_f value of an ion has been obtained by means of IE or AE measurements, it may be compared with literature or estimated values.

One may estimate heats of formation of ions by studying correlations within homologous series. The equation, $\Delta H_f(ion) = A - Bn + C/n$, where A, B and C are constants and n is the number of atoms in the molecule can give fairly acceptable values **[12]**.

Many factors have to be considered when estimating ΔH_f(ions): location of the charge on the ion **[13]**, nature of substituent **[14]**, multiple substitution effects **[15]** and the

relationship between stabilization energy and ion size **[16]**. However, although the ΔH_f value of an ion is an excellent criterion for its structure assignment, it should not be solely used because isomers may have similar ΔH_f values. A good example of such a possibility is that of the $C_2H_5Cl^{+\bullet}$ isomers, for which the $\Delta H_f(CH_3CH_2Cl^{+\bullet})$ was found to be 227.1 kcal mol^{-1} vs 227.3 kcal mol^{-1} for its ylid counterpart $CH_3CHClH^{+\bullet}$ **[17]**. Another problem may arise if the structure of the neutral is not known. An example is found in the fragmentation of ionized aniline **[18]** which produces $C_5H_6^{+\bullet}$ and [H,C,N] with an AE value 0.8 eV above the calculated threshold for $C_5H_6^{+\bullet}$ + HCN. It was proposed that the neutral is HNC for which ΔH_f is 0.6 eV higher than HCN. This proposition was confirmed by performing a collision induced dissociative ionization (CIDI) experiment (see section 4.3.4) on the neutral product to establish its structure **[16]**.

4.3 Ion Dissociation Characteristics

Ion dissociation characteristics are primordial in the identification of ion and neutral species in the gas phase. These may be separated into spontaneous and collision induced dissociation (CID). The important difference between these techniques is that ions having different internal energies are being sampled. Therefore ions which may be indistinguishable from their metastable ion (MI) dissociative characteristics may be clearly identifiable from CID experiments (see section 4.3.2).

The reactions concerning the topics presented in this thesis include metastable ion

(MI) dissociations and dissociations resulting from the collision of fast moving ionic or neutral species with a stationary target gas. Experiments falling in the latter category include, collision induced dissociation (CID), collision induced dissociative ionization (CIDI) and neutralization-reionization (NR) mass spectrometry. In the following sections, each of the above mentioned techniques will be discussed individually.

4.3.1 Metastable Ion (MI) Mass Spectrometry

As defined in section 3.2.4, a metastable ion is one which has enough energy to exit the ionization chamber but decomposes before reaching the detector **[8]**. Such ions have a small excess energy above the minimum for fragmentation and a lifetime of ca 1-10 μs. Metastable ion dissociations have been observed in early mass spectrometry studies and the first scientists to use the term "metastable ions" were Hipple and Condon **[20]** in 1945.

The detection of metastable ion dissociation products is possible only if the appropriate fragmentation took place in the field free regions of the apparatus (i.e. between the ion source and magnet, 1FFR, or between the magnetic and electrostatic sectors, 2FFR). Suppose that an ion, $M_1^{+\bullet}$, metastably decomposes in the first field free region of the VG ZAB-2F yielding a daughter ion, $M_2^{+\bullet}$, and a neutral fragment, M_3. Assuming that the velocity of both fragments is virtually unchanged, and that the law of conservation of momentum has to be obeyed, the kinetic energy of the products will be a fraction of the kinetic energy of the precursor ion.

$$1/2\ m_2v_2^2 = m_2/m_1\ \ x\ \ zV_{acc} \qquad (4.5)$$

$$1/2\ m_3v_3^2 = m_3/m_1\ \ x\ \ zV_{acc} \qquad (4.6)$$

In other words the initial kinetic energy, $1/2\ m_1v_1^2$, will be equal to the total kinetic energy of the fragments and it can be seen that this kinetic energy is shared between the fragments in the ratio of their masses.

$$1/2\ m_1v_1^2 = 1/2\ m_2v_2^2 + 1/2\ m_3v_3^2 \qquad (4.7)$$

From equation (2.3) and keeping in mind conservation of momentum, $M_2^{+\bullet}$ will have a kinetic energy of

$$zV'_{acc} = 1/2\ m_2v_1^2 \qquad (4.8)$$

where $V'_{acc} = (m_2/m_1)\ V_{acc}$

Combined with equation (2.4) one obtains

$$(m_2^2/m_1)\ /\ z = B^2r^2\ /\ 2\ V_{acc} \qquad (4.9)$$

and therefore metastably generated $M_2^{+\bullet}$ will have an apparent mass, m^*, given by

$$m^* = m_2^2/m_1 \qquad (4.10)$$

Therefore metastably generated ions $M_2^{+\bullet}$ will be transmitted through the magnetic analyser with such an apparent mass, but because they have a fraction m_2/m_1 of the kinetic energy of the precursor ion, $M_1^{+\bullet}$, they will be detected only if the ESA is set at the appropriate voltage, corresponding to $m_2/m_1 \times V_{acc}$.

For metastable ions dissociating in the second field free region (those of major interest for this thesis), they are mass-selected by the magnetic analyser whereafter they enter the 2FFR and the masses of the fragmentation products are determined by scanning the electric sector. Along with metastable fragmentation products determination, metastable peak shapes and kinetic energy release (KER) measurements, recorded under good resolution conditions, can give further and valuable information on the ion of interest. These two criteria will be discussed in some detail below.

4.3.1.1 Resolution

For the VG ZAB-2F one may speak in terms of mass or energy resolution. Mass resolution is a measure of the ability to separate two ions, M_1^+ and M_2', of any defined mass difference, $\Delta M = m_2 - m_1$. The peaks are resolved when $h/H \leq 0.1$ (Figure 4.6) and the resolution, R, is given by

$$R = m_1 / \Delta m \qquad (4.11)$$

The resolution power of the VG ZAB-2F is approximately 1000 when all the variable slits (Y_1 - Y_5) are fully open. Narrowing the slits permits one to achieve greater resolution at the expense of signal intensity.

The energy resolution is measured by the energy recorded at half height of the peak (Figure 4.6). The "real" voltage scanned by the electrostatic analyser is 0-483 Volts, but since an accelerating voltage of 8000 V is given to the ions, the sector voltage is scaled to 8000 V. Therefore at 483 V, the ions are considered to have 8000 V. An energy resolution of 5 Volts is considered acceptable.

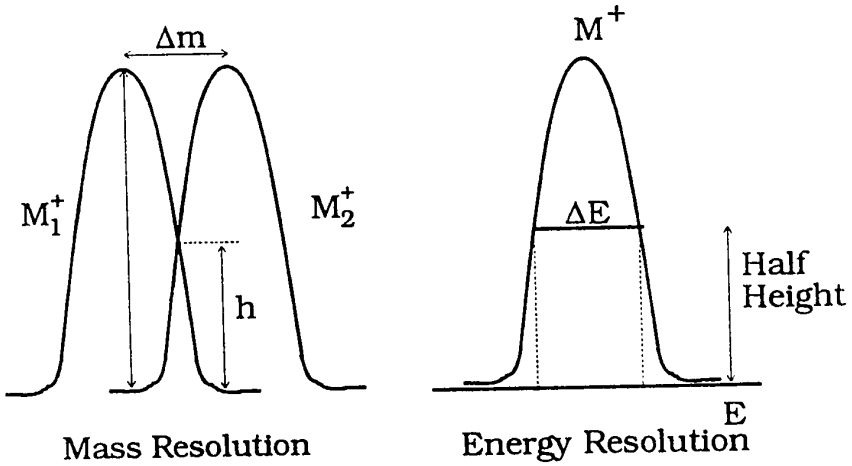

Figure 4.6 *Diagram showing the difference between mass and energy resolution.*

4.3.1.2 Metastable Peak Shapes and Kinetic Energy Release (KER)

It was mentioned in section 4.2.2 that for an ion to dissociate, an excess of internal energy is required. When metastable ions fragment, this excess of internal energy may be released as kinetic energy given to the fragments, and as a result, the metastable peaks are broadened relative to a beam of non dissociating ions. The magnitude of this peak broadening is dependent upon the reverse activation energy (ε_r) as well as on the kinetic shift ($\varepsilon^{\neq}$). If there is a large ε_r and/or $\varepsilon^{\neq}$ then there will usually (but not always) be a large kinetic energy release (large $T_{0.5}$ value, see below) and a dish-shaped metastable peak. On the other hand, if the reaction takes place near threshold then there will always be a small KER and a narrow Gaussian metastable peak. It should be mentioned that the fundamental difficulty associated with the evaluation of the way in which the internal energy of a fragmenting ion is partitioned among the translational degrees of freedom of the products, is that no simple method exists for the simultaneous and accurate measurement of internal energy content and the kinetic energy release **[21]**. In essence this means that a measured $T_{0.5}$ value has no special significance. Nevertheless, $T_{0.5}$ values are still of great importance because fragmenting ions having the same reacting configuration should show similar $T_{0.5}$ values **[22]**.

Experimentally, kinetic energy release values are measured under high energy resolution conditions. The ion of interest is mass-selected through the magnet and then the electric sector is scanned slowly over a small voltage range close to that of the ion

fragment's energy. For a given metastable fragmentation process, $M_1^{+\bullet} \rightarrow M_2^{+} + M_3^{\bullet}$, the $T_{0.5}$ value associated with the metastable peak M_2^{+} is then calculated by the following equation **[8]**.

$$T_{0.5} = (\Delta E_2^2 - \Delta E_1^2) \times m_1^2 / 16 \times m_2 \times m_3 \times V_{acc} \qquad (4.12)$$

Where ΔE_2 and ΔE_1 are the peak widths at half height of the metastable peak, M_2^{+}, and the metastable precursor ion, $M_1^{+\bullet}$, respectively. V_{acc} is the accelerating voltage. Note that the $T_{0.5}$ values are usually given in meV, because peak widths at half heights are normally measured in volts. $T_{0.5}$ values are obtained with an uncertainty of ±5 meV.

Another important criterion of metastable ion studies is the shape of a metastable peak. Metastable peak shapes are generally classified as Gaussian, flat-topped and dished, or composite (see Figure 4.7).

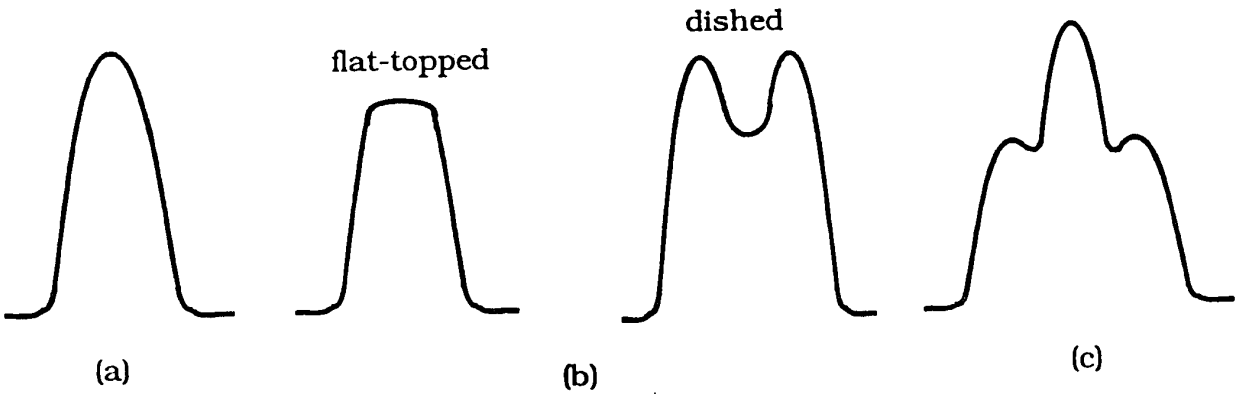

Figure 4.7 *Metastable peak shapes: (a) Gaussian, (b) flat-topped and dished, (c) composite.*

Gaussian-type metastable peaks are the most commonly observed and are usually associated with small kinetic energy releases; typically $T_{0.5}$ values of up to 80 meV. Flat-topped and dished metastable peaks are associated with larger KER due to reactions having significant reverse activation energy. The dish observed in such peaks is not of physicochemical origin but is produced by z-axial discrimination against the ion beam. The fragment ions which contain large amount of kinetic energy in the plane of the long axis of the energy resolving slit are not fully transmitted because the slit is of finite length.

Composite metastable peaks may consist of the combination of a Gaussian peak atop a dished peak or a pair of superimposed dished peaks **[23]**. They can arise (i) from two isomeric ions which lose a common neutral fragment to yield one or two daughter ion structures (ii) from a single precursor ion structure which fragments to yield a pair of isomeric daughter ions and (iii) from a pair of isomeric precursor ions fragmenting to yield a common daughter ion via different reacting configurations.

4.3.1.3 Metastable Peak Intensities

The possibility that there is a relationship between relative metastable peak intensities and the structure of a fragmenting ion was proposed by Shannon and McLafferty **[24]** following a related study of Rosenstock et al. **[25]**. It is based on the premise that when two (or more) competing fragmentations from the same ion give reasonably intense metastable peaks, then the ratio of their abundances may be used as a criterion for ion

structure. Therefore, if dissociating ions of a given m/z ratio and having the same molecular formula, obtained from a variety of different precursor species, all display very closely similar metastable peak abundance ratios, it provides good circumstantial evidence, but not proof, that ions having the same reacting configurations are being observed. However, care must be taken such that all fragmenting ions are observed under identical experimental conditions of e.g. ionizing electron energy, ion lifetime (reacting region) and energy resolution. If such care is taken, metastable peak abundance ratios are reproducible and may be obtained with an uncertainty of ± 1 relative units.

4.3.2 Collision Induced Dissociation (CID) Mass Spectrometry

The collision induced dissociation of ions was first described by Jennings **[26]** and Hadden and McLafferty **[27]**. In their paper, Hadden and McLafferty **[27]** suggested that the structure of an ion can be characterized by its CID mass spectrum and that the technique would provide an additional characteristic of broad applicability. Indeed some twenty years later, CID experiments are widely used and have proven to be of prime importance in the study of gas phase ion structure and fragmentation mechanisms **[7, 28]**. For example the use of CID in the investigation of $C_3H_8O^{+\bullet}$ ions has shown the existence of two new isomers of 1-propanol ions $CH_3CH_2CH_2OH^{+\bullet}$ of structures $CH_2CH_2CH_2OH_2^{+\bullet}$ and $CH_3CHCH_2OH_2^{+\bullet}$ **[29]**.

With the VG ZAB-2F, the second collision gas cell situated in the second field free

region (see Figure 4.8) is used to perform CID experiments. Ions of interest, $M_1^{+\bullet}$, are mass-selected with the magnet, travel through the 2FFR and enter gas cell 2 in which they collide with a target gas, T (usually He or O_2). The fragment ions are then analysed by scanning the ESA and detected. The mass-selected ions which suffer collision induced dissociation, are ions originating from the ion source which have insufficient energy to fragment on the μs (metastable ion) time-scale. When these ions collide with a neutral target, some of their translational energy may be converted into internal energy inducing unimolecular fragmentation of the ions.

$$M_1^{+\bullet} + T \rightarrow M_1^{*+\bullet} \rightarrow M_2^{+} + M_3^{\bullet} \qquad (413)$$

The ions which undergo collision induced dissociation possess a broad range of internal energies, from the IE (AE) of the ion up to and including energies appropriate to metastable fragmentations in the 2FFR. If the precursor ion ($M_1^{+\bullet}$) retains its initial structure (no rearrangement) over this whole range of internal energies then the CID mass spectrum can be taken as structure specific for $M_1^{+\bullet}$ and should resemble the normal mass spectrum of the molecule M_1. Therefore in cases where at energies appropriate to metastable fragmentation, isomers freely interconvert and the isomers cannot be distinguished based on their MI mass spectrum, one may be able to distinguish the isomers based on their CID characteristics since ions of lower internal energy are being sampled (see Figure 3.4(ii)).

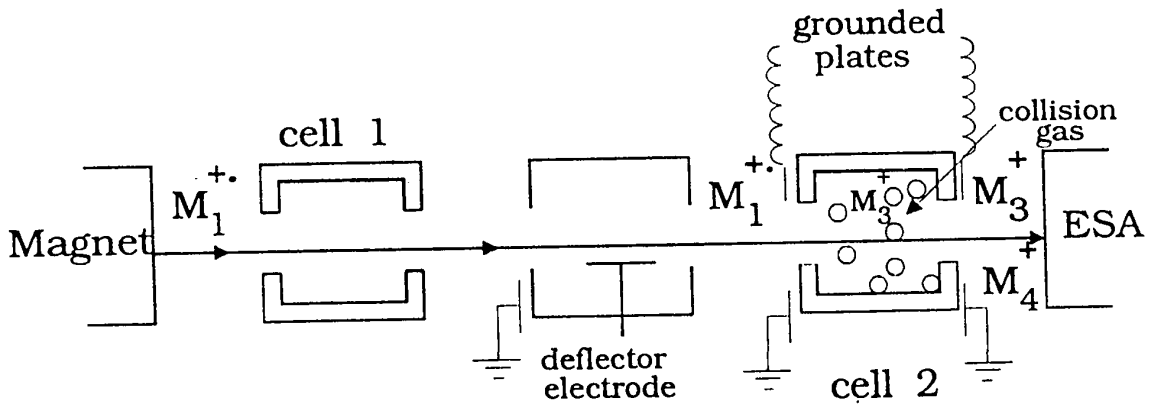

Figure 4.8 Collision induced dissociation experiment performed in the second field free region of the VG ZAB-2F.

4.3.2.1 Nature and Pressure of the Collision Gas

These are the factors which most affect a CID mass spectrum. The most widely used target gases for CID experiments are He and O_2, although N_2, H_2, Xe and other gases have also been used. Target gases mainly fall into two categories **[30]**, soft targets (O_2, NO_2, Cl_2) which provide less fragmentation and hard targets (He, CH_4, SF_6) which provide more, whereas N_2 is considered an intermediate strength target. The choice of gas will therefore depend on the type of information needed **[31]**.

Normally, the actual pressure of gas within the collision cell is not measured and so it is monitored at some nearby station in the mass spectrometer. Thus a more convenient way of reporting experimental pressure conditions, is to report the percentage

reduction of the ion main beam, e.g. gas pressure causing a 10% reduction of the mass-selected ion beam is normally used to record CID mass spectra. As the main ion beam becomes more and more reduced, multiple collisions become more important and the yield of fragments resulting from high dissociation energy pathways increases. For example Figure 4.9 shows that at a 10% reduction of the incident ion beam, >95% of the collisions are single encounters whereas at 60% beam reduction, double and triple encounters now make up 20% and 5% of the collision events respectively.

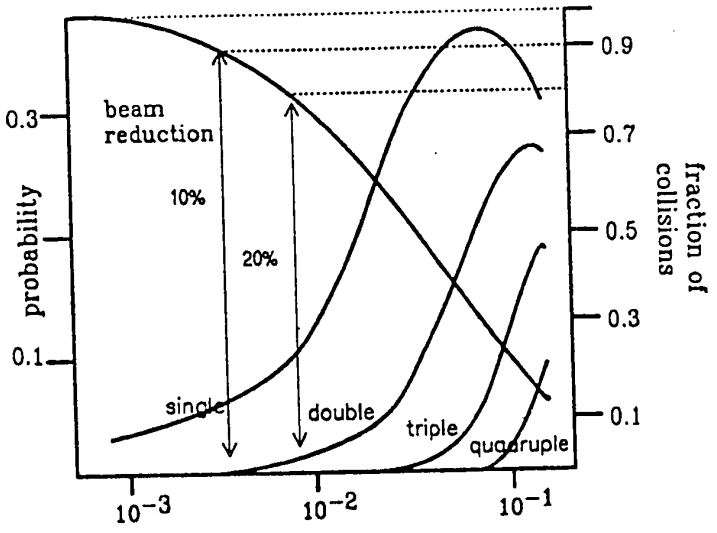

Figure 4.9 *Total collision probability and the fractions of single and multiple collision processes as a function of collision gas pressure.*

Thus it is obvious that in order to obtain reproducible results care must be taken in the choice of the collision gas and in the pressure at which the experiments are performed. Note that for this thesis, He and O_2 were used as target gases at pressures corresponding to a 10% beam reduction to obtain essentially single collision conditions.

4.3.2.2 Metastable Peak or Collision Induced Dissociation Peak?

As for MI peaks, those originating from CID processes will have a width related to the KER for their fragmentation. In general the CID peak will be wider since there is a larger range of internal energies involved and a larger time scale for the CID relative to metastable ion decomposition.

The cross section for CID may be very high and so peaks which appear to be metastable instead may be due to CID. One way to determine whether a peak is due to a CID process and not to a metastable process, is to measure the width of the peak (under energy resolution conditions) in the absence of and in the presence of increasing amounts of collision gas. If the width of the peak is <u>independent</u> of collision gas pressure then the peak is very likely to originate from a CID process.

Another method to discriminate MI from CID peaks is to put a positive or negative voltage (typically ± 1000 V) on the collision gas cell. Consider the dissociation process, $M_1^{+\bullet} \rightarrow M_2^{+} + M_3^{\bullet}$, and assume that a negative voltage, -V, is applied to the collision cell.

Two possibilities may occur. $M_1^{+\bullet}$ fragments within the collision cell (CID process) or it also fragments outside the collision cell (MI fragmentation). For a voltage -V applied to the cell, the ions $M_1^{+\bullet}$ entering the cell with an energy V_{acc} will acquire +V translational energy i.e. their kinetic energy will be raised to V_{acc} + V. The fragments M_2^+ produced from $M_1^{+\bullet}$ in the cell will then have a fraction of the energy, $[m_2/m_1 \times z(V_{acc} + V)-V]$, as they exit the cell. The fragments produced before and after the cell will have an energy of $m_2/m_1 \times zV_{acc}$ and are not affected by the voltage applied to the cell. Thus MI and CID peaks are separated from one another (see Figure 4.10).

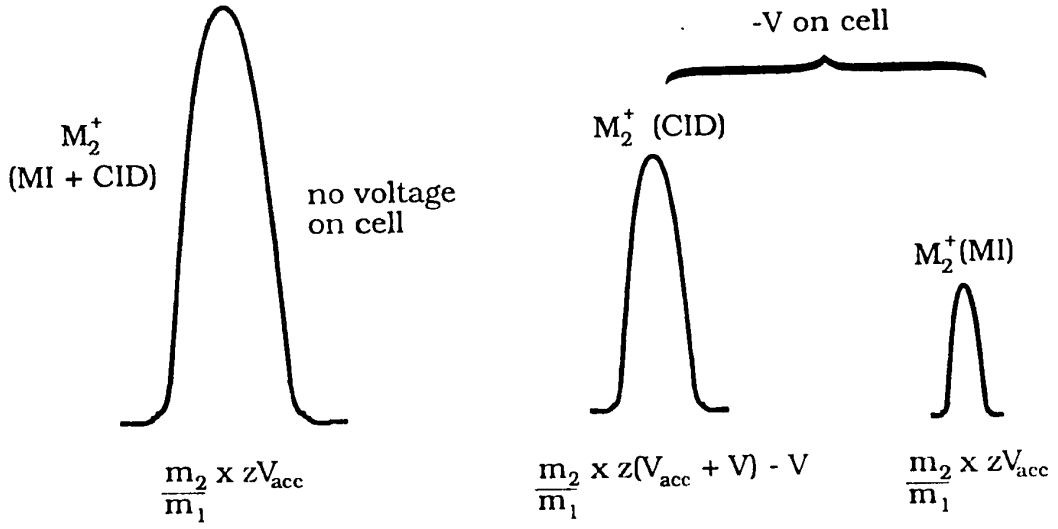

Figure 4.10 The usefulness of applying a voltage -V on the collision cell to separate MI and CID peaks.

4.3.3 Charge Stripping (CS) Mass Spectrometry

This process was first described by Cooks at al. in 1972 **[32]**. As for CID processes, charge stripping reactions arise from collisions between high energy ions and a target gas, but now to produce doubly charged ions.

$$M^+ + T \rightarrow M^{2+} + T + e \qquad (4.14)$$

They are characterized by very sharp peaks in the CID mass spectrum which appear at half the ESA voltage required to transmit the precursor ion. Due to the large energy required to generate them, CS peaks are much less intense than CID signals and may sometimes be very difficult to observe. Since this technique was not used in the present thesis, it will not be discussed in further detail. However valuable examples of the utility of the technique in the determination of structure of ions may be found in reference 33.

4.3.4 Collision Induced Dissociative Ionization (CIDI) Mass Spectrometry

The dissociation of metastable ions gives rise to the formation of ion and neutral fragments. The CIDI technique allows one to study the neutral fragments generated from metastable ion dissociations.

The method consists in mass-selecting an ion $M_1^{+\bullet}$ which traverses the 2FFR of the

VG ZAB-2F where it dissociates unimolecularly prior to the deflector electrode. Consider such an ion which undergoes only one metastable dissociation i.e. $M_1^{+\bullet} \rightarrow M_2^{+\bullet} + M_3$. A positive charge is placed on the electrode such that all the ions are deflected away and only the fast neutrals, produced during the metastable dissociation, continue on to collision cell 2. The high velocity neutral species M_3 then collide with the target gas (typically He or O_2) and if sufficient translational energy is converted into internal energy, ionization and/or fragmentation take place (see Figure 4.11).

$$M_3 + T \rightarrow M_3^{+\bullet} \rightarrow M_4^{+} + M_5^{\bullet} \qquad (4.15)$$

The resulting CIDI mass spectrum is obtained by analysis of the new ions using the electrostatic sector.

Note that for such experiments to produce unequivocal results, the unimolecular fragmentation of the mass-selected ion must generate a sufficiently intense metastable peak. Moreover the collision gas pressure should be restricted to concentrations which lead to essentially only single collision events within the cell. The latter restriction is of great importance since it has been proposed that an increase in collision gas pressure could convey energy to the neutrals allowing them to isomerize and/or decompose before collision induced ionization **[34]**. Nevertheless the CIDI technique has proven to be of great use in the assignment of the structure of many neutral fragments **[34, 35]**, sometimes with unexpected results **[19, 36]**.

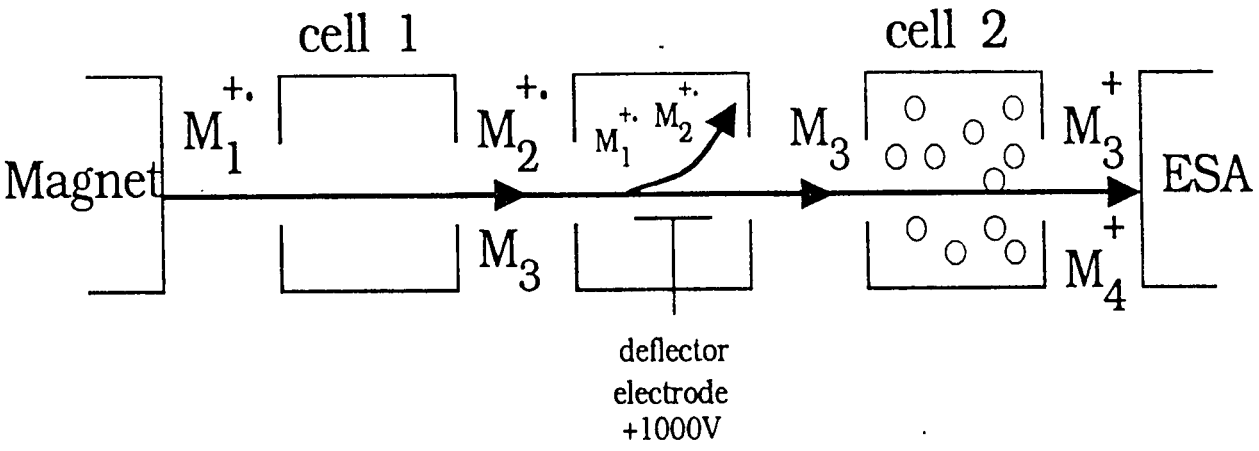

Figure 4.11 *Collision induced dissociative ionization of a neutral fragment, M_3, produced from the metastable fragmentation of a mass-selected ion, $M_1^{+\bullet}$.*

4.3.5 Neutralization-Reionization Mass Spectrometry (NRMS)

Reactions involving neutral species also include the NRMS technique which is used to study and characterize the neutral counterpart of new and unconventional ions.

The term NRMS appeared in 1983 when Danis et al. **[37]** showed that this experimental method could provide valuable information on the structure and chemistry of neutrals, ions and molecules. Since then, due to the pioneering work of J.L. Holmes, F.W. McLafferty, R.F. Porter, H. Schwarz and J.K. Terlouw, much progress has been made and the technique is well established **[38-41]**.

The technique is simple. First the desired ion is mass-selected using the magnetic

sector. The ion beam is then neutralized by charge exchange with a target gas, N (usually monoatomic), in the first collision cell. Then, as in CIDI experiments, all remaining ions are deflected from the flight path by applying a positive voltage to the deflector electrode. The neutrals enter cell 2 where they are ionized by collision with a second target gas, R, and finally the reionized neutrals and their fragment ions are separated (based on their kinetic energy) by scanning the ESA.

Therefore in the following discussion, the term NRMS will apply to the mass spectra resulting from the collisional reionization of neutrals generated from mass-selected positive ions by electron transfer from a target gas, equations (4.16) and (4.17).

$$M^+ + N \rightarrow M + N^+ \qquad (4.16)$$

$$M + R \rightarrow M^+ + R + e \qquad (4.17)$$

4.3.5.1 Neutralization

The first neutralization-reionization experiments were performed using metal vapours (Hg, Na, K, Zn) **[37, 39]**. However in 1985 Holmes, Terlouw and coworkers have shown that Xenon and other permanent gases can also conveniently be used for neutralization **[42]**.

As stated above neutralization will occur via charge exchange (Equation 4.16). Because interaction between cations and a monoatomic target will involve a time of only

approximately 10^{-16} s, the electron transfer will be considered as a vertical Franck-Condon process **[41]**. Hence if the geometries of the ion and corresponding neutral are closely similar, stable neutrals will be generated upon neutralization of the ion. However if the geometries are markedly different, their transitions to an unstable part of the potential energy surface of the neutral may take place; resulting in the decomposition of the transient neutral (see Figure 4.12).

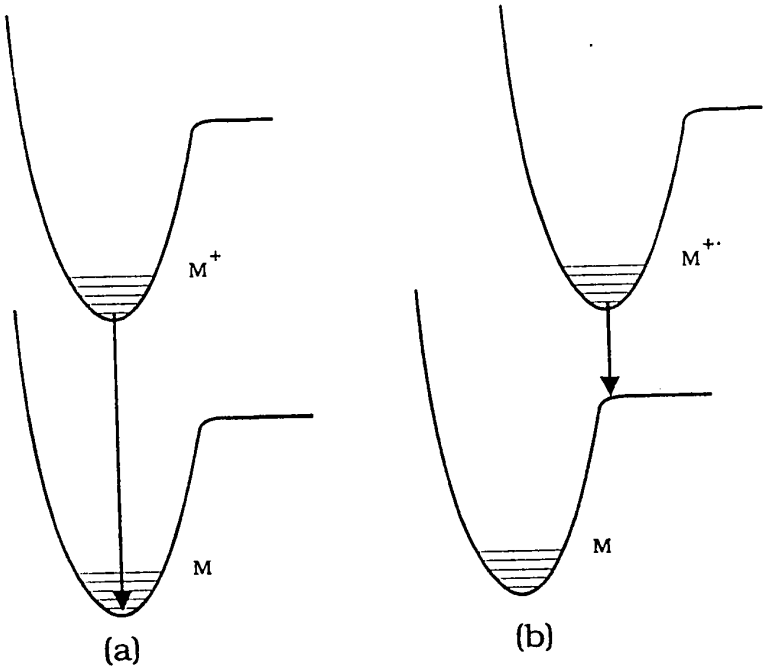

Figure 4.12 Vertical neutralization of an ion M^+ giving rise to the formation of (a) a stable neutral and (b) a dissociative neutral species.

The efficiency of electron transfer and its consequences depend upon the energy balance, Q_N, of reaction (4.16).

$$Q_N = IE(N) - NE_v(M^+) \qquad (4.18)$$

Where IE(N) is the ionization energy of the electron transfer target and $NE_v(M^+)$ is the vertical neutralization energy of the selected ion M^+. There are three situations to consider, (i) resonant electron transfer, (ii) endothermic electron transfer and (iii) exothermic electron transfer.(i)

(i) Resonant electron transfer ($Q_N \sim 0$)

For monoatomic and diatomic species, near resonant electron transfer has been shown to be very efficient. However for polyatomic molecules, where there is a significant geometry change, use of M as the neutralization target will not be resonant since $IE_v \neq NE_v$. Acetone, for which endothermic neutralization is more efficient, is a good example of the latter situation **[43]**.

(ii) Endothermic electron transfer ($Q_N > 0$)

In these situations the energy deficit (extra energy required for electron transfer) is provided by the translational energy of the projectile ions M^+. Thus Hg (IE = 10.4 eV) and Xe (IE = 12.1 eV), commonly used as neutralization agents, have proved to be excellent electron transfer targets for organic cations corresponding to neutral species with IE values as low as 6 eV.

(iii) Exothermic electron transfer ($Q_N < 0$)

If the charge exchange process is exothermic, excited neutral species are generated which might have enough energy for decomposition and/or rearrangement. These conditions may be achieved by the use of alkali metal vapours as the target atoms for the neutralization of M^+. This is due to the low IE of such atoms (e.g. IE(Na) = 5.1 eV, IE(K) = 4.3 eV).

4.3.5.2 Collision Induced Reionization

Similarly to CIDI, this process (Equation 4.15) occurs in the second collision cell. Reionization is usually with O_2 or He. The extent of fragmentation immediately after reionization depends on the internal energy of the ion generated vertically from the neutral.

4.3.5.3 General Remarks on NRMS

For the experiment to be considered a possible success, a reionized species having the correct m/z ratio (recovery signal M^+) must be observed indicating that neutral species M have been generated as stable species on the time scale of the experiment, Typically 1-10 μs.

Often, the NR mass spectra of molecular ions are similar to their EI and CID mass spectra. This indicates that the species do not undergo major rearrangement during the

neutralization and/or reionization processes. When no recovery signal is recorded it indicates either that neutralization has led to the formation of an unstable neutral species or that a dissociative ion was formed upon reionization. Alternatively, if a recovery signal is recorded but the NR mass spectrum differs significantly from the CID mass spectrum, it may indicate that the stable neutral has undergone rapid isomerization into a more stable neutral form.

Whenever possible, CIDI experiments should be performed in parallel with NRMS. This is because for a CIDI experiment the neutral will mostly be in its ground state whereas in NRMS the neutral will often be formed with an excess of energy. Dissimilarities between an ion's NR and CIDI mass spectra must then be reconciled with the properties of the ion and the neutral, and this may well give some insight into the neutralization process itself.

4.4 Isotopic Labeling

Isotopic labeling experiments are used as a tool to probe and clarify fragmentation mechanisms of positive ions examined by mass spectrometry. The most commonly used labels are D, ^{13}C and ^{18}O. The goal of most isotopic labeling experiments is to discover which atoms are involved in a given dissociation. It also gives insight as to the nature of the transition state involved in the fragmentation pathways. A review concerning the use of labeling studies as an aid to investigate the fragmentation of ions has been published

[44] and the utility of such experiments is provided by the studies carried out in Chapters 7 and 8.

REFERENCES - CHAPTER 4

1. K. Levsen, ***Fundamental Aspects of Organic Mass Spectrometry***, vol 4, New-York, (1978).
2. S.G. Lias, J.E. Bartmess, J.F. Liebman, J.L. Holmes, R.D. Levin and W.G. Mallard, ***J. Phys. Chem. Ref. Data***, 17, Suppl.1 (1988).
3. J.B. Pedley, R.D. Naylor and S.P. Kirby, ***Thermochemical Data of Organic Compounds***, 2nd Ed., London, N.Y. Chapman and Hall (1986).
4. S.W Benson, ***Thermochemical Kinetics***, 2nd Ed. Wiley-Interscience, New-York (1976).
5. P.C. Burgers and J.L. Holmes, ***Int. J. Mass Spectrom. Ion Processes***, 58, 15 (1984).
6. P.C. Burgers, J.L. Holmes and J.K. Terlouw, ***J. Chem. Soc. Chem. Comm.*** 642 (1984).
7. J.L. Holmes, ***Org. Mass Spectrom.***, 20, 169 (1985).
8. R.G. Cooks, J.H. Beynon, R.M. Caprioli and G.R. Lester, ***Metastable Ions***, Elsevier Scientific Publishing Co. Amsterdam (1973).
9. K.C. Kim, J.H. Beynon and R.G. Cooks, ***J. Chem. Phys.*** 61, 1305 (1974).
10. (a) K. Maeda, G.P. Semeluk and F.P. Lossing, ***Int. J. Mass Spectrom. Ion Phys.*** 1, 395 (1968). (b) F.P. Lossing and J.C. Traeger, **Idem**, 19, 9 (1976).
11. P.C. Burgers and J.L. Holmes, ***Org. Mass Spectrom.*** 17, 123 (1982).
12. J.L. Holmes, M. Fingas and F.P. Lossing, ***Can J. Chem.*** 59, 80 (1981).
13 F.P. Lossing, ***J. Am. Chem. Soc.*** 99, 7526 (1977).

REFERENCES - CHAPTER 4

14. J.L. Holmes, F.P. Lossing and R.A. McFarlane, ***Int. J. Mass Spectrom. Ion Processes,*** 86, 209 (1988).

15. J.L. Holmes and F.P. Lossing, ***Can. J. Chem.*** 60, 2365 (1982).

16. F.P. Lossing and J.L. Holmes, ***J. Am. Chem. Soc.*** 106, 6917 (1984).

17. J.L. Holmes, P.C. Burgers, J.K. Terlouw, H.Schwarz, B. Ciommer and H. Halim, ***Org. Mass Spectrom.*** 18, 208 (1983).

18. C. Lifshitz, P. Gotchiguian and R. Roller, ***Chem. Phys. Lett.*** 95, 106 (1983).

19. P.C. Burgers, J.L. Holmes, A.A. Mommers, J.E. Szulejko and J.K. Terlouw, ***Org. Mass Spectrom.*** 19, 442 (1984).

20. J.A. Hipple and E.U. Condon, ***Phys. Rev.*** 29, 54 (1945).

21. J.L. Holmes and J.K. Terlouw, ***Org. Mass Spectrom.*** 15, 383 (1980).

22. E.G. Jones, L.E. Baumann, J.H. Beynon and R.G. Cooks, ***Org. Mass Spectrom.*** 7, 185 (1973).

23. J.L. Holmes, A.D. Osborne and G.M. Weese, ***Org. Mass Spectrom.*** 10, 867 (1975).

24. T.W. Shannon and F.W. McLafferty, ***J. Am. Chem. Soc.*** 88, 5021 (1966).

25. H.M. Rosenstock, V.H. Dibeler and F.N. Harllee, ***J. Chem. Phys.*** 40, 591 (1964).

26. K.R. Jennings, ***Int. J. Mass Spectrom. Ion Phys.*** 1, 227 (1968).

27. W.F. Hadden and F.W. McLafferty, ***J. Am. Chem. Soc.*** 90, 4745 (1968).

28. (a) K. Levsen and H. Schwarz, ***Mass Spectrom. Rev.*** 2, 77 (1983). (b) F.W. McLafferty (Ed.), ***Tandem Mass Spectrometry.*** Wiley-Interscience, New-York (1983).

REFERENCES - CHAPTER 4

29. J.L. Holmes, A.A. Mommers, J.E. Szulejko and J.K. Terlouw, ***J. Chem. Soc. Chem. Comm.*** 165, (1984).

30. P.O. Danis, R. Feng and F.W. McLafferty, ***Anal. Chem.*** 58, 355 (1986).

31. F.W. McLafferty, P.F. Bente, III, R. Kornfeld, S-C. Tsai and I. Howe, ***J. Am. Chem. Soc.*** 95, 2120 (1973).

32. R.G. Cooks, J.H. Beynon and T. Ast, ***J. Am. Chem. Soc.*** 94, 1004 (1972).

33. (a) D.L. Kemp, J.H. Beynon and R.G. Cooks, ***Org. Mass Spectrom.*** 11, 857 (1976). (b) J.L. Holmes, J.K. Terlouw, P.C. Burgers and R.T.B. Rye, ***Org. Mass Spectrom.*** 15, 51 (1980). (c) D. Harnish, J.L. Holmes, F.P. Lossing, A.A. Mommers, A. Maccoll and M.N. Mruzek, ***Org. Mass Spectrom.*** 25, 381 (1990).

34. P.C. Burgers, J.L. Holmes, A.A. Mommers, J.E. Szulejko and J.K. Terlouw, ***Org. Mass Spectrom.*** 18, 208 (1983).

35. (a) P.C. Burgers, J.L. Holmes, A.A. Mommers and J.K. Terlouw, ***Chem. Phys. Lett.*** 102, 1 (1983). (b) R. Clair, J.L. Holmes, A.A Mommers and P.C. Burgers, ***Org. Mass Spectrom.*** 20, 207 (1985).

36. (a) P.C. Burgers, J.L. Holmes, C.E.C.A. Hop and J.K. Terlouw, ***Org. Mass Spectrom.*** 21, 549 (1986). (b) C.E.C.A. Hop, M. Dakubu and J.L. Holmes, Org. Mass Spectrom. 23, 609 (1988).

37. P.O. Danis, C. Wesdemiotis and F.W. McLafferty, ***J. Am. Chem. Soc.*** 105, 7454 (1983).

REFERENCES - CHAPTER 4

38. C. Wesdemiotis and F.W. McLafferty, ***Chem. Rev.*** 87, 485 (1987).

39. G.I. Gellene and R.F. Porter, ***Acc. Chem. Res.*** 16, 200 (1983).

40. J.K. Terlouw and H. Schwarz, ***Ang. Chem. Int. Ed. Engl.*** 26, 805 (1987).

41. J.L. Holmes, ***Mass Spectrom. Rev.*** 8, 513 (1989).

42. J.K. Terlouw, W.M. Kieskamp, J.L. Holmes, A.A. Mommers and P.C. Burgers, ***Int. J. Mass Spectrom. Ion Processes,*** 64, 245 (1985).

43. P.O. Danis, R. Feng and F.W. McLafferty, ***Anal. Chem.*** 58, 348 (1986).

44. E. Buncel, C.C. Lee, ***Isotopes in Organic Chemistry,*** Elsevier (1975), Chapter 3 by J.L. Holmes.

CHAPTER 5
THE LOW ENERGY FRAGMENTATIONS OF FIVE ISOMERIC $[H_3,C,N,O_2]^{+\bullet}$ IONS

Org. Mass Spectrom. 25, 167 (1990)

5.1 Overview

The low energy fragmentation characteristics of the $[H_3,C,N,O_2]^{+\bullet}$ isomers $H_3CNO_2^{+\bullet}$, **1**, $H_2C{=}N(O)OH^{+\bullet}$, **2**, $H_3CONO^{+\bullet}$, **3**, $HC(O)NHOH^{+\bullet}$, **4**, and $HC(OH){=}NOH^{+\bullet}$, **5**, were studied in detail by metastable ion mass spectrometry. In agreement with most earlier observations, appearance energy measurements established the potential energy surface of the isomers **1**, **2** and **3**, showing the intricate interrelations between them. It was concluded that **1** isomerizes into **2** prior to fragmentation by loss of $^{\bullet}OH$ and H_2O and into **3** before loss of $^{\bullet}H$ and $CH_3O^{\bullet}$. Moreover the reverse reactions do not take place on the metastable time-frame. The dominant metastable process for isomers **4** and **5** (obtained via HCN loss from glyoxime) was generation of $H_2NOH^{+\bullet}$. For isomer **5** this process was proposed to involve a rate determining isomerization into **4**. It was concluded that isomers **4** and **5** do not intercommunicate with ions **1**, **2** and **3** prior to fragmentation. Neutralization-reionization mass spectrometry established that the enol form of formohydroxamic acid is stable in the gas phase.

5.2 Introduction

The low energy dissociations of molecular ions in the gas phase often only occur from isomeric ions generated via extensive rearrangement processes. This is especially true for (but by no means limited to) those ions which have lifetimes of $\geq 10^{-6}$ s, i.e. the metastable ions which decompose in the drift regions of a mass spectrometer. This is well illustrated by the metastable fragmentation characteristics of the isomeric nitromethane, **1**,

[1-7], aci-nitromethane, **2**, **[5,7]**, and methylnitrite, **3**, **[3-5, 7-15]** radical cations.

$H_3C\text{-}NO_2^{+\bullet}$ **1** $\quad$ $H_2C{=}N(O)OH^{+\bullet}$ **2** $\quad$ $H_3C\text{-}ONO^{+\bullet}$ **3**

Egsgaard et al. **[5]** have studied the metastable and the collision induced dissociations of the isomers **1, 2** and **3** to investigate the concurrent rearrangements of the nitromethane radical cation into its isomers. For isomer **1,** they reported five metastable processes: generation of m/z 60 ($H_2CNO_2^+$), m/z 46 (NO_2^+) (although Lifshitz et al. **[6]** have shown that this ion is generated solely by collision), m/z 44 (H_2CNO^+), m/z 43 ($HCNO^{+\bullet}$) and m/z 30 (NO^+). It was proposed that the signal observed at m/z 44 is due to a **1** → **2** rearrangement en route to dissociation and the m/z 30 signal was ascribed to O-N bond cleavage in $H_3CONO^{+\bullet}$ after a **1** → **3** rearrangement. Isomer **2**, obtained via C_2H_4 loss from nitropropane ions, only displayed metastable loss of $^{\bullet}OH$ and H_2O (generation of m/z 44 and 43), which indicates that a **2** → **1** isomerization does not take place. With regard to isomer **3**, it displayed only one major fragmentation in the metastable time frame, namely the generation of $H_2COH^+ + NO^{\bullet}$ **[8-10,15]**. In the metastable ion mass spectrum presented by Egsgaard et al. **[5]** signals at m/z 30 (NO^+), and 29 (HCO^+), were also present, but these were later ascribed to collision induced fragmentations **[12]**.

In addition to the above three species, more $[H_3,C,N,O_2]^{+\bullet}$ isomers are known. Formohydroxamic acid was first synthesized by Nef **[16]** and Schroeter **[17]**. Two structures were proposed: the keto and enol tautomers. Based on its infrared spectrum, the keto structure has been assigned to formohydroxamic acid **[18]**. Although formohydroxamic acid has been the source of much biochemical interest, its molecular ion, **4**, has not been investigated mass spectrometrically. The molecular ion of the enol tautomer, **5**, and its neutral counterpart have not yet been identified. Recently, carbamic acid radical cations, **6**, were identified as stable species in the gas phase **[19]**.

$[HC(O)\text{-}NHOH]^{+\bullet}$ **4** $\quad$ $[HC(OH){=}NOH]^{+\bullet}$ **5** $\quad$ $[H_2N\text{-}C(O)OH]^{+\bullet}$ **6**

In this study the metastable fragmentation characteristics of the isomers **1**, **2** and **3** have been reinvestigated in order to establish an unambiguous potential energy surface showing their possible isomerizations (see Figure 5.1). Isomers **4** and **5** have been identified as stable species in the gas phase and their possible interconversion will be discussed. Lastly, using the relatively new neutralization-reionization technique **[20-22]** the first experimental evidence for the stability of the enol form of formohydroxamic acid will be presented.

5.3 Experimental

All experiments were performed using the VG Analytical ZAB-2F double focussing mass spectrometer of reversed geometry modified for neutralization-reionization (NR) mass spectrometry as described in Chapter 2. Metastable ion (MI), collision induced dissociation (CID) and neutralization-reionization (NR) mass spectra were recorded as previously described (see Chapter 4). Helium was used as target gas in the CID experiments. In the NR experiments the mass-selected ions were neutralized by charge exchange with Xe (cell 1). After separating the neutrals from the ions by means of a charged electrode, the former were reionized by collision with O_2.

In the above experiments all slits were fully open to obtain maximum signal strength and to minimise energy resolving effects. The kinetic energy releases ($T_{0.5}$) for the various metastable processes were obtained from the peak widths at half-height measured under high energy resolution conditions **[23]**. The appearance energies (AE) of metastable processes were measured with the Kratos AEI MS 902S mass spectrometer (see Chapter 2) using a comparative method and with iodobenzene and diethylether as standards **[24]**. Daughter ion appearance energies were obtained with an apparatus comprising an electrostatic electron monochromator with a quadrupole mass analyser and a minicomputer data system **[25]**.

Methylnitrite was obtained by mixing CH_3OH, $NaNO_2$ and dilute H_2SO_4. The

gaseous methylnitrite was introduced into the mass spectrometer without further purification. Formohydroxamic acid was synthesized as described by Fishbein et al. **[26]**. All other compounds were commercially available.

5.4 Results and Discussion

5.4.1 Metastable Ion and Collision Induced Dissociation Experiments

The metastable ion mass spectra of $H_3CNO_2^{+\bullet}$, the $H_2C{=}\dot{N}(O)OH^{+\bullet}$ daughter ions from ionized nitropropane **[5, 27]**, $H_3CONO^{+\bullet}$, $HC(O)NHOH^{+\bullet}$ and the $[H_3,C,N,O_2]^{+\bullet}$ daughter ions from glyoxime are presented in Table 5.1.

Although the m/z 61 signal in the mass spectrum of glyoxime was only 0.1 % of m/z 44 (the most intense signal), it was a single peak under high resolution conditions and an exact mass measurement showed that it indeed corresponded with $[H_3,C,N,O_2]^{+\bullet}$; its generation and observation were reproducible. The production of $[H_3,C,N,O_2]^{+\bullet}$ from glyoxime molecular ions can be considered an OH shift accompanied by loss of [H,C,N], most likely HCN (Equation (5.1)).

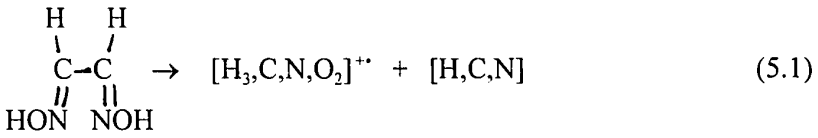

(5.1)

The MI mass spectra of **1**, **2** and **3** were in good agreement with those reported in ref. **[5]**, except for the complete absence of m/z 46 and m/z 15 in the MI mass spectrum of nitromethane ions (as has been reported by Lifshitz et al. **[6]**) and m/z 30 and m/z 29 in that of methylnitrite ions. These differences can be explained by lower background pressures in the present experiments resulting in minimal contributions from collision induced dissociation processes.

CID mass spectra were also recorded; those of **1**, **2** and **3** were close to those

published earlier **[5,7]** and those of $HC(O)NHOH^{+\bullet}$ and the $[H_3,C,N,O_2]^{+\bullet}$ ions from ionized glyoxime are shown in Figure 5.2.

*Table 5.1. Metastable ion mass spectra of the isomeric ions $H_3CNO_2^{+\bullet}$, **1**, $H_2C{=}N(O)OH^{+\bullet}$, **2**[a], $H_3CONO^{+\bullet}$, **3**, $HC(O)NHOH^{+\bullet}$, **4** and the $[H_3,C,N,O_2]^{+\bullet}$ from ionized glyoxime, **5**.*

Isomers	m/z					
	30	31	33	43	44	60
1	21	1		2	44	32
2				13	86	1
3		87				13
4			100			
5			79	2	19	

(a) Obtained via a 1,5-hydrogen shift in the molecular ion of 1-nitropropane as shown in reference 27.

5.4.2 Potential Energy Surface of $H_3CNO_2^{+\bullet}$, $H_2C{=}N(O)OH^{+\bullet}$ and $H_3CONO^{+\bullet}$

The appearance energies and the kinetic energy releases of the metastable decompositions of the isomers **1**, **2** and **3** are reported in Table 5.2. The potential energy surface of the three isomers, derived from the above data, is shown in Figure 5.1 and will be discussed in detail below.

Table 5.2. Appearance energies and kinetic energy releases, $T_{0.5}$, of the metastable processes of the nitromethane, aci-nitromethane and methylnitrite radical cations[a].

Metastable Process	Equation No.	Appearance Energy (eV)	$T_{0.5}$ value (meV)
$H_3CNO_2^{+\bullet} \rightarrow NO^+ + H_3CO^\bullet$	(5.2)	12.0 ± 0.1[b] (11.75 ± 0.05)[c]	47 (58[c])
$H_3CNO_2^{+\bullet} \rightarrow H_2CNO^+ + {}^\bullet OH$	(5.3)	12.0 ± 0.1[b] (11.75 ± 0.05)[c]	25 (30,[c] 24[d])
$H_3CNO_2^{+\bullet} \rightarrow HCNO^{+\bullet} + H_2O$	(5.4)	~12.4[b]	34
$H_3CNO_2^{+\bullet} \rightarrow H_2CONO^+ + H^\bullet$	(5.5)	12.1 ± 0.1[b] (11.8 ± 0.1)[c]	324 (320[c])
$H_2CNO_2H^{+\bullet} \rightarrow H_2CNO^+ + {}^\bullet OH$	(5.6)	12.9 ± 0.1[b]	14 (15[d])
$H_2CNO_2H^{+\bullet} \rightarrow HCNO^{+\bullet} + H_2O$	(5.7)	(Too weak)	33
$H_2CNO_2H^{+\bullet} \rightarrow H_2CONO^+ + H^\bullet$	(5.8)	(Too weak)	37 (320[c])
$H_3CONO^{+\bullet} \rightarrow H_2COH^+ + NO^\bullet$	(5.9)	11.0 ± 0.2[d] (10.69 ± 0.03)[f]	79 (93,[e] 54[f])
$H_3CONO^{+\bullet} + H_2CONO^+ + H^\bullet$	(5.10)	11.5 ± 0.1[b] (11.20 ± 0.05)[b]	39 (38[c])

(a) Appearance energies of source generated fragment ions and $T_{0.5}$ values obtained from previous studies are given in parentheses.

(b) See Experimental

(c) From Ref. 6.

(d) From Ref. 5.

(e) From Ref. 9.

(f) From Ref. 8.

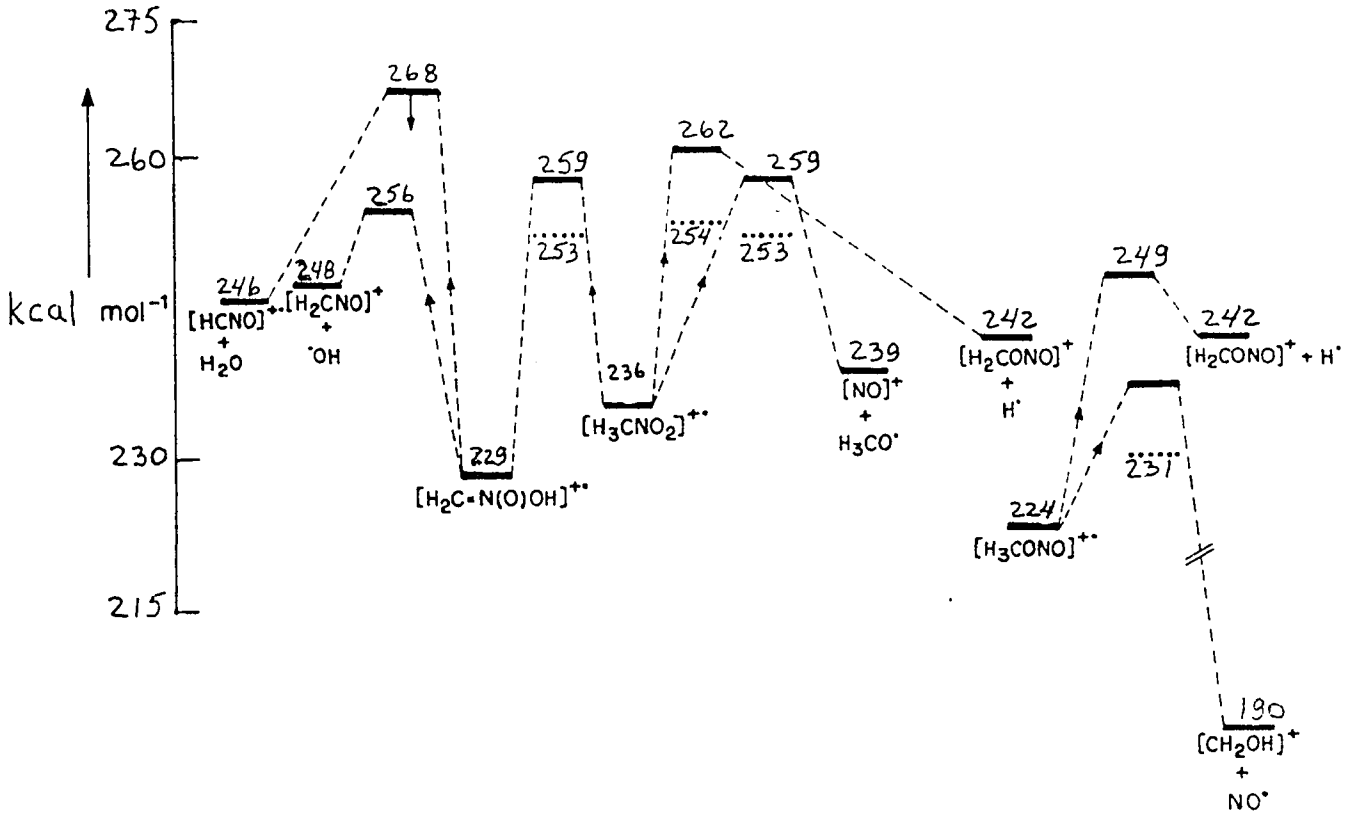

Figure 5.1 *Potential energy surface of nitromethane, aci-nitromethane and methyl nitrite radical cations and their metastable fragmentation routes. All ΔH_f values are from References 28, except $\Delta H_f(HCNO^{+\cdot})$ and $\Delta H_f(H_2CNO^+)$, which are from References 34 and 30 respectively, and $\Delta H_f(H_2C{=}NO_2H^{+\cdot})$ and $\Delta H_f(H_2CONO^+)$ which have been determined in this work. The energies for the transition states are calculated from the data in Table 5.2; underlined in bold are the transition states for metastable reactions and dots indicate those determined from daughter ion appearance energies.*

First we shall consider the H· loss process. In agreement with Lifshitz et al. **[6]**, we find that the CID mass spectra of the m/z 60 ions from these three precursors are identical within experimental error and assign them the structure H_2CONO^+. This structure has also been assigned to this ion on the basis of ab initio molecular orbital theory calculations **[28]**, which lead to an energy of 232 kcal mol^{-1} for the sum of $\Delta H_f(H_2CONO^+) + \Delta H_f(H^\cdot)$. This energy is below that measured from H_3CONO using energy selected electrons, 242 kcal mol^{-1} (see Figure 5.1), but the latter should be regarded as an upper limit in view of the kinetic energy release.

Generation of H_2CNO^+ from metastable nitromethane radical cations and its aci form must involve complex rearrangements; these processes will be discussed below. Note, however, that in contrast with an earlier report **[6]**, the kinetic energy releases are markedly different, 324 and 37 meV respectively indicating that different processes are involved.

Generation of NO^+, process (5.2), for ionized nitromethane takes place via a **1** → **3** rearrangement **[5]**. A priori this is unexpected because m/z 31, H_2COH^+, is the dominant process for metastable methylnitrite ions and generation of m/z 30 does not take place on the metastable time-scale. To explain this behaviour we propose that isomerization of **1** into **3** yields highly excited ions (~36 kcal mol^{-1} of internal energy, see Figure. 5.1), which will favour a fragmentation reaction with a high frequency factor (see section 4.2.3), i.e. O-N bond cleavage, instead of a complex rearrangement. This is in good agreement with the breakdown graph, derived from the photoelectron spectrum of methylnitrite, which shows that at high energy the generation of m/z 30 is favoured over m/z 31 **[3,8]**.

The occurrence of the **1** → **3** rearrangement also explains the metastable $H^\cdot$ loss, because $H_3CNO^{+\cdot}$ loses $H^\cdot$ metastably. In addition, the measured transition state energy for $H^\cdot$ loss is, within experimental error, equal to that for the **1** → **3** rearrangement (see Figure 5.1). This barrier gives rise to the large kinetic energy release for $H^\cdot$ loss.

To explain the generation of H_2CNO^+ (Equation (5.3)) by nitromethane molecular ions, a **1** → **2** rearrangement was proposed **[5]**. The AE of metastably generated H_2CNO^+ was measured to be 12.0 eV, resulting in a transition state energy of the rate determining step of 259 kcal mol^{-1} ($\Delta H_f(H_3CNO_2)$ = -18 kcal mol^{-1} **[29]**).

No details were given by Egsgaard et al. **[5]** for the third and fourth metastable processes, generation of $HCNO^{+\cdot}$ (Equation (5.4)), and H_2CNO^+ (Equation (5.5)). The AE of metastably generated m/z 43 from nitromethane, 12.4 eV, yields a transition state energy of 268 kcal mol^{-1}. However, m/z 43 is only a minor peak in the MI mass spectrum of nitromethane ions (see Table 5.1) and so a competitive shift can be expected, making

the measured AE too high. Moreover, C-N bond cleavage, which has the same apparent (calculated) energy requirement ($\Delta H_f(NO_2^+) + \Delta H_f(^{\bullet}CH_3)$ = 268 kcal mol^{-1} **[29]**) is not an observed metastable process for nitromethane ions. Note that the above AE's are those of metastable processes, i.e. ions fragmenting after ~10^{-6} s. The AE's of some of the daughter ions have also been measured by photoionization **[6]** at extended lifetimes and so those AE values are consistently lower than the present results (see Table 5.2).

The aci form of nitromethane was obtained via a 1,5-hydrogen shift in the molecular ion of 1-nitropropane **[27]**. The AE of the $H_2C{=}N(O)OH^{+\bullet}$ daughter ion, measured using energy selected electrons, 11.75 eV, gave ΔH_f(**2**) = 229 kcal mol^{-1} ($\Delta H_f(C_3H_7NO_2)$ = -30 kcal mol^{-1} and $\Delta H_f(C_2H_4)$ = 12 kcal mol^{-1} **[29]**), assuming that there is no excess energy involved in the reaction. Thus, **2** is more stable than **1** (ΔH_f(**1**) = 236 kcal mol^{-1} **[29]**) by 7 kcal mol^{-1}, which is considerably less than the difference obtained by Egsgaard et al. **[5]**, 19 kcal mol^{-1}, also based on an AE measurement.

With regard to its metastable processes, aci-nitromethane ions yield H_2CNO^+ + $^{\bullet}OH$ (Equation (5.6)), $HCNO^{+\bullet}$ + H_2O (Equation (5.7)) and H_2CONO^+ + $H^{\bullet}$ (Equation (5.8)). Note that the metastable peaks for these three reactions arise from an ion of low abundance in the normal mass spectrum of nitropropane (only ~1.5% of the base peak). Only the metastable peak for reaction (5.6) was sufficiently intense for a reasonably accurate AE determination. The transition state for the reaction $H_2C{=}N(O)OH^{+\bullet} \rightarrow HCNO^{+\bullet} + H_2O$ (Equation (5.7)) could only be roughly estimated as lower than ~268 kcal mol^{-1} and certainly no less than that for reaction (5.6). The $H^{\bullet}$ loss metastable peak was the weakest. The AE of metastable reaction (5.6), 12.9 eV, gave a transition state energy of 256 kcal mol^{-1} for $^{\bullet}OH$ loss from **2**. The latter is lower than the transition state energy for $^{\bullet}OH$ loss from **1** via **2** (Equation (5.3)), 259 kcal mol^{-1} (see above). Thus, the rate determining step for dissociation of $H_3CNO_2^{+\bullet}$ into H_2CNO^+ + $^{\bullet}OH$ is the isomerization into the aci form, $H_2C{=}N(O)OH^{+\bullet}$; this is supported by the $T_{0.5}$ value for reaction (5.3) being larger than the $T_{0.5}$ value for reaction (5.6), 25 versus 14 meV (see Table 5.2).

It now remains to explain the metastable generation of $HCNO^{+\bullet}$ from isomers **1** and **2**. Since the $T_{0.5}$ values of both metastable peaks are the same (see Table 5.2), we propose that for nitromethane ions a **1** → **2** isomerization takes place prior to dissociation of $H_2C{=}N(O)OH^{+\bullet}$ into $HCNO^{+\bullet} + H_2O$, with the latter step being rate determining. Note that the inverse process, **2** → **1**, does <u>not</u> take place because m/z 30 is not produced metastably by the aci form. Since the transition state energy for the **2** → **1** → $NO^+ + H_3CO^\bullet$ process is only 259 kcal mol^{-1} (see Fig. 5.1), the barrier for H_2O loss from $H_2C{=}N(O)OH^{+\bullet}$, a metastable process, is most likely considerably lower than the value given in Figure 5.1, 268 kcal mol^{-1}. Additionally, H_2O loss could be kinetically favoured over the **2** → **1** → $NO^+ + H_3CO^\bullet$ process because it involves a less complex mechanism, i.e. one instead of two rearrangement reactions.

The highest energy fragmentation for the metastable fragmentation $H_2CN(O)OH^{+\bullet}$ ions is $H^\bullet$ loss. The reaction sequence **2** → **1** → **3** can be ruled out because the aci form does not isomerize to nitromethane (see above). Although the kinetic energy releases for $H^\bullet$ loss from $H_2CN(O)OH^{+\bullet}$ and $H_3CONO^{+\bullet}$ are similar, the MI mass spectra (Table 5.1) do not provide support for a direct **2** → **3** isomerization.

Finally, for the methylnitrite radical cation, thermodynamically the most stable of the three isomers (ΔH_f(**3**) = 223 kcal mol^{-1} **[29]**), the absence of m/z 44 and 43 in its MI and CID mass spectra indicates that it does not communicate with isomers **1** and **2**. The potential energy surface, Figure 5.1, shows that dissociations into $H_2COH^+ + NO^\bullet$ and $NO^+ + H_3CO^\bullet$ are thermochemically much more favourable than the **3** → **1** isomerization. The metastable generation of H_2COH^+ has been the subject of numerous investigations **[8-15]** and will not be discussed further.

5.4.3 Characterization of $HC(O)NHOH^{+\bullet}$ and its Tautomer $HC(OH){=}NOH^{+\bullet}$

The MI mass spectra of $HC(O)NHOH^{+\bullet}$ and the $[H_3,C,N,O_2]^{+\bullet}$ daughter ions from glyoxime are both dominated by m/z 33, but the latter spectrum also contains peaks at m/z

44 and 43 (see Table 5.1). In addition the $T_{0.5}$ values of the m/z 33 signals are different, 21 and 113 meV respectively (the $T_{0.5}$ value for m/z 44 in the MI mass spectrum of the m/z 61 daughter ions from glyoxime is 49 meV). This shows that we are dealing with two different $[H_3,C,N,O_2]^{+\bullet}$ isomers, and this is confirmed by their having different CID mass spectra, see Figure 5.2. The ions m/z 32 and 29 are relatively more intense in the CID mass spectrum of $HC(O)NHOH^{+\bullet}$. In contrast, the CID mass spectrum of the m/z 61 ions from ionized glyoxime has relatively more intense signals at m/z 44, 43 and 30.

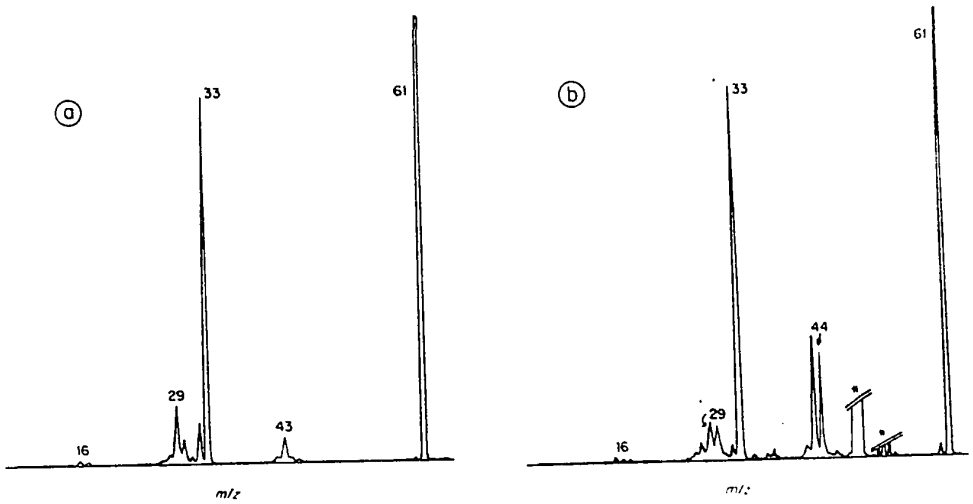

Figure 5.2 CID mass spectra of (a) $HC(O)NHOH^{+\bullet}$ and (b) the $[H_3,C,N,O_2]^{+\bullet}$ daughter ions of ionized glyoxime.

The CID mass spectrum of the $[H_3,N,O]^{+\bullet}$ ions generated metastably in the first field-free region from ionized formohydroxamic acid is identical with that of the source generated $[H_3,N,O]^{+\bullet}$ daughter ions and that of ionized hydroxylamine (ionized hydroxylamine was obtained via thermolysis of hydroxylamine hydrochloride). The high mass regions of these spectra are dominated by m/z 32, 30 and 31 and the low mass regions by m/z 16 and 17, in decreasing order of intensity. Thus the $[H_3,N,O]^{+\bullet}$ ions generated metastably from ionized formohydroxamic acid have the $H_2NOH^{+\bullet}$ structure. It is worth noting that the NR mass spectrum of $H_2NOH^{+\bullet}$ has m/z 33 as base peak and closely resembles the CID mass spectrum, which is in keeping with the stability of H_2NOH **[30]**.

Generation of $H_2NOH^{+\bullet}$ via a 1,2-hydrogen shift in $HC(O)NHOH^{+\bullet}$ can be ruled out, because the ion thus obtained, $OCNH_2OH^{+\bullet}$, would be expected to dissociate into H_2NCO^+ + $^\bullet OH$, the bond cleavage of lower energy requirement ($\Sigma\Delta H_f(H_2NCO^+ + {}^\bullet OH)$ = 170 kcal mol^{-1} **[29, 31]** and $\Sigma H_f(H_2NOH^{+\bullet} + CO)$ = 185 kcal mol^{-1} **[29]**). By analogy with the mechanism proposed for the generation of $CH_3OH_2^+$ from ionized ethylene glycol **[32]**, odd electron, hydrogen bridged species are suggested intermediates:

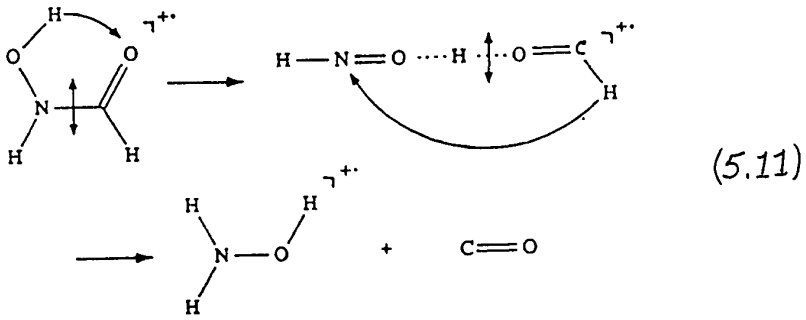

(5.11)

Two mechanisms can be proposed for the generation of m/z 61 from glyoxime: an OH shift to the carbon atom yielding $HC(OH)=NOH^{+\bullet}$, **5**, (Equation (5.12a)) or an OH shift to the nitrogen atom yielding $HCN(OH)_2^{+\bullet}$, **7** (Equation (5.12b)). Ab initio molecular orbital theory calculations **[10]** predicted the heat of formation of **5** to be 28 kcal mol^{-1} lower than that of **1**, i.e. $\Delta H_f(HC(OH)=NOH^{+\bullet})$ = 208 kcal mol^{-1}. No experimental or theoretical results were available for ion **7**.

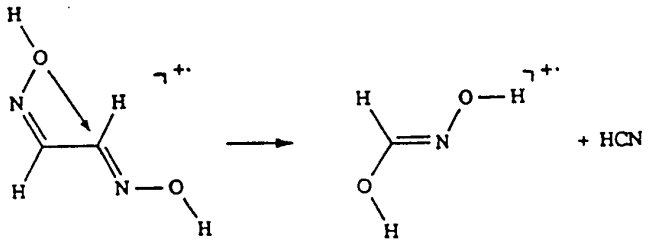

(5.12a)

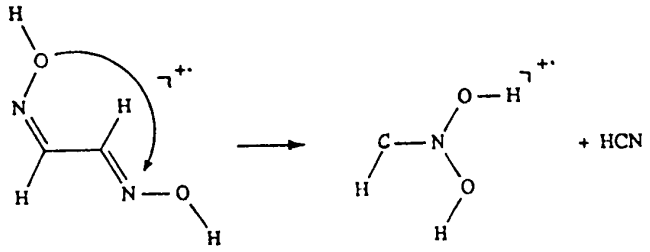

(5.12b)

Considering structures **5** and **7**, the metastably generated m/z 44 and 43 ions are most likely $HCNOH^+$ and $HCNO^{+\bullet}$ and the calculated difference between the sum of the heats of formation of the fragmentation products ($\Delta H_f(HCNOH^+) + \Delta H_f(^{\bullet}OH)$ = 239 kcal mol^{-1} **[29, 31]** and $\Delta H_f(HCNO^{+\bullet}) + \Delta H_f(H_2O)$ = 246 kcal mol^{-1} **[29, 33]**) is in keeping with the ratio of the two signals in the MI mass spectrum, ~8 : 1. Generation of $[H_3,N,O]^{+\bullet}$ is the most intense metastable process and consequently the energy of the transition state for this process is expected to be somewhat lower than 239 kcal mol^{-1}. The $T_{0.5}$ value for m/z 33, 113 meV, indicates that this is not a threshold process, a considerable barrier for the reverse reaction is expected. Note that generation of $[H_3,N,O]^{+\bullet}$ involves a complex rearrangement. Assuming that the $[H_3,C,N,O_2]^{+\bullet}$ daughter ions from ionized glyoxime have structure **5**, two hydrogen atoms have to be transferred. If the m/z 61 ions have structure **7**, an OH transfer has to take place as well as the transfer of two hydrogen atoms. At this point, the former argument seems more feasible than the latter.

To aid structure assignment of the m/z 61 daughter ions of ionized glyoxime, the NR mass spectrum of these ions was recorded, see Figure 5.3b. The spectrum is clearly different from that of ionized formohydroxamic acid, see Figure 5.3a. Since the contributions from metastable fragmentation of ions are reduced in NR mass spectra compared to those in CID mass spectra **[34]**, it can be safely stated that the NR and CID mass spectra of the m/z 61 daughter ions of ionized glyoxime are in good agreement. Note that the signal at m/z 28 is due to ionization of metastably generated CO. An important feature of the NR mass spectrum is the presence of a recovery signal at m/z 61, indicating that the neutral counterpart of the mass-selected m/z 61 ions is a stable species in the gas phase. Unfortunately, the NR mass spectrum of the $[H_3,C,N,O_2]^{+\bullet}$ species, is not of great help for an unambiguous structure assignment, because in essence, both structures **5** and **7** could explain the NR mass spectrum. However, as stated above, a **5** $\rightarrow$ **4** rearrangement prior to the production of $H_2NOH^{+\bullet}$ is more straightforward than a **7** $\rightarrow$ **4** isomerization .

Thus, we propose that the $[H_3,C,N,O_2]^{+\bullet}$ ions from ionized glyoxime have structure **5**, the enol form of formohydroxamic acid. The m/z 33 peak in the MI mass spectrum is

then explained by a rate determining isomerization of the enol form into the keto form (a 1,3-hydrogen shift) followed by the mechanism depicted in equation (5.11). The rate determining character of the **5** → **4** isomerization explains the $T_{0.5}$ value of m/z 33 for isomer **5** being larger than that for isomer **4**, 113 meV versus 21 meV.

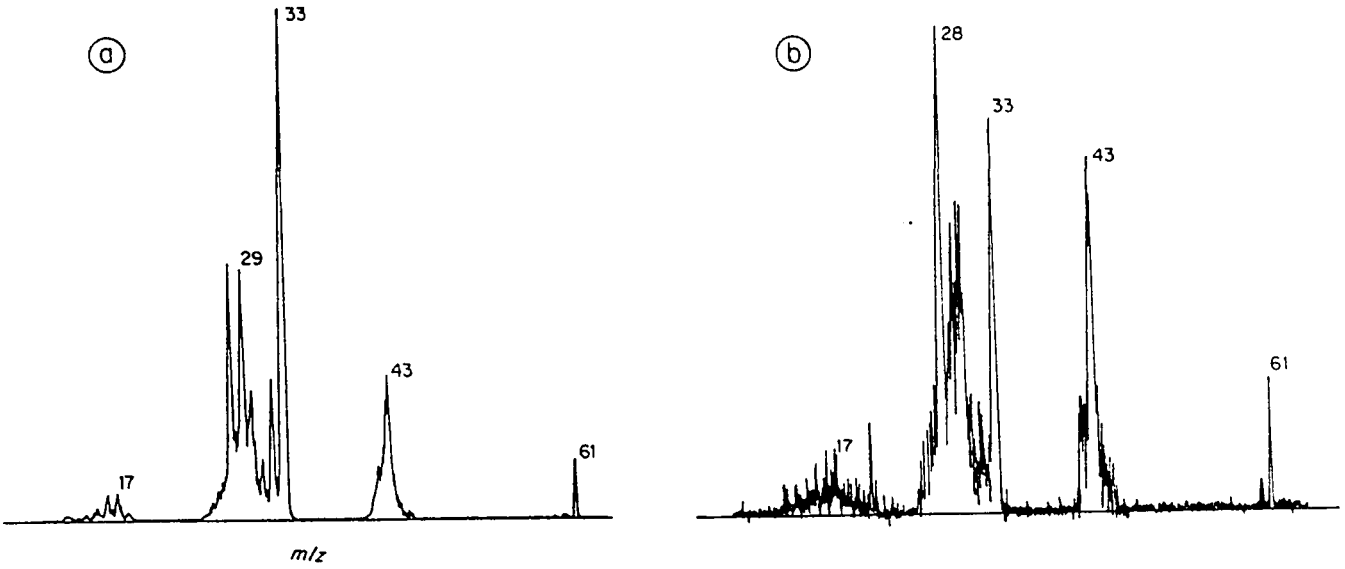

Figure 5.3 NR mass spectra of (a) $HC(O)NHOH^{+\bullet}$ and (b) $[H_3,C,N,O_2]^{+\bullet}$ daughter ions of ionized glyoxime.

5.5 Conclusions

The low energy fragmentations of nitromethane, **1**, aci-nitromethane, **2**, methylnitrite, **3**, formohydroxamic acid, **4** and the enol form of formohydroxamic acid, **5**, ions were studied in detail by metastable ion mass spectrometry. For ionized nitromethane **1**, it was concluded that the generation of NO^+ (m/z 30), takes place via a **1** → **3** isomerization and a **1** → **2** rearrangement was introduced to explain the production of $H_2CNO^{+\bullet}$ and $HCNO^{+\bullet}$ (m/z 44 and 43). It is noteworthy that the reverse reactions do not take place on the metastable time-scale. By means of appearance energy measurement the potential energy surface of these three isomers was constructed, showing their interrelationships.

Based on metastable ion and neutralization-reionization mass spectra, structure **5**, the enol form of formohydroxamic acid, was assigned to the $[H_3,C,N,O_2]^{+\bullet}$ daughter ions from ionized glyoxime. The metastable ion mass spectra of isomers **4** and **5** were dominated by m/z 33, $H_2NOH^{+\bullet}$. Generation of $H_2NOH^{+\bullet}$ by ionized formohydroxamic acid could not be explained by a conventional 1,2-hydrogen shift. Therefore, $HNO{\bullet\bullet\bullet}H{\bullet\bullet\bullet}OCH^{+\bullet}$, a hydrogen bridged ion, was proposed as intermediate. A 1,5-hydrogen shift in the latter ion yields $H_2NOH^{+\bullet}$. For isomer **5** we proposed that metastable generation of $H_2NOH^{+\bullet}$ takes place via a **5** $\rightarrow$ **4** isomerization and that the latter process is rate determining, which explains the $T_{0.5}$ value of m/z 33 being larger for this isomer.

The relatively new neutralization-reionization technique was used to establish the stability of the enol form of formohydroxamic acid in the gas phase.

REFERENCES - CHAPTER 5

1. S. Meyerson and E.K. Ellis, ***Org. Mass Spectrom.*** 9, 485 (1974).
2. J.P. Gilman, T. Hsieh and G.G. Meisels, ***J. Chem. Phys.*** 78, 1174 (1983).
3. I.K. Ogden, N. Shaw, C.J. Danby and I. Powis, ***Int. J. Mass Spectrom. Ion Processes*** 54, 41 (1983).
4. M.L. Mckee, ***J. Phys. Chem.*** 90, 2335 (1986).
5. H. Egsgaard, L. Carlsen and S. Elbel, ***Ber. Bunsenges. Phys. Chem.*** 90, 369 (1986)
6. C. Lifshitz, M. Rejwan, I. Levin and T. Peres, ***Int. J. Mass Spectrom. Ion Processes*** 84, 271 (1988).
7. H. Egsgaard, L. Carlsen, H. Florencio, T. Drewello and H. Schwarz, ***Ber. Bunsenges. Phys. Chem.*** 93, 76 (1989).
8. G.G. Meisels, T. Hsieh and J. Gilman, ***J. Chem. Phys.*** 73, 4126 (1980).
9. P.C. Burgers and J.L. Holmes, ***Org. Mass Spectrom.*** 19, 452 (1984).
10. T. Baer and J.R. Hass, ***J. Phys. Chem.*** 90, 451 (1986).
11. E.E. Ferguson, ***Chem. Phys. Letters***, 138, 450 (1987).
12. H. Egsgaard and L. Carlsen, ***Chem. Phys. Letters***, 147, 30 (1988).
13. M.P. Irion, A. Selinger, A.W. Castleman Jr., E.E. Ferguson and K.G. Weil, ***Chem. Phys. Letters***, 147, 33 (1988).
14. B. Leyh-Nihant and J.C. Lorquet, ***J. Chem. Phys.*** 88, 5606 (1988).
15. T. Baer, personal communication.
16. J.U. Nef, ***Justus Liebigs Ann. Chem.*** 298, 202 (1897).
17. (a) G. Schroeter, ***Chem. Ber.*** 31, 2190 (1898). (b) G. Schroeter, ***Chem. Ber.*** 33, 1975 (1900).
18. W.J. Orville-Thomas and A.E. Parsons, ***J. Mol. Spectrosc.*** 2, 203 (1958).
19. K.J. van den Berg, C.B. Lebrilla, J.K. Terlouw and H. Schwarz, ***Chimia***, 41, 122 (1987).
20. C. Wesdemiotis and F.W. McLafferty, ***Chem. Rev.*** 87, 485 (1987).
21. J.K. Terlouw and H. Schwarz, ***Angew. Chem. Int. Ed. Engl.*** 26, 805 (1987).

REFERENCES - CHAPTER 5

22. J.L. Holmes, ***Mass Spectrom. Rev.*** 8, 513 (1989).

23. J.L. Holmes and J.K. Terlouw, ***Org. Mass Spectrom.*** 15, 383 (1980).

24. P.C. Burgers and J.L. Holmes, ***Org. Mass Spectrom.*** 17, 123 (1982).

25. F.P. Lossing and J.C. Traeger, ***Int. J. Mass Spectrom. Ion Phys.*** 19, 9 (1976).

26. W.N. Fishbein, J. Daly and C.L. Streeter, ***Anal. Biochem.*** 28, 13 (1969).

27. S.K. Hindawi, R.H. Fokkens, F.A. Pinkse and N.M.M. Nibbering, ***Org. Mass Spectrom.*** 21, 243 (1986).

28. T. Baer, Personal Communication.

29. S.G. Lias, J.E. Bartmess, J.F. Liebman, J.L. Holmes, R.D. Levin and W.G. Mallard, ***J. Phys. Chem. Ref. Data***, 17, Suppl. 1 (1988).

30. J.A. Pople, K. Raghavachari, M.J. Frisch, J.S. Binkley and P. v. R. Schleyer, ***J. Am. Chem. Soc.*** 105, 6389 (1983).

31. C.E.C.A. Hop, J.L. Holmes, P.J.A. Ruttink, G. Schaftenaar and J.K. Terlouw, ***Chem. Phys. Letters***, 156, 251 (1989).

32. P.C. Burgers, J.L. Holmes, C.E.C.A. Hop, R. Postma, P.J.A. Ruttink and J.K. Terlouw, ***J. Am. Chem. Soc.*** 109, 7315 (1987).

33. C.E.C.A. Hop, K.J. van den Berg, J.L. Holmes and J.K. Terlouw, ***J. Am. Chem. Soc.*** 111, 72 (1989).

34. C.E.C.A. Hop, J.L. Holmes, K.J. van den Berg and J.K. Terlouw, ***Rapid Commun. Mass Spectrom.*** 1, 52 (1987).

CHAPTER 6

THE NEUTRAL COUNTERPARTS OF THE $C_2H_7O^+$ ISOMERS

Org. Mass Spectrom. 25, 481 (1990)

Org. Mass Spectrom. Submitted

6.1 Overview

The neutral counterparts of the $C_2H_7O^+$ isomers, $CH_3O^+(H)CH_3$, $CH_3CH_2OH_2^+$ and C_2H_4•••H-OH_2^+ have been studied by means of neutralization-reionization (NR) mass spectrometry. Protonated dimethyl ether as well as its O-(D) analogue were produced by protonation (deuteronation) of dimethyl ether and also generated as daughter ions from (labeled) $CH_3OCH_2CH(OH)CH_3^{+\bullet}$ by loss of $CH_3CO^{\bullet}$. It was observed that the internal energy of protonated (deuteronated) dimethyl ether ions is directly related to the stability of the neutrals generated by electron transfer, and on their dissociations.

With regard to $CH_3CH_2OH_2^+$ (a), it was produced as a daughter ion from $CH_3CH(OH)CH(OH)CH_3^{+\bullet}$ by loss of $CH_3CO^{\bullet}$. The last isomer studied, C_2H_4•••H-$OH_2^{\bullet}$ (b), was obtained by reacting $C_2H_5^{\bullet}$ ions (from $C_2H_5Br^{+\bullet}$) with water in the ion source. The reversibility of the isomerization of (a) into (b) prior to the metastable generation of $H_3O^{\bullet}$ and C_2H_4 will be discussed. Finally, it will be shown that isomer (a) can be obtained as a neutral species in the gas phase whereas neutral isomer (b) could not be produced.

6.2 Introduction

In the mid-1980's Neutralization-Reionization mass spectrometry was introduced as a new and successful technique for the generation and characterization of novel neutral molecules and free radicals **[1]**. Use of this method together with other techniques such as collision induced dissociation (CID) mass spectrometry has proved to be a valuable tool in structural characterization of positive and negative ions and in the determination of fragmentation mechanisms **[2]**. This aspect of the field was very well reviewed by F.W McLafferty at the last International Mass Spectrometry Conference in Amsterdam **[3]**.

In this study, a beam of fast neutrals is produced via charge exchange neutralization of a beam of positively charged, mass selected ions, $M^{+\bullet}$, (having 8 keV translational energy) with a target gas, N (Equation (6.1)), in a collision cell located in the second field free region.

$$M^{+\bullet} + N \rightarrow M + N^{+\bullet} \qquad (6.1)$$

Surviving ions exiting the first collision cell are electrostatically repelled from the ion-beam path, and by ionizing the neutral downstream in a second collision cell containing a target gas, R (Equation (6.2)), and scanning the electrostatic analyser, a neutralization-reionization (NR) mass spectrum of the mass selected ions is obtained.

$$M + R \rightarrow M^{+\bullet} + N + e \qquad (6.2)$$

NR mass spectrometry has proved to be particularly useful in the preparation and characterization of unusual neutral species such as hypervalent radicals. However, the investigation of the latter has provided ample controversy. For example, stable high Rydberg methonium radicals have only been produced by neutralization of CH_5^+ and CD_5^+ with zinc vapor **[4]**, a result which seems unique to the element. $H_3^\bullet$ has been studied in remarkable detail **[5]** and $ND_4^\bullet$ (not $NH_4^\bullet$) is a well authenticated radical **[6]**. Stable neutral $H_3O^\bullet$, $D_3O^\bullet$ and isotopically ladeled $CH_3OH_2^\bullet$ have proved elusive to some and detectable by others; for a full discussion see reference 1(d) and the original work. More recently, we have shown **[7]** that stable $CH_3O(H)CH_3^\bullet$ can be obtained by neutralization of vibrationally highly excited protonated dimethyl ether. Also Wesdemiotis et al. **[8]** have reported the observation of stable $CH_3CH_2OH_2^\bullet$ from excited protonated ethanol.

In the present Chapter the generation of stable hypervalent $CH_3O(H)CH_3^\bullet$ is discussed in detail. We have used NR mass spectrometry together with other techniques (MI and CID) in order to investigate the possible isomerization process between the classical, $CH_3CH_2OH_2^+$, and non-classical, C_2H_4•••H-OH_2^+, forms of protonated ethanol, a process which has also been the subject of two theoretical studies **[9, 10]**. The involvment of a Rydberg state in the observation of stable $C_2H_7O^\bullet$ will also be discussed.

6.3 Experimental

All experiments were performed using the VG Analytical ZAB-2F mass spectrometer of reversed geometry **[11]** modified for neutralization-reionization (NR) mass spectrometry as described earlier **[12, Chapter 2]**. Metastable ion (MI) and collision induced dissociation (CID) mass spectra were recorded by standard procedures **[13, Chapter 4]**. Oxygen was used as target gas in the CID experiments. In the NR experiments, the mass selected ions were neutralized by charge exchange with xenon. After separating the neutrals from the ions by means of a charged electrode, the former were reionized by collision with O_2. Isotopic contributions from ions of lower mass were negligible, unless stated otherwise.

The appearance energies (AE) of metastable processes were measured with a Kratos AEI MS 902S mass spectrometer using a comparative method with diethyl ether as standard **[14]**. Daughter ion appearance energies were obtained with an apparatus consisting of an electrostatic electron monochromator with a quadrupole mass analyser and a minicomputer data system **[15]**.

$CH_3OCH_2CD(OH)CH_3$ was synthesized by reducing methoxyacetone with $LiAlD_4$ **[16]** in anhydrous ether. All other chemicals were commercially available and used without further purification.

6.4 Results and Discussion

6.4.1 Protonated Dimethyl Ether and Isotopomers

Protonated dimethyl ether and its O-D analogue have been produced from two different reactions: (i) by protonation (deuteronation) of dimethyl ether using H_3O^+ (D_3O^+) as reagent and (ii) as a fragment ion produced from ionized 1-methoxy 2-propanol as shown by the following reactions:

$$CH_3OCH_2CH(OH)CH_3^{+\bullet} \rightarrow C_2H_7O^+ + C_2H_3O^{\bullet} \qquad (6.3)$$

$$CH_3OCH_2CD(OH)CH_3^{+\bullet} \rightarrow C_2H_6DO^+ + C_2H_3O^{\bullet} \qquad (6.4)$$

The structure of the $C_2H_7O^+$ fragment ion (from reaction (6.3)) was confirmed to be protonated dimethyl ether by two types of experiments. First the dissociation of the metastable $C_2H_7O^+$ ions showed a broad dished peak at m/z 31, CH_2OH^+, having a shape identical with that from the MI mass spectrum of protonated dimethyl ether **[17]**. The identity of the neutral $C_2H_3O^{\bullet}$ fragment was determined from its collision induced dissociative ionization (CIDI) mass spectrum (see Chapter 4) and was found to be identical with that of the radical produced in the metastable dissociation of ionized biacetyl, showing it to have the acetyl structure $CH_3CO^{\bullet}$ **[18]**.

The second experiment was to measure the appearance energy (AE) of m/z 47, 9.54

± 0.05 eV, using energy selected electrons. With $\Delta H_f(CH_3OCH_2CH(OH)CH_3)$ = -97 kcal mol^{-1} **[19]** and $\Delta H_f(CH_3CO^{\bullet})$ = -6 kcal mol^{-1} **[20]**, $\Delta H_f(C_2H_7O^+)$ = 129 kcal mol^{-1}, in excellent agreement with the literature value of 130 kcal mol^{-1} derived from the proton affinity of dimethyl ether **[20]**.

The m/z 48 ($C_2H_6DO^+$) ion produced from ionized $CH_3OCH_2CD(OH)CH_3$ (reaction (6.4)) very largely loses CH_4 in its MI mass spectrum (see Table 6.1), the ratio m/z 32 : m/z 31 being ~ 13 : 1. Therefore, the deuterium atom in the $C_2H_6DO^+$ species must be bonded to oxygen, because only CH_4 is lost metastably (not CH_3D) in the MI mass spectrum of $CH_3O^+(D)CH_3$ (produced by direct deuteronation of CH_3OCH_3) whereas for $CH_2DO^+(H)CH_3$ (produced by protonation of CH_2DOCH_3 with H_3O^+) m/z 31 (loss of CH_3D) and m/z 32 (loss of CH_4) were found to be in a ratio of 1.6 : 1 (see Table 6.1).

Table 6.1. Metastable ion (MI) mass spectra of protonated dimethyl ethers.

Ion	Fragment ion abundance	
	m/z 31	32
$CH_3O^+(H)CH_3$ (m/z 47)	1.0	-
$CH_3O^+(D)CH_3$ (m/z 48)	-	1.0
$CH_3O^+(H)CH_2D$ (m/z 48)	1.6	1.0
m/z 48 from $CH_3OCH_2CD(OH)CH_3$	1.0	13

Figure 6.1 was obtained by measuring the appearance energy (see Chapter 4) of the m/z 31 ion arising from the metastable process

$$CH_3O^+(H)CH_3 \rightarrow CH_2OH^+ + CH_4 \qquad (6.5)$$

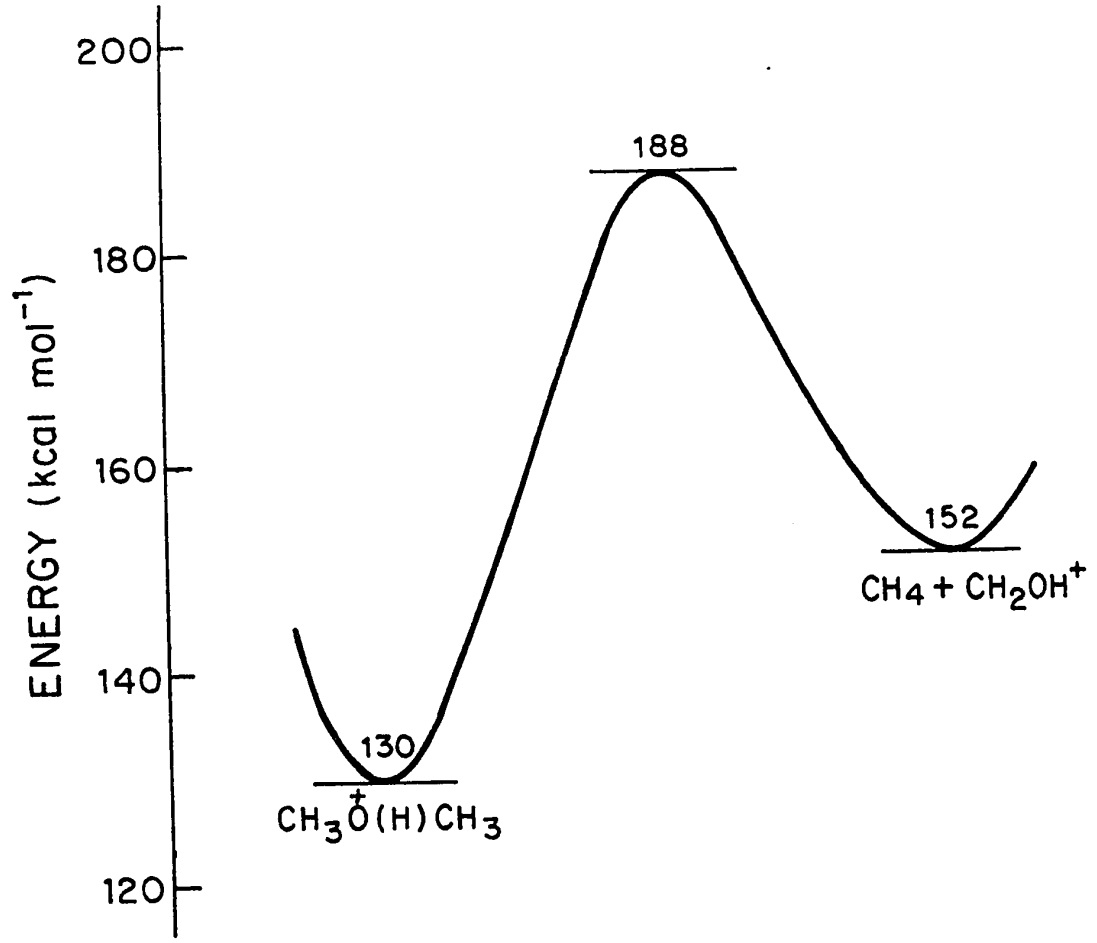

Figure 6.1. Energy diagram for the metastable fragmentation of protonated dimethyl ether.

AE = 12.1 ± 0.1 eV and using the established thermochemical data for the reactant and product enthalpies, $\Delta H_f(CH_3CO^{\bullet})$ = -6 kcal mol^{-1}, $\Delta H_f(CH_2OH^+)$ = 168 kcal mol^{-1} and $\Delta H_f(CH_4)$ = -16 kcal mol^{-1}, all data from reference 20. Note the large reverse energy barrier, 36 kcal mol^{-1}, which is in keeping with the broad dished m/z 31 metastable peak shape and the large associated kinetic energy release ($T_{0.5}$ = 420 meV). Also note that the $CH_3O^+(H)CH_3$ ions occupy a deep potential well of 58 kcal mol^{-1}, which can explain the pressure effect (described below) observed for the metastable fragmentation of protonated (deuteronated) dimethyl ether produced from direct protonation (deuteronation) of dimethyl ether in the ion source.

With H_3O^+ as protonating agent, the reaction

$$(CH_3)_2O + H_3O^+ \rightarrow CH_3O^+(H)CH_3 + H_2O \qquad (6.6)$$

is 24.8 kcal mol^{-1} exothermic ($\Delta H_f(H_3O^+)$ = 141 kcal mol^{-1}; $\Delta H_f(CH_3OCH_3)$ = -44 kcal mol^{-1}; $\Delta H_f(CH_3O^+(H)CH_3)$ = 130 kcal mol^{-1} and $\Delta H_f(H_2O)$ = -57.8 kcal mol^{-1} (all data from Ref. 20). When $CH_3O^+(H)CH_3$ and its O-D analogue were produced by direct protonation (deuteronation) of dimethyl ether, observations of the metastable fragmentation of these ions showed that increasing the pressure of H_2O (D_2O) in the ion source reduced the fraction of energy rich species (see Figure 6.2a). By varying the measured source pressure by an order of magnitude, from 10^{-5} to 10^{-4} mbar, the relative abundance of the metastable peak for m/z 47 $\rightarrow$ m/z 31 + CH_4 to the m/z 47 ion beam, m^*_{31} / $I.B._{47}$, changed from

0.1 x 10^{-4} to 2.0 x 10^{-4}.

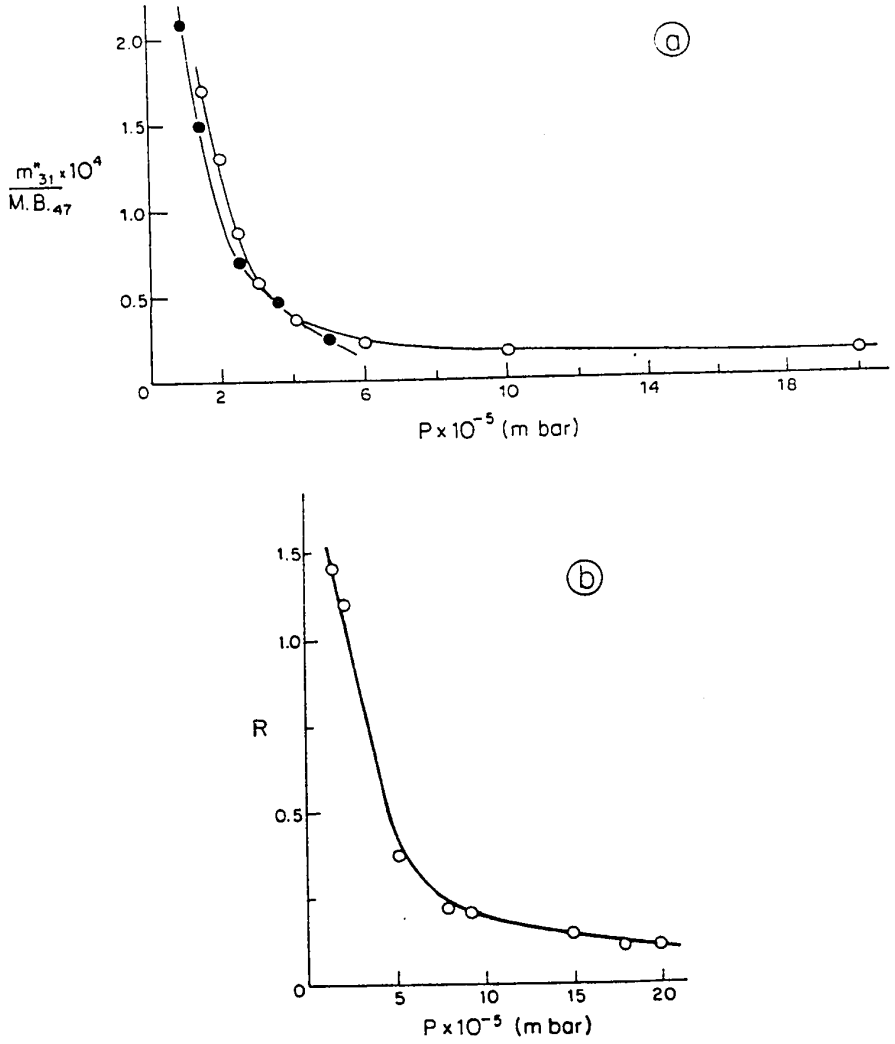

Figure 6.2. (a) Effect of pressure on the internal energy of protonated (o) and deuteronated (•) dimethyl ether as measured by the relative abundance of the metastable peak to the ion beam. (b) Effect of pressure on the intensity of the recovered m/z 47 as measured by the ratio R = intensity of recovered m/z 47 over the intensity of fragment ion m/z 46 in the Xe/O_2 NR mass spectra of protonated dimethyl ether.

Since the activation energy for the metastable fragmentation of $CH_3O^+(H)CH_3$ is 58 kcal mol^{-1} (see Figure 6.1) it is not surprising that ions of lower energy (high ion source pressure conditions) hardly dissociate metastably. At low ion source pressures, ions having greater internal energy are being formed and can therefore dissociate more easily. Figure 6.2b shows that the lower the ion source pressure, the greater the intensity of the recovery signal m/z 47 (reionized $CH_3O(H)CH_3$) in the NR mass spectrum of protonated dimethyl ether.

The behaviour of ionized deuteronated dimethyl ether was the same and the greatest yield of hypervalent radicals (see Figure 6.3a) was obtained from $CH_3O^+(D)CH_3$ under CI conditions which produced energy rich ions (low ion source pressure). Figure 6.3b represents the NR mass sepctrum of $CH_3O^+(D)CH_3$ produced from $CH_3OCH_2CD(OH)CH_3^+$ (see reaction (6.4)) and it can be seen that the yield of stable hypervalent radicals is much less than that obtained from excited deuteronated dimethyl ether. The latter observation is due to the m/z 48 ions produced from reaction (4) being much "colder". This is shown by the ratio of $m^*_{32}/I.B._{48}$being 0.28×10^{-4} vs 2.1×10^{-4} for that of highly excited $CH_3O^+(D)CH_3$ produced by deuteronation of dimethyl ether. Note that neutralization with Xe, Hg and Cd generally produced similar neutralization-reionization phenomena, but with Na, dissociation of the hypervalent species was dominant. A result which is not surprising since the energy balances, Q_N (see Chapter 4), given by

$$Q_N = IE(N) - NE_V(M^+) \qquad (6.7)$$

where IE(N) is the ionization energy of the electron transfer target and $NE_V(M^+)$ is the vertical neutralization energy of the selected ion M^+, were estimated to be 6.8, 5.1, 3.7 and -0.2 eV for Xe (IE = 12.1 eV), Hg (IE = 10.4 eV), Cd (IE = 9.0 eV) and Na (IE = 5.1 eV, all IE values from Ref. 20) respectively. Note that the value $NE_V(CH_3O^+(H)CH_3)$ was estimated as follows: first $\Delta H_f(CH_3O^{\bullet}(H)CH_3)$ was calculated from the sum $\Delta H_f(CH_3OCH_3)$ + $\Delta H_f(H^{\bullet})$ = -44 kcal mol^{-1} + 52 kcal mol^{-1} = 8 kcal mol^{-1} **[20]** = $\Delta H_f(CH_3O^{\bullet}(H)CH_3)$, this assumes no binding energy between the hydrogen atom and the ether molecule. Any binding energy would necessarily lower this value. Then $NE_V(CH_3O^+(H)CH_3)$ = $\Delta H_f(CH_3O^+(H)CH_3)$ - $\Delta H_f(CH_3O^{\bullet}(H)CH_3)$ > 122 kcal mol^{-1} or $NE_V(CH_3O^+(H)CH_3)$ > 5.3 eV. Now introducing the latter value in equation (6.7), we obtained the energy balances, Q_N, mentioned above.

We conclude that the vertical neutralization process which gives hypervalent radicals, stable on the time scale of the present experiment (~1-2 μs) arises only from vibrationally highly excited protonated (deuteronated) dimethyl ether. To our knowledge, kinetic studies **[21, 22]** have never provided any evidence for the existence of stable $CH_3O^{\bullet}(H)CH_3$. For example, Meagher and co-workers **[21]** have shown that the mechanism of the reaction of H and D atoms with CH_3OCH_3 resulted in a bimolecular abstraction of the type

$$H^{\bullet} \text{ (or } D^{\bullet}) + CH_3OCH_3 \rightarrow H_2 \text{ (or HD)} + {}^{\bullet}CH_2OCH_3 \qquad (6.8)$$

for which the activated complexes are H•••H•••CH_2-OCH_3 and D•••H•••CH_2-OCH_3. Therefore we propose that a Rydberg state wherein the ion core is stable may be

responsible for the observation of stable $CH_3O(H)CH_3$ and its O-D analogue. Note that such a Rydberg state would make the Q_N values mentioned above more endothermic, since it would lie at an energy somewhere between 8 and 122 kcal mol^{-1}.

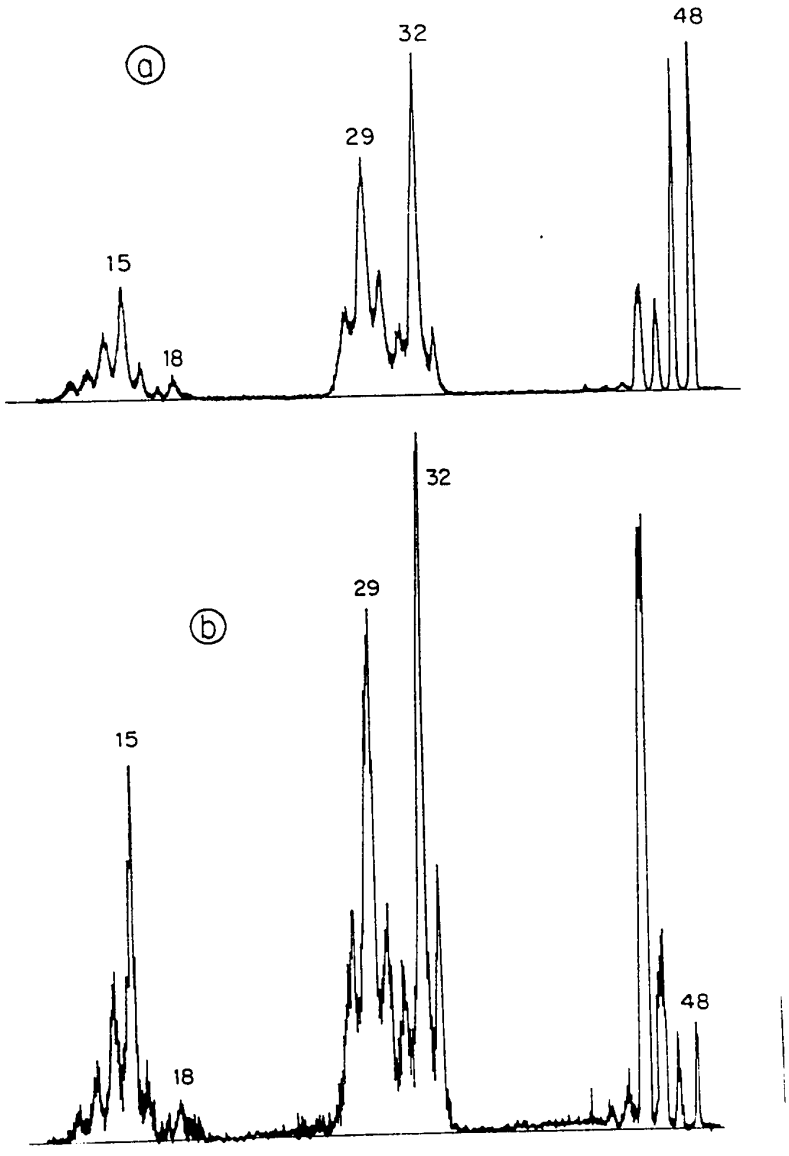

Figure 6.3. Neutralization (Xe) - reionization (O_2) mass spectra of $CH_3O^+(D)CH_3$ obtained (a) from $CH_3OCH_3 + D_3O^+$ and (b) as a daughter ion from $CH_3OCH_2CD(OH)CH_3^{+\bullet}$

6.4.2 Protonated Ethanol and its Non-Classical Form

Wesdemiotis et al. **[8]** concluded from ethanol autoprotonation, that the classical ion, $[CH_3CH_2OH_2]^+$ (a), and its non-classical structure, $[C_2H_4{\bullet\bullet\bullet}H{\bullet\bullet\bullet}OH_2)^+$ (b), can coexist and that the stable hypervalent radicals observed in their NR Hg/O_2 mass spectra arise from excited ions having the classical structure. The isomerization process was proposed **[8]** to explain the extensive H/D scrambling observed in the CID mass spectra of a series of labeled protonated ethanols. Such scrambling was also observed by Harrison **[23]** and Jarrold et al. **[17]** and was explained by the interconversion of $[C_2H_4{\bullet\bullet\bullet}H{\bullet\bullet\bullet}OH_2]^+$ and $[C_2H_4{\bullet\bullet\bullet}OH_3]^+$, en route to the elimination of either H_2O or C_2H_4. Recently the calculations of Swanton et al. **[10]** (which are in good agreement with those of Bouchoux and Hoppilliard **[9]**) showed that a species which resembles a complex of ethene plus oxonium ion, $[C_2H_4{\bullet\bullet\bullet}H\text{-}OH_2]^+$ (c), lies some 13 kcal mol^{-1} higher than (a) (see Figure 6.4) and thus can explain the extensive H/D mixing discussed above. Also it was calculated that the (a) $\rightarrow$ (c) isomerization requires an activation energy of 23 kcal mol^{-1} and that the elimination of C_2H_4 and H_2O from (c) can occur at threshold.

In order to investigate the (a) $\rightarrow$ (c) isomerization process, we have generated them (as well as some of their isotopomers) seperately from different precursors. The ion $[CH_3CH_2OH_2]^+$, was produced from ionized 2,3-butanediol by loss of $CH_3CO^{\bullet}$. The structure of the $C_2H_7O^+$ ion was assigned by measuring the AE of the m/z 47 ion, 10.00 $\pm$ 0.05 eV. Using $\Delta H_f(CH_3CH(OH)CH(OH)CH_3)$ = -115 kcal mol^{-1} **[24]** and $\Delta H_f(CH_3CO^{\bullet})$

= -6 kcal mol^{-1} **[20]** we obtained $\Delta H_f(C_2H_7O^+)$ = 122 kcal mol^{-1}, in excellent agreement with the literature value of 121 kcal mol^{-1} **[20]** obtained from the proton affinity of ethanol. With regard to isomer (c), since H_2O is a small molecule, reacting it with $C_2H_5^+$ is more likely to give rise to the formation of the non-classical structure, (c), because we have shown **[25, Chapter 7]** that when a ROR′ molecule is small, it reacts in great extent with the more stable form of the ethyl cation i.e. the non-classical one **[26]**.

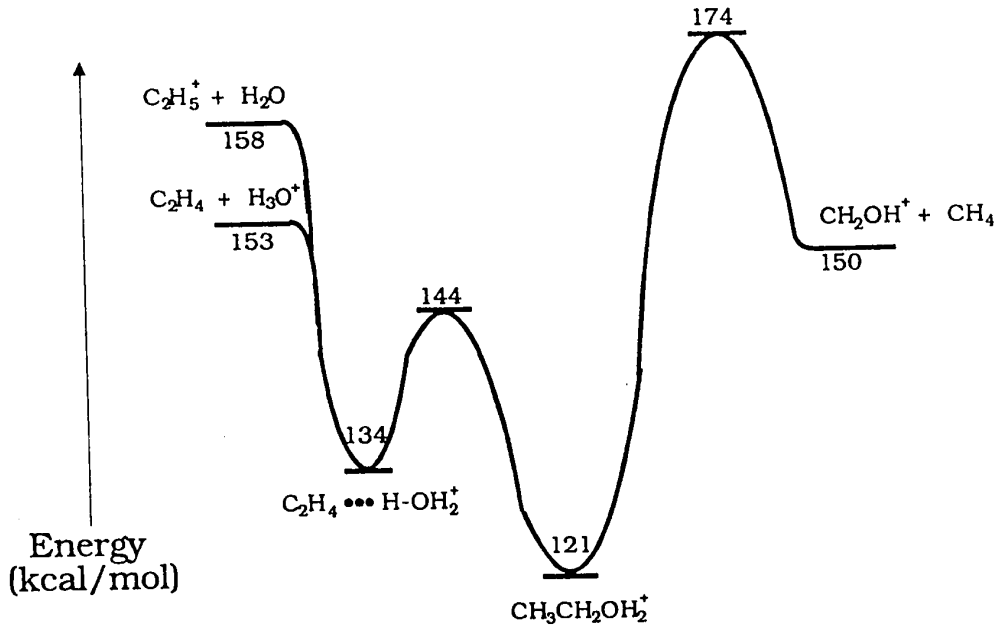

Figure 6.4 *Schematic potential energy profile describing unimolecular fragmentation reactions of protonated ethanol. All thermochemical values are from Ref. 20, except for $\Delta H_f(C_2H_4$•••$H\text{-}OH_2^+)$ and the transition states, which are from Ref. 10.*

First note that both ions (a) and (c) displayed the same single metastable peak, m/z 19 (H_3O^+). The kinetic energy release at half height ($T_{0.5}$ value) was measured to be 2 meV in both cases, indicating that there is no significant barrier to the reverse association, a finding which is in good agreement with theoretical calculations **[10]**.

Figure 6.5 shows the CID mass spectra of m/z 47 generated from $CH_3CH(OH)CH(OH)CH_3^+$ and from $C_2H_5^+ + H_2O$, and m/z 52 obtained from $CD_3CD(OH)CD(OH)CD_3^+$ and from $C_2D_5^+ + H_2O$. Also shown are the CID mass spectra of the metastably generated ions 47 and 52 from the corresponding diols. From Figures 6.5a and 6.5b it can be noticed that the source and metastably generated ions have the same structure or mixture of structures. The peak at m/z 33 in Figure 6.5a was found to be an artifact signal which is confirmed by the latter being absent in Figure 6.5b. When comparing Figures 6.5a and 6.5b with Figure 6.5c, one can see that H_3O^+ (m/z 19) is produced in greater abundance from the m/z 47 ion when the latter is produced by the reaction $C_2H_5^+ + H_2O$ rather than from ionized 2,3-butanediol, whereas $C_2H_5^+$ (m/z 29), CH_2OH^+ (m/z 31) and $CH_2OH_2^+$ (m/z 32) are relatively less intense. This observation is interpreted as showing that when the $C_2H_7O^+$ ions are produced from $C_2H_5^+ + H_2O$, the former have the non-classical structure (c) and they can either lose C_2H_4 and H_2O (in small extent) or isomerize to (a) and then lose H_2O (in greater extent than from (c)), CH_4 and $CH_3^{\cdot}$. On the other hand, when ions of mass 47 are generated from ionized 2,3-butanediol, a greater yield of protonated ethanol is being initially produced and therefore the peaks at m/z 29, 31 and 32 are more intense. Nevertheless, note that upon collision , the

rearrangement (a) → (c) also occurs since a peak at m/z 19 is also observed when excited ions (a) are formed. The latter statement is supported by the extensive H/D scrambling observed in the CID mass spectra of the labeled species (see Figure 6.5d). Such mixing has also been observed by others **[8, 17 and 23]**. Therefore we propose the following scheme in order to explain the results discussed above.

$$[C_2H_4\bullet\bullet\bullet H\text{-}OH_2]^+ \rightarrow H_3O^+ + C_2H_4 \quad (6.9)$$

$$\rightarrow C_2H_5^+ + H_2O \text{ (minor)} \quad (6.10)$$

$$[CH_3CH_2OH_2]^+ \rightarrow C_2H_5^+ + H_2O \text{ (major)} \quad (6.11)$$

$$\rightarrow CH_2OH^+ + CH_4 \quad (6.12)$$

$$\rightarrow CH_2OH_2^{+\bullet} + CH_3^{\bullet} \quad (6.13)$$

The sum of the heats of formation $\Delta H_f(H_3O^+) + \Delta H_f(C_2H_4)$ = 153 kcal mol^{-1} vs 158 kcal mol^{-1} for that of $C_2H_5^+ + H_2O$, all data from ref. 20. Since it has been calculated **[10]** that both processes occur at threshold when produced from isomer (c), m/z 29 should never be more intense than m/z 19 (since the latter process is less energy demanding), unless most of the $C_2H_5^+$ is produced from (a), a process which necessitates only a simple C-O bond cleavage. The thermodynamically favoured process, $CH_2OH^+ + CH_4$ ($\Delta H_f(CH_2OH^+) + \Delta H_f(CH_4)$ = 150 kcal mol^{-1} **[20]**) was calculated **[10]** to occur with a large energy barrier, 53 kcal mol^{-1} vs 23 kcal mol^{-1} for that of the isomerization process (a) → (c) (see Figure 6.4) and therefore the peak at m/z 31 is relatively less intense than those at m/z 19 and 29.

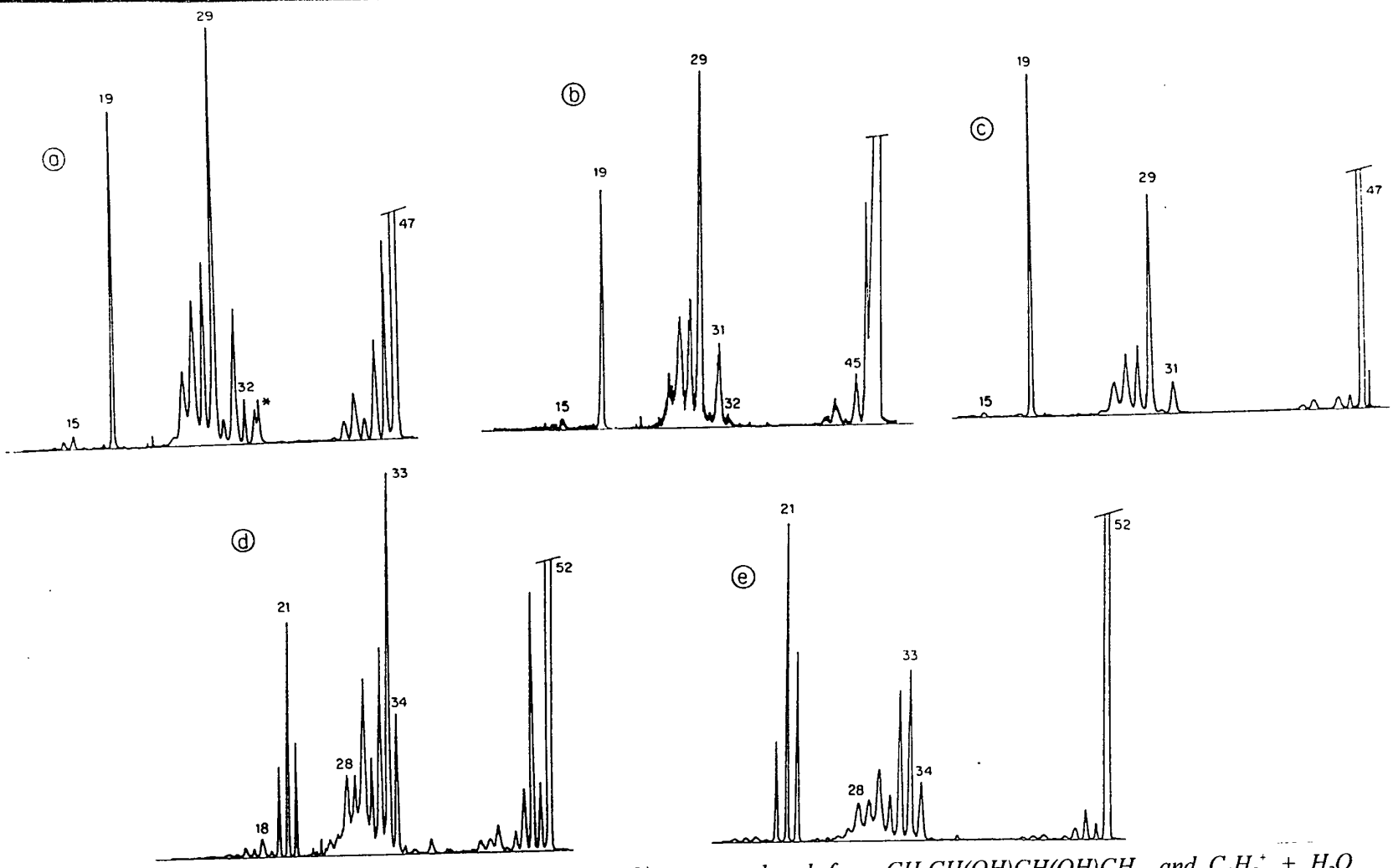

Figure 6.5. (a) and (c) CID mass spectra of $C_2H\text{-}O^+$ ions produced from $CH_3CH(OH)CH(OH)CH_3$ and $C_2H_5^+ + H_2O$ respectively. (b) CID mass spectrum of metastably generated $C_2H_7O^+$ from $CH_3CH(OH)CH(OH)CH_3^{+\bullet}$. (d) and (e) CID mass spectra of $C_2D_5H_2O^+$ ions obtained from $CD_3CD(OH)CD(OH)CD_3^{+\bullet}$ and $C_2D_5^+ + H_2O$ respectively.

In order to aid distinguishing between isomers (a) and (c), the Xe/O_2 NR mass spectra of the above species were recorded, see Figure 6.6. Note that the NR mass spectra of the $C_2H_7O^+$ isomers and their isotopomers are identical (see Figures 6.6a, b, c and d) suggesting that only one of the two isomers has survived to the neutralization step. For the unlabeled isomers (m/z 47), very small recovery signals were observed, but the formation of peaks at m/z 31 ($CH_2OH_2^+$) and m/z 18 (H_2O) are more likely to have occured from the dissociation of reionized $CH_3CH_2OH_2$ (see discussion above). For the labeled species $C_2H_2D_5O^+$ (m/z 52), much more intense recovery signals were observed (see Figures 6.6c and 6.6d), showing that a stable hypervalent radical was formed upon neutralization with xenon. Also note the presence of fragment ions at m/z 33 ($CHDOHD^+$) and m/z 18 (H_2O^+). These results lead us to propose (in agreement with Wesdemiotis et al. **[8]**) that the hypervalent radicals are produced by neutralization of the classical ion (a). Similarly to protonated dimethyl ether, a Rydberg state of the most stable isomer, $CH_3CH_2OH_2^+$ can explain the observation of a recovery signal in the present NR mass spectra.

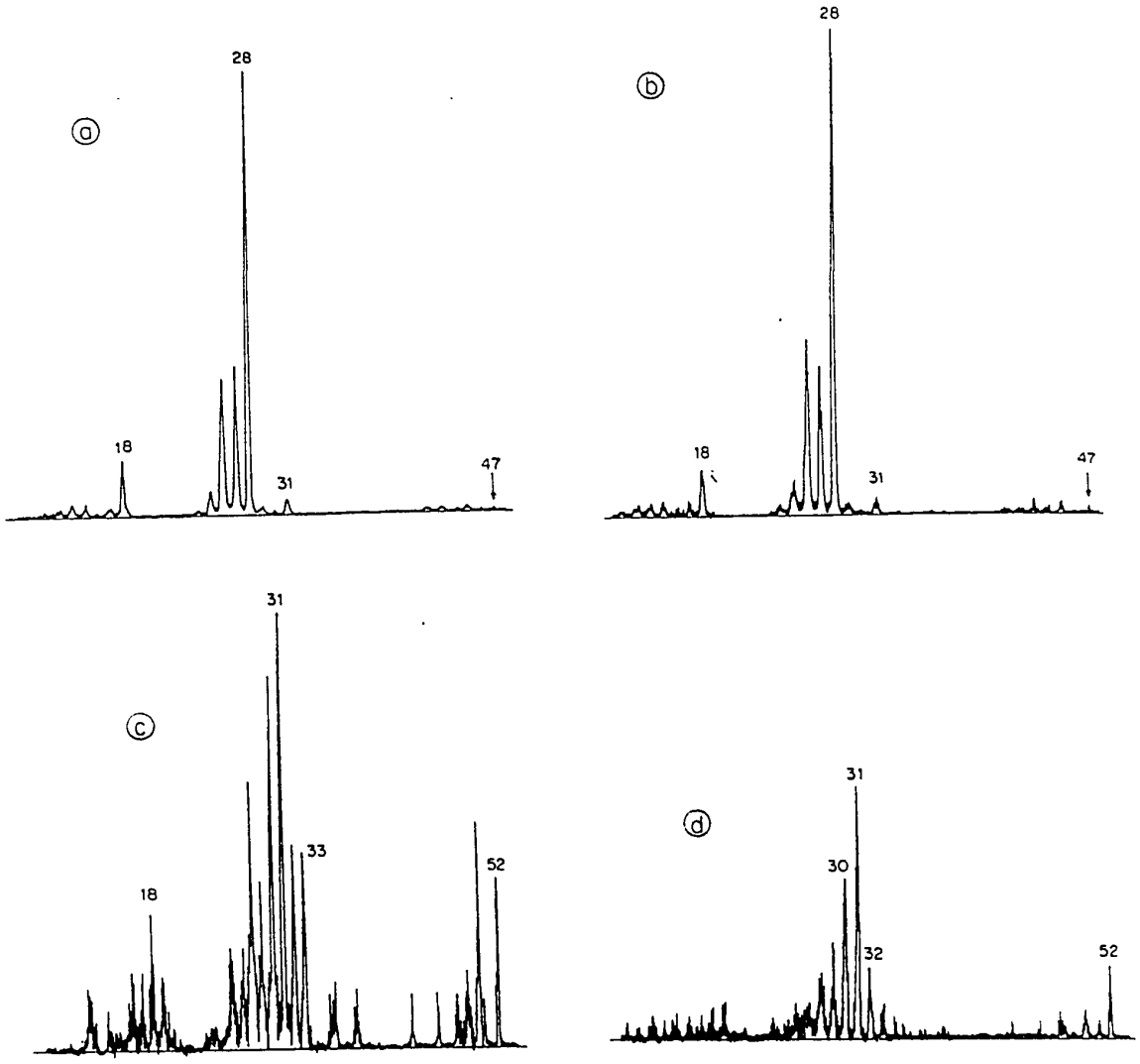

Figure 6.6. *(a) and (b) Xe/O_2 NR mass spectra of $C_2H_7O^+$ produced from $CH_3CH(OH)CH(OH)CH_3^{+\bullet}$ and $C_2H_5^+ + H_2O$ respectively. (c) and (d) Xe/O_2 NR mass spectra of $C_2D_5H_2O^+$ generated from $CD_3CD(OH)CD(OH)CD_3^{+\bullet}$ and $C_2D_5^+ + H_2O$ respectively.*

6.5 Conclusions

It was shown that stable hypervalent radicals, $CH_3O(H)CH_3^{\bullet}$ and $CH_30(D)CH_3^{\bullet}$, are produced via the vertical neutralization of vibrationally highly excited protonated (deuteronated) dimethyl ether.

For protonated ethanol, stable hypervalent radicals are proposed to arise by neutralization of the classical ion, $CH_3CH_2OH_2^+$.

For both $C_2H_7O^+$ isomers, we suggest that a Rydberg state in which the ion core is stable may explain the observation of recovery signals in the NR mass spectra.

REFERENCES - CHAPTER 6

1. (a) G.I Gellene and R.F. Porter, ***Acc. Chem. Res.*** 16, 200 (1985). (b) C. Wesdemiotis and F.W McLafferty, ***Chem. Rev.*** 87, 485 (1987). (c) J.K. Terlouw and H.Schwarz, ***Angew. Chem. Int. Ed. Engl.*** 26, 805 (1987). (d) J.L. Holmes, ***Mass Spectrom. Rev.*** 8, 573 (1989).
2. F.W. McLafferty and C. Wesdemiotis, ***Org. Mass Spectrom.*** 24, 663 (1989).
3. F.W. McLafferty, ***Private communication.***
4. S.F. Selgren and G.I. Gellene, ***J. Chem. Phys.*** 87, 5804 (1987).
5. S.F. Selgren and G.I. Gellene, ***Chem. Phys. Lett.*** 146, 485 (1988).
6. S-J. Jeon, A.B. Raksit and R.F. Porter, ***J. Am. Chem. Soc.*** 107, 4129 (1985).
7. J.L. Holmes and M. Sirois, ***Org. Mass Spectrom.*** 25, 481 (1990).
8. C. Wesdemiotis, A. Fura and F.W. McLafferty, ***J. Am. Soc. Mass Spectrom.*** 2, 459 (1991).
9. G. Bouchoux and Y. Hoppilliard, ***J. Am. Chem. Soc.*** 112, 9110 (1990).
10. D.J. Swanton, D.C.J. Marsden and L. Radom, ***Org. Mass Spectrom.*** 26, 227 (1991).
11. P.C. Burgers, J.L. Holmes, A.A. Mommers, J.E. Szulejko and J.K. Terlouw, ***Org. Mass Spectrom.*** 19, 442 (1984).
12. J.L. Holmes, A.A. Mommers, J.K. Terlouw and C.E.C.A. Hop, ***Int. J. Mass Spectrom. Ion Processes,*** 68, 249 (1986).
13. J.K. Terlouw, P.C. Burgers and J.L. Holmes, ***Org. Mass Spectrom.*** 14, 387 (1979).
14. P.C. Burgers and J.L. Holmes, ***Org. Mass Spectrom.*** 17, 123 (1982).

REFERENCES - CHAPTER 6

15. F.P. Lossing and J.C. Traeger, ***Int. J. Mass Spectrom. Ion Processes,*** 19, 9 (1976).

16. A. Streitwieser Jr. and C.H. Heathcock, ***Introduction to Organic Chemistry***, 3rd edition, MacMillan Publishing Company, New York, 1985.

17. M.F. Jarrold, J. Kirchner, S. Liu and M.T. Bowers, ***J. Phys. Chem.*** 90, 78 (1986).

18. B.L.M. Van Baar, P.C. Burgers, J.L. Holmes and J.K. Terlouw, ***Org. Mass Spectrom.*** 23, 355 (1988).

19. By group additivity, S.W. Benson, ***Thermochemical kinetics,*** 2nd Ed. Wiley, New-York, 1976.

20. S.G. Lias, J.E. Bartmess, J.F. Liebman, J.L. Holmes, R.D. Levin and W.G. Mallard, ***J. Phys. Chem. Ref. Data*** Suppl. 1, 1988.

21. J.F. Meagher, P. Kim, J.H. Lee and R.B. Timmons, ***J. Phys. Chem.*** 28, 2650 (1974).

22. F. Slemr and P. Warneck, ***Int. J. Chem. Kinet.*** 9, 267 (1977).

23. A.G. Harrison, ***Org. Mass Spectrom.*** 22, 637 (1987).

24. J.B. Pedley, R.D. Naylor and S.P. Kirby, ***Thermochemical Data of Organic Compounds,*** 2nd Ed. London, N.Y. Chapman and Hall (1986).

25. M. Sirois, M. George, J.R. Cao and J.L. Holmes, ***J. Am Chem Soc.*** Submitted.

26. M-W. Wang, J. Baker, R.H. Nobes and L. Radom, ***J. Am. Chem. Soc.*** 109, 2245 (1987).

CHAPTER 7

CLASSICAL AND NON-CLASSICAL FORMS OF THE ETHYL CATION AND THEIR PARTICIPATION IN THE IONS $RO^+(C_2H_5)R'$

J. Am. Chem. Soc. Submitted

7.1 Overview

Ion-molecule reactions of the type $C_2H_5^+ + ROR' \rightarrow RO^+(C_2H_5)R'$ (where R and/or R′ = H, CH_3, C_2H_5 and $CH(CH_3)_2$) were performed to probe the participation of the low energy (non-classical) and higher energy (classical) forms of the ethyl cation in these ethylated ROR′ species, all of which are metastable with respect to C_2H_4 loss. Significant H/D mixing was observed only when a labeled ethyl cation was reacted with a non-labeled ROR′ molecule, and the degree of H/D mixing depends only on the size of R and R′, being independent of the observational timeframe from 1-30 μs. When non-labeled ethyl cations were reacted with labeled ROR′ molecules, H/D mixing was not observed. The results were interpreted as arising from the classical and non-classical forms of the ethyl cation having different reactivities with ethers of different sizes.

7.2 Introduction

Since the early 1970's there has been considerable interest in the structure of the ethyl cation among both experimentalists **[1-3]** and theoreticians **[4-8]**, but agreement between the various results has been disappointing. For example, from the ion cyclotron resonance mass spectral study of a series of dialkyl-N-nitrosamines, Jaffé and Billets **[1]** observed that the $C_2H_5^+$ ion produced from ionized diethyl-N-nitrosamine transfers a proton to the neutral molecule. The $CD_3CH_2^+$ ion was found, in a double resonance experiment, to transfer only D^+. They proposed that the $C_2D_3H_2^+$ ion exists either as a localized ion (classical form) $CD_3CH_2^+$, or it exists as a bridged ion (non-classical form) in which the bridge atom is only deuterium. In neither structure was H/D scrambling permitted to occur, even though this seemed to them highly improbable. On the other hand, based on the H^- (D^-) transfer reaction $C_2D_3H_2^+$ ($C_2D_2H_3^+$) + RH (RD) $\rightarrow$ $C_2D_3H_3$ + R^+, Ausloos et al. **[2]** concluded that their results could only be explained by invoking statistical scrambling of the hydrogen (deuterium) atoms in the ethyl cation, regardless of its structure. This result was in agreement with the later observations of Vorachek et al. **[3]** who used high pressure mass spectrometry with CD_3CH_2I as the source of the ethyl cations as well as the proton acceptor. They considered the excess energy in the ethyl ion produced by photolysis or electron impact to be sufficient to overcome the barrier between the classical and H-bridged forms of $CH_3CH_2^+$, then believed **[5]** (on the basis of ab initio molecular orbital theory calculations) to be at least 1 kcal mol^{-1}. To avoid this potential problem, they generated ethyl cations with two vibrational energies by reacting CD_3CH_2F in SbF_5 in SO_2

solution at -78 °C. The $CD_3CH_2^+SbF_6^-$ complexes were found to react with hydride donors to produce mixtures of ethane whose mass spectra were only compatible with there having been complete randomization of H/D among the (CD_3CH_2) moieties prior to reaction.

In the early 1970's ab initio molecular orbital theory calculations favored the classical form of $C_2H_5^+$ as the lower energy species, whereas semiempirical calculations favored a non-classical protonated ethene structure. More recent and higher level calculations **[9]** have shown that there is no energy barrier between the classical and non-classical forms and that the non-classical form is the more stable by 6-7 kcal mol^{-1}. This result could explain the observed statistical H/D scrambling within the ethyl cation observed by Ausloos et al. **[2]** and Vorachek et al. **[3]**, if only energy rich (> 6 kcal mol^{-1}) ethyl cations were involved in the reactions studied by them.

In order to probe the possible participation of the classical and non-classical forms of the ethyl cation in ethylated ROR′ species (where R and/or R′ = H, CH_3 ,C_2H_5 and $CH(CH_3)_2$) we have performed ion-molecule reactions of the type

$$C_2H_5^+ + ROR' \rightarrow RO^+(C_2H_5)R' \qquad (7.1)$$

in the ion source of a reversed geometry double focusing mass spectrometer (see section 7.3).

When R = R′ = C_2H_5, reaction (7.1) leads to the formation of the triethyloxonium

ion. This species possibly could have a structure $H_3O^+(C_2H_4)_3$ if non-classical forms of the ethyl cation only are involved. It is noteworthy that electrostatic interactions between the hydroxonium ion, H_3O^+, and simple polar organic compounds, X, have been shown to lead to stable cluster ions of general formula $H_3O^+X_{(1,2\ or3)}$. The complexes for X = CH_3CN have been described by both theory and experiment **[10-12]** and the results were best described by treating the ion $H_3O^+(CH_3CN)_3$, as a symmetrical species with an H_3O^+ core to which the acetonitrile molecules are electrostatically attached through linear O-H-N bridges. The dissociation behaviour of these ions, induced by high (kV) and low (V) energy collisions with an inert target gas, is to lose CH_3CN. Similar structures, were also proposed for the $H_3O^+(acetone)_3$ **[13]** and $H_3O^+(methanol)_3$ **[14]** complexes. Also related to the present work, theoretical **[15]** and experimental **[16-18]** investigations have both shown that protonated ethanol rearranges reversibly to $[H_2O\text{-}H^+\bullet\bullet\bullet C_2H_4]$, at energies below the two dissociation channels of the $C_2H_7O^{+\bullet}$ ion which yield H_3O^+ and $C_2H_5^+$.

7.3 Experimental

All experiments were performed on the extended VG Analytical ZAB-2F (geometry $B_1E_1B_2$) mass spectrometer **[19]**. Metastable ion (MI) and collision induced dissociation (CID) mass spectra (using helium as the target gas) were recorded by standard procedures **[20]** (also see Chapter 4). Ethene loss ratios were also determined by MS/MS/MS experiments and metastably generated (in the first field-free region) daughter ion intensities were measured, allowing for the observation of metastable ion fragmentations occuring in

different timeframes. Ion-molecule reactions were performed in the ion source by first introducing the ROR′ species to a pressure of 10^{-6} mbar. The C_2H_5X compound was then admitted to the ion source until a total pressure of 10^{-4} mbar was reached. Note that results were independent of yet higher or lower ion source pressure.

$CD_3CH_2OCH_2CH_3$, $CH_3CD_2OCH_2CH_3$ and $CD_3CD_2OCH_2CH_3$ were prepared by reacting CH_3CD_2I, CD_3CH_2Br or CD_3CD_2Br respectively, with CH_3CH_2ONa in excess ethanol **[21]**. $CD_3CH_2NO_2$ was prepared by reacting $AgNO_2$ with CD_3CH_2Br **[22]**. All other compounds were commercially available and were used without further purification.

7.4 Results and Discussion

7.4.1 Triethyloxonium Ion and Isotopomers

Triethyloxonium ions, m/z 103, were produced by reacting an ethyl cation (from CH_3CH_2Br, CH_3CH_2I or $CH_3CH_2NO_2$) with a diethylether molecule under chemical ionization conditions in the ion source. The only dissociation channel observed for the metastable m/z 103 ion corresponds to the loss of ethene, C_2H_4 (see Table 7.1), for which the kinetic energy release calculated from the peak width at half height, $T_{0.5}$, was measured to be 45 meV. The reactions leading to C_2H_4 loss involve a β-H transfer to oxygen, $RR'O^+CH_2CH_3 \rightarrow RR'O^+H + C_2H_4$. The He collision induced dissociation (CID) mass spectrum of the m/z 103 ions, irrespective of the origin of the $C_2H_5^+$ ions, showed major peaks at m/z 75 ($-C_2H_4$),

Table 7.1. Metastable ion (MI) and partial collision induced dissociation (CID) mass spectra of triethyloxonium ions and isotopomers.

Reaction		Ion peak abundance m/z				
		75	76	77	78	80
$(C_2H_5)_2O + C_2H_5^+ \rightarrow [C_6, H_{15}, O]^+$	MI	100				
m/z 103	CID	100				
$(C_2H_5)_2O$ self-ethylation $\rightarrow [C_6,H_{15},O]^+$	MI	100				
m/z 103	CID	100				
$(C_2H_5)_2O + C_2D_5^+ \rightarrow [C_6, H_{10}, D_5, O]^+$	MI		19			81
m/z 108						
$C_2H_5OC_2D_5 + C_2H_5^+ \rightarrow [C_6, H_{10}, D_5, O]^+$	MI		19			81
m/z 108						
STATISTICAL RATIO			33			66
$(C_2H_5)_2O + CH_3CD_2^+ \rightarrow [C_6,H_{13},D_2,O]^+$		MI	22	7	71	
m/z 105	CID	26	6	68		
$CH_3CD_2OCH_2CH_3 + C_2H_5^+ \rightarrow [C_6,H_{13},D_2,O]^+$	MI	29	-	71		
m/z 105	CID	30	-	70		
STATISTICAL RATIO		60	40			
$(C_2H_5)_2O + CD_3CH_2^+ \rightarrow [C_6,H_{12},D_3,O]^+$	MI	10	14		76	
m/z 106	CID	10	15		75	
$CD_3CH_2OCH_2CH_3 + C_2H_5^+ \rightarrow [C_6,H_{12},D_3,O]^+$	MI	<1	21		79	
m/z 106	CID	<1	22		78	
STATISTICAL RATIO		40	60			

m/z 47 ($-2C_2H_4$) and minor signals at m/z 59, 29 and 19 ($-3C_2H_4$). As shown in Table 7.1, triethyloxonium ions could also be produced by auto-ethylation of the diethylether cation and their dissociation characteristics were the same as those of the other m/z 103 ions referred to above.

The unimolecular dissociations of the deuterium labeled isotopomer $[C_6, H_{10}, D_5, O]^+$, m/z 108, obtained by reacting $C_2D_5^+$ with $C_2H_5OC_2H_5$ or by self-ethylation of $C_2D_5OC_2H_5$ were found to be identical, producing only m/z 80 ions (loss of C_2H_4) and m/z 76 ions (loss of C_2D_4) in a ratio of 81:19. This shows that H/D exchange between the ethyl groups does not occur but that there is an isotope effect acting against C_2D_4 loss i.e. H^+ transfer preferred over D^+ transfer. The metastable m/z 80 ions, $[C_4,H_6,D_5,O]^+$ also lost C_2H_4 and C_2D_4, producing protonated ethanol, but in a ratio of 76 : 24 indicating a larger isotope effect.

Two other isotopomers of the triethyloxonium ion were studied, $[C_6,H_{13},D_2,O]^+$, m/z 105 and $[C_6,H_{12},D_3,O]^+$, m/z 106. Note that (see Table 7.1) for these isotopomers, H/D mixing prior to ethene loss from metastable ions was observed only when the deuterium atoms were present in the reacting ethyl cation,

e.g. $(C_2H_5)_2O + CH_3CD_2^+$ or $CD_3CH_2^+ \rightarrow [C_6,H_{13},H_2,O]^+$ or $[C_6,H_{12},D_3,O]^+$ (7.2)

When <u>labeled</u> diethylether was reacted with a <u>non-labeled</u> ethyl cation

e.g. $CH_3CD_2OC_2H_5$ or $CD_3CH_2OC_2H_5 + C_2H_5^+ \rightarrow [C_6,H_{13},D_2,O]^+$ or $[C_6,H_{12},D_3,O]^+$ (7.3)

no (or very little) positional mixing of H and D atoms was observed. For the metastable $[C_6, H_{12}, D_3, O]^+$ ions from reaction (7.2) the H/D scrambling was found to be nearly statistical for the loss of C_2D_3H and $C_2D_2H_2$ i.e. m/z 75 and m/z 76 were in a ratio of 42 : 58; the statistical ratio for 3 deuterium and 2 hydrogen atoms is 40 : 60. Note that this ratio became exactly 40 : 60 in the CID mass spectrum. For $[C_6,H_{13},D_2,O]^+$ from reaction (3) the H/D mixing was not statistical, possibly due to a small isotope effect. Nevertheless significant H/D scrambling was observed only when a labeled triethyloxonium ion was formed from the reaction between a non-labeled diethylether molecule and a labeled ethyl cation. Possible explanations for these results will be discussed below. However since H/D mixing was not observed between the ethyl groups (see above), the mixing has to arise within the reactant, label-containing ethyl group.

7.4.2 Protonated Diethylether and Isotopomers

The collision induced dissociation (CID) mass spectrum of unlabeled protonated diethylether, obtained by using H_3O^+ as the protonating agent, has been reported earlier **[23]**. Metastable protonated diethylether ions lose only C_2H_4, with $T_{0.5}$ = 25 meV, and isotopomers were prepared via different routes (see Table 7.2). It was again found that considerable H/D mixing occured only when $[C_4,H_9,D_2,O]^+$ or $[C_4,H_8,D_3,O]^+$ ions were obtained via ethene loss from labeled triethyloxonium ions, which had been produced by reacting a non-labeled diethylether molecule with a labeled ethyl cation. When labeled

protonated diethylether was produced via any other route, only a very small amount of H/D mixing was observed, even in the CID mass spectra. Note therefore, that for the reactions $CH_3CH_2OH + CH_3CD_2^+$ or $CD_3CH_2^+ \rightarrow [C_4,H_9,D_2,O]^+$ or $[C_4,H_8,D_3,O]^+$, very little H/D scrambling preceded ethene loss, even though a labeled ethyl cation had been reacted with a non-labeled ethanol.

Table 7.2. Metastable ion (MI) and partial collision induced dissociation (CID) mass spectra of protonated diethyl ether and isotopomers.

Reaction		Ion peak abundance, m/z			
		47	48	49	50
$CH_3CH_2O^+(H)CH_2CH_3$ From self-protonation m/z 75	MI	100			
	CID	100			
$CH_3CH_2OCH_2CH_3 + D_3O^+ \rightarrow CH_3CH_2O^+(D)CH_2CH_3$ m/z 76	MI		100		
	CID		100		
$(C_2H_5)_2O + CH_3CD_2^+ \rightarrow [C_6,H_{13},D_2,O]^+$ $\downarrow -C_2H_4$ $[C_4, H_9, D_2, O]^+$ m/z 77	MI	27	13	60	
	CID	24	21	55	
$CH_3CD_2OCH_2CH_3 + C_2H_5^+ \rightarrow [C_6,H_{13},D_2,O]^+$ $\downarrow -C_2H_4$ $[C_4,H_9,D_2,O]^+$ m/z 77	MI	41	<1	58	
	CID	43	3	54	
$CH_3CD_2O^+(H)CH_2CH_3$ from self-protonation m/z 77	MI	42	<1	57	
	CID	41	6	53	
$CH_3CD_2OH + C_2H_5^+ \rightarrow CH_3CD_2O^+(H)CH_2CH_3$ m/z 77	MI	42	<1	57	
	CID	41	3	56	
$CH_3CH_2OH + CH_3CD_2^+ \rightarrow CH_3CD_2O^+(H)CH_2CH_3$ m/z 77	MI	44	2	54	
	CID	44	6	50	
STATISTICAL RATIO		60	40		

Table 7.2. cont'd

$(C_2H_5)_2O + CD_3CH_2^+ \rightarrow [C_6,H_{12},D_3,O]^+$					
$\downarrow -C_2H_4$					
$[C_4,H_8,D_3,O]^+$	MI	18	17		65
m/z 78	CID	19	20		61
$CD_3CH_2OCH_2CH_3 + C_2H_5^+ \rightarrow [C_6,H_{12},D_3,O]^+$					
$\downarrow -C_2H_4$					
$[C_4,H_8,D_3,O]^+$	MI	<1	29		71
m/z 78	CID	4	39		57
$CD_3CH_2O^+(H)CH_2CH_3$ From self-protonation	MI	<1	30		70
m/z 78	CID	3	36		61
$CH_3CH_2OH + CD_3CH_2^+ \rightarrow CH_3CH_2O^+(H)CH_2CD_3$		MI	4	29	67
m/z 78	CID	6	42		52
STATISTICAL RATIO		40	60		

7.4.3 Protonated Ethanol and Isotopomers

Labeled protonated ethanol, the lowest member of the series, was also produced by several reactions and the results were in good agreement with earlier reports **[16-18]** (see also Chapter 6). However, no matter how the protonated ethanol cations had been formed, see Table 7.3, identical results (within experimental error) were observed, all showing extensive H/D scrambling prior to either loss of C_2H_4 or H_2O among metastable ions. This behavior has already been rationalized in terms of a facile isomerization between the non-classical $[C_2H_4\cdots H\text{-}OH_2]^+$, and the classical form, $[CH_3CH_2OH_2]^+$, of protonated ethanol, and need not be discussed further; for more details see references 16-18 (see also Chapter 6).

Table 7.3. Metastable ion (MI) and partial collision induced dissociation (CID) mass spectra of protonated ethanol and isotopomers.

Reaction		Ion peak abundance m/z			
		19	20	21	22
$(C_2H_5)_2O + CH_3CD_2^+ \rightarrow [C_6,H_{13},D_2,O]^+$					
$\downarrow -2C_2H_4$					
$[C_2,H_5,D_2,O]^+$	MI	54	37	9	
m/z 49	CID	33	53	14	
$CH_3CD_2OCH_2CH_3 + CH_3CH_2^+ \rightarrow [C_6,H_{13},D_2,O]^+$					
$\downarrow -2C_2H_4$					
$[C_2,H_5,D_2,O]^+$	MI	53	37	10	
m/z 49	CID	33	53	14	
$D_2O + CH_3CH_2^+ \rightarrow [C_2,H_5,D_2,O]^+$	MI	53	38	9	
m/z 49	CID	32	53	15	
$CH_3CD_2O^+(H)CH_2CH_3$ From self-protonation					
$\downarrow -C_2H_4$					
$[C_2,H_5,D_2,O]^+$	MI	50	40	10	
m/z 49	CID	33	52	15	
STATISTICAL RATIO		29	57	14	
$(C_2H_5)_2O + CD_3CH_2^+ \rightarrow [C_6,H_{12},D_3,O]^+$					
$\downarrow -2C_2H_4$					
$[C_2,H_4,D_3,O]^+$	MI	36	43	18	3
m/z 50	CID	15	50	31	4
$CD_3CH_2OCH_2CH_3 + C_2H_5^+ \rightarrow [C_6,H_{12},D_3,O]^+$					
$\downarrow -2C_2H_4$					
$[C_2,H_4,D_3,O]^+$	MI	28	46	21	4
m/z 50	CID	14	50	31	4
$CD_3CH_2^+ + H_2O \rightarrow [C_2,H_4,D_3,O]^+$	MI	27	46	23	4
m/z 50	CID	13	50	34	3
STATISTICAL RATIO		11	51	34	3

In summary, labeled triethyloxonium ions, M_3^+, produced by reaction (7.2) display extensive H/D mixing only within the reactant ethyl group. This mixing is reproduced in the dissociation behavior of the $[M_3 - C_2H_4]^+$ and $[M_3 - (C_2H_4)_2]^+$ fragment ions. The last ion, a labeled $[C_2H_5OH_2]^+$ species, when produced by protonation of ethanol or by the reaction of ethyl ions with H_2O also showed complete H/D mixing prior to metastable dissociation. In marked contrast, if the ion corresponding to $[M_3 - C_2H_4]^+$ was produced by direct reactions of labeled ethyl cations with ethanol or by protonation of labeled diethylether, then ethene loss from such metastable ions shows only a small amount of H/D mixing. Four possibilities that could explain the above results will now be discussed.

7.4.4 H/D Mixing Within the Reactant Ethyl Cation

The CID mass spectra of $CD_3CH_2^+$ obtained from two different precursors, CD_3CH_2Br and $CD_3CH_2NO_2$, were identical, with m/z 17, CD_2H^+, and m/z 18, CD_3^+, in a ratio of 4 : 1 (the statistical ratio being 6 : 1) showing a certain degree of mixing, which in principle could have taken place both prior to and after the collisional excitation. Nevertheless, if the mixing in the ethyl cation took place before reaction with ROR′, the same degree of mixing should be observed for all the products irrespective of the ROR′ species. However (see Tables 7.1 and 7.2) this is not the case. In order to investigate this further, labeled ethyl cations were reacted with more ROR′ species, see Table 7.4, and it was found that the product ions are mixed in small and to different extents. For example metastable $CH_3O^+(H)CH_2CD_3$ loses CH_2CD_2 and $CHDCD_2$ in a ratio of 90 : 10 and $CH_3O^+(CH_3)CH_2CD_3$ loses the same two molecules in a ratio of 86 : 14, the statistical ratios

being 60 : 40. It should be noted moreover, that the ethene loss ratios were independent of the observation time for the metastable ion fragmentations, from 1 to 30 μs (see section 7.3)). These observations lead us to suggest that either the H/D mixing observed in the CID mass spectrum of the $CD_3CH_2^+$ cation is mostly post-collision, or (see below) that the reactants in the present ethyl cationization study have been misidentified.

According to the theoretical calculations **[9]** the energy required to scramble the H/D atoms in the labeled non-classical ethyl cation is 6-7 kcal/mol and so a considerable fraction of the non-classical ethyl cations will not have enough internal energy to interconvert with the classical form and so mix the H/D atoms, except when excess energy is provided by collisional activation. Rapid dissociation after collision would result in incomplete statistical mixing.

7.4.5 Misidentification of the Reactants

Although it was assumed that reaction (7.1) produced the ethylated cations, two other reactions, (7.4) and (7.5), must be considered.

$$ROR' + Et^+ \rightarrow RO^+(Et)R' \qquad (7.1)$$

$$ROR' + EtX^{+\bullet} \rightarrow RO^+(Et)R' + X^\bullet \qquad (7.4)$$

$$ROR'^{+\bullet} + EtX \rightarrow RO^+(Et)R' + X^\bullet \qquad (7.5)$$

Table 7.4. Metastable ion (MI) and partial collision induced dissociation (CID) mass spectra of various labeled $RO^+(Et)R'$ ions.

Reaction		Ion peak abundance			
		m/z	33	34	
$CH_3OH + CH_3CD_2^+ \rightarrow CH_3CD_2O^+(H)CH_3$		MI		98	2
m/z 63	CID.		95	5	
		m/z	33	34	
$CH_3OH + CD_3CH_2^+ \rightarrow CD_3CH_2O^+(H)CH_3$		MI		10	90
m/z 64	CID		14	86	
		m/z	47	48	
$CH_3OCH_3 + CH_3CD_2^+ \rightarrow CH_3O^+(CH_3)CD_2CH_3$	MI		96	4	
m/z 77	CID		89	11	
		m/z	47	48	
$CH_3OCH_3 + CD_3CH_2^+ \rightarrow CH_3O^+(CH_3)CH_2CD_3$	MI		14	86	
m/z 78	CID		15	85	
		m/z	61	62	63
$CH_3CH_2OCH_3 + CH_3CD_2^+ \rightarrow CH_3CH_2O^+(CD_2CH_3)CH_3$	MI		45	4	51
m/z 91	CID		50	4	46
		m/z	61	62	64
$CH_3CH_2OCH_3 + CD_3CH_2^+ \rightarrow CH_3CH_2O^+(CH_2CD_3)CH_3$	MI		6	31	63
m/z 92	CID		4	38	58

Because identical results were found when X = NO_2 or I, reaction (7.4) can be ruled out because the molecular ion of $CH_3CH_2NO_2^{+\bullet}$, m/z 75, is not present in its EI mass spectrum. In order to determine which of reactions (7.1) or (7.5) is thermodynamically favored, the difference $\Delta H_5 - \Delta H_1$ for the reactions was calculated. $\Delta H_5 - \Delta H_1$ = AE (Et^+ from EtX) - IE (ROR'). The appearance energy (AE) of Et^+ can be calculated from $C_2H_5X \rightarrow C_2H_5^+ + X^\bullet$ and using the values $\Delta H_f(C_2H_5I)$ = -2.2 kcal mol^{-1}, $\Delta H_f(C_2H_5NO_2)$ = -24.4 kcal mol^{-1}, $\Delta H_f(C_2H_5^+)$ = 216 kcal mol^{-1}, $\Delta H_f(I^\bullet)$ = 25.5 kcal mol^{-1} and $\Delta H_f(NO_2^\bullet)$ = 8 kcal mol^{-1} (all values from ref. 24), then AE = 244 kcal mol^{-1} for X = I and 248 kcal mol^{-1} when X = NO_2. It can be seen from Table 7.5 that reaction (7.1) is always energetically favored except for ROR'= CH_3OH.

Table 7.5. Appearance energy (AE) of the ethyl cation (from CH_3CH_2X) and Ionization energy (IE) of the ROR' species. All values from ref. 24.

Species	AE[a] kcal mol^{-1}	IE kcal mol^{-1}	$\Delta H_5 - \Delta H_1$[a]
$C_2H_5^+$ From CH_3CH_2I	244		
$C_2H_5^+$ From $CH_3CH_2NO_2$	248		
$CH_3CH_2OCH_2CH_3$		219	25[b], 29[c]
CH_3CH_2OH		241	3[b], 7[c]
CH_3OH		249	-5[b], -1[c]
CH_3OCH_3		231	13[b], 17[c]

a. See text for calculation.

b. When AE = 244 kcal mol^{-1}

c. When AE = 248 kcal mol^{-1}

7.4.6 Formation of a Complex of a Special Kind

With the non-classical form of the ethyl cation being the lower energy species [9], it is possible that the ROR' species would preferentially react with it. Diethylether reacting with a non-classical ethyl cation could form a triethyloxonium ion possessing a non-classical moiety which then could undergo an isomerization process (see below) which could give rise to the observed localized H/D mixing.

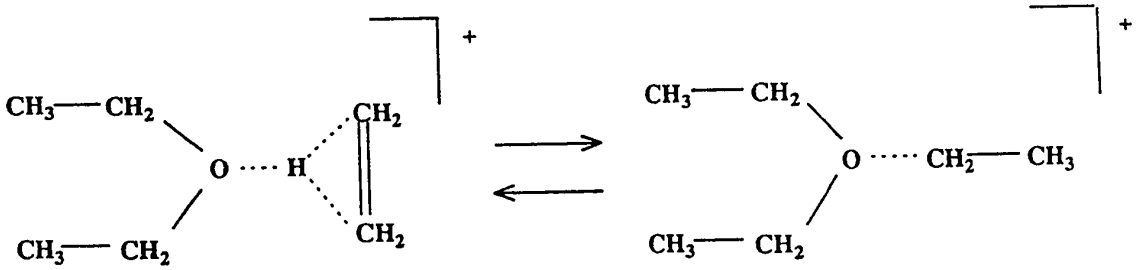

However this possibility must be excluded. Labeled triethyloxonium ions show extensive H/D scrambling only when they are produced via reaction (7.2), not by reaction (7.3). If the above reaction took place, the latter result would have to be explained by non-ergodic behavior, a rare observation, and unlikely in the present system because the metastable ion and CID mass spectra of the m/z 108, $[CD_3CD_2O(C_2H_5)_2]^+$ ions are identical, irrespective of the reaction used for their production, see Table 7.1.

Note also that all the other ROR′ species that were reacted with a labeled ethyl cation showed only a small degree of H/D mixing, which indicates that an isomerization process within the newly attached ethyl group cannot have occurred.

7.4.7 Reactivity Competition Between the High Energy (Classical) and Low Energy (Non-Classical) Forms of the Ethyl Cation

Table 7.4 shows that the observed degree of H/D mixing is small, but increases with increase of the size of R and R′. The exception, as described above, is for R = R′ =H. For example, when CH_3OH was reacted with $CD_3CH_2^+$ to form $CD_3CH_2O^+(H)CH_3$, the observed m/z 33 to m/z 34 ratio (losses of C_2D_3H and $C_2H_2D_2$ respectively) in the MI mass spectrum of the latter was found to be 10 : 90. When the same reaction was performed with CH_3CH_2OH, ionized labeled protonated diethylether was obtained, and the corresponding ethene losses giving m/z 47 and m/z 48 were in the ratio 12 : 88. When $CH_3CH_2OCH_3$ is the ROR′ species (R and R′ ≠ H) a ratio of 16 : 84 was observed for the metastable peaks at m/z 61 and 62, C_2D_3H and $C_2D_2H_2$ losses, respectively. Thus as the size of R and R′ is increased, the observed H/D mixing becomes greater. We propose that this result is best explained by different reactivities of the classical and non-classical forms of the ethyl cation. If R and R′ are relatively large, it becomes less easy for the non-classical form to react with the ROR′ species. Note that the observations did not change at the highest ion source pressures and so the inverse statement of the preceding sentence cannot apply i.e. collisional stabilization of a classical ethyl cation adduct should have been dependent on

total ion source pressure. Classical ethyl cations (which by virtue of their internal energy content will have randomized H/D positions before reaction with the substrate) can react with ROR' with less size constraint. The low energy (non-classical) $C_2H_5^+$ ions react most readily with small ROR' giving rise to the observed marked reduction in H/D positional mixing in the ethene lost from metastable adduct ions. This trend is clearly illustrated in Figure 7.1.

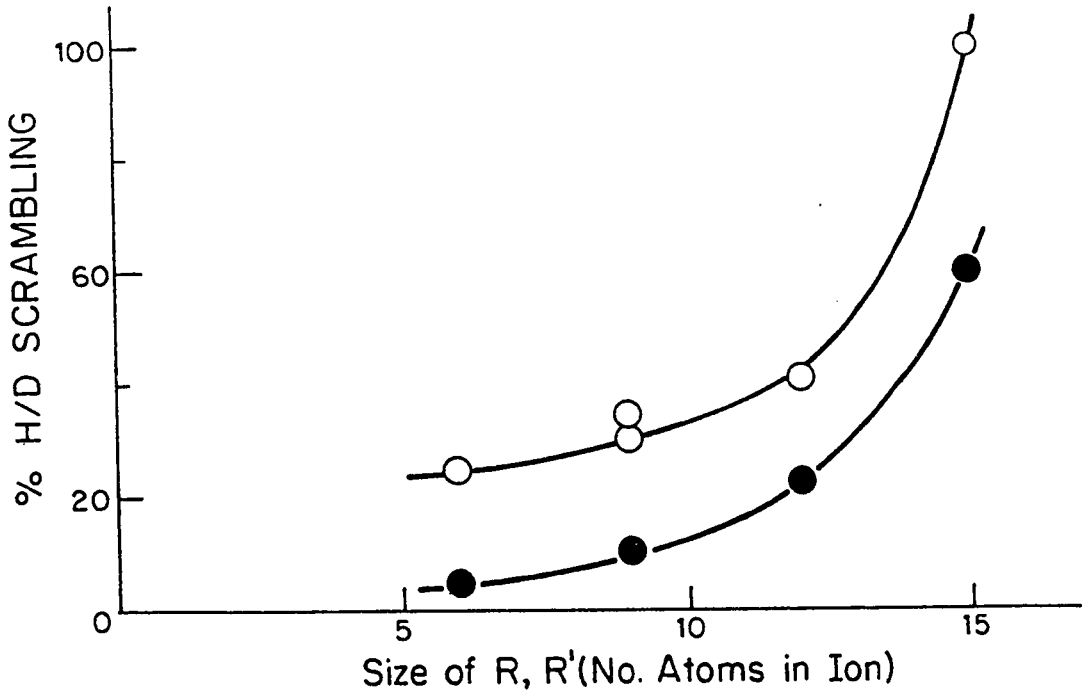

Figure 7.1. Mixing of H/D atoms in the ethene lost from labeled metastable $RR'O^+C_2H_5$ ions. The percentage mixing is expressed as the relative abundance of the C_2H_3D loss (when $CH_3CD_2^+$ is the reactant) or the C_2D_3H loss (when $CD_3CH_2^+$ is the reactant) over the corresponding statistical relative abundance i.e. 40.

Also note from Tables 7.1, 7.2 and 7.4 that for a given ROR′ species, a greater degree of H/D mixing is always observed when the latter was reacted with $CD_3CH_2^+$ rather than with $CH_3CD_2^+$. This may be explained by the non-classical form of $CH_3CD_2^+$ having a hydrogen ion in the bridge whereas for $CD_3CH_2^+$ a deuterium ion serves as the bridging species. If the non-classical form of $CH_3CD_2^+$ reacts more readily than that of $CD_3CH_2^+$ then relatively less H/D mixing will be observed for the former because a greater proportion of non-classical ethyl cations will have reacted with ROR′.

When R = R′ = C_2H_5 it was found that H/D mixing was nearly statistical in labeled triethyloxonium ions, see Table 7.1. It was therefore predicted that when R and R′ ≥ C_2H_5, extensive H/D mixing should always be observed. When $CH_3CH_2OCH(CH_3)_2$ was reacted with labeled ethyl cations, see Table 7.6, the resulting metastable m/z 119 and 120 ions first lose C_3H_6, producing ionized labeled protonated ethanol (m/z 77 and 78 respectively), for which the MI and CID mass spectra showed the expected extensive H/D mixing in the ethene loss (see Table 7.6), thus confirming the above prediction. However note that (see Table 7.6) in the metastable ion mass spectrum of $CH_3CH_2O^+(H)CH_2CD_3$ m/z 47 (loss of C_2D_3H) and m/z 48 (loss of $C_2D_2H_2$) were in a ratio of 53 : 47 (the statistical ratio is 40:60), showing a rather large isotope effect in favor of H^+ transfer. As expected this isotope effect became less important in the CID mass spectrum of the m/z 78 ions (see Table 7.6). This last argument also applies for the m/z 78 daughter ion obtained by ethene loss from labeled triethyloxonium ions which had been produced by the reaction between diethylether and $CD_3CH_2^+$ (see Table 7.2).

Table 7.6. *Metastable ion (MI) and partial collision induced dissociation (CID) mass spectra of labeled protonated diethylether ions produced from ethylated ethyl iso-propylether.*

Reaction	Ion peak abundance m/z			
	m/z	47	48	49
$C_2H_5OCH(CH_3)_2 + CH_3CD_2^+ \rightarrow C_2H_5O^+(CD_2CH_3)CH(CH_3)_2$				
m/z 119				
$\downarrow -C_3H_6$	MI	30	10	60
$CH_3CH_2O^+(H)CD_2CH_3$	CID	33	11	56
m/z 77				
STATISTICAL RATIO		60	40	
	m/z	47	48	50
$C_2H_5OCH(CH_3)_2 + CD_3CH_2^+ \rightarrow C_2H_5O^+(CH_2CD_3)CH(CH_3)_2$				
m/z 120				
$\downarrow -C_3H_6$	MI	18	16	66
$CH_3CH_2O^+(H)CH_2CD_3$	CID	19	20	61
m/z 78				
STATISTICAL RATIO		40	60	

REFERENCES - CHAPTER 7

1. H.H. Jaffé and S. Billets, ***J. Am. Chem. Soc.*** 94, 674 (1972).
2. P. Ausloos, R.E. Rebbert, L.W. Sieck and T.O. Tiernan, ***J. Am. Chem. Soc.*** 94, 8939 (1972).
3. J.H. Vorachek, G.G. Meisels, R.A. Geanangel and R.H. Emmel, ***J. Am. Chem. Soc.*** 95, 4078 (1973).
4. W.A. Lathan, W.J. Hehre and J.A. Pople, ***J. Am. Chem. Soc.*** 39, 808 (1971).
5. P.C. Hariharan, W.A. Lathan and J.A. Pople, ***Chem. Phys. Lett.*** 14, 385 (1972).
6. B. Zurawski, R. Ahlrichs and W. Kritzelnigg, ***Chem. Phys. Lett.*** 21, 309 (1973).
7. H. Lischka and H-J. Kohler, ***J. Am. Chem. Soc.*** 100, 5297 (1978).
8. K. Hirao and S. Yamabe, ***Chem. Phys.*** 89, 237 (1984).
9. (a) M-W. Wong, J. Baker, R.H. Nobes and L. Radom, ***J. Am. Chem. Soc.*** 109, 2245 (1987). (b) B. Ruscic, J. Berkowitz, L.A. Curtiss and J.A. Pople, ***J. Chem. Phys.*** 91, 114 (1989). (c) G. Trinquier, ***J. Am. Chem. Soc.*** 114, 6807 (1992).
10. C.A. Deakyne, M. Meot-Ner, C.L. Campbell, M.G. Hughes and S.P. Murphy, ***J. Chem. Phys.*** 84, 4958 (1986).
11. M. Iraki and C. Lifshitz, ***Int. J. Mass Spectrom. Ion Proc.*** 71, 245 (1986).
12. S.T. Graul and R.R. Squires, ***Int. J. Mass Spectrom. Ion Processes.*** 94, 41 (1989).
13. S. Wei, W.B. Tzeng, R.G. Keesee and A.W. Jr Castleman, ***J. Am, Chem. Soc.*** 113, 1960 (1991).
14. M. Iraki and C. Lifshitz, ***Int. J. Mass Spectrom. Ion Processes.*** 88, 45 (1989).

REFERNCES - CHAPTER 7

15. (a) D.J. Swanton, D.C.J. Marsden and L. Radom, ***Org. Mass Spectrom.*** 26, 227 (1991). (b) G. Bouchoux and Y. Hopilliard, ***J. Am. Chem. Soc.*** 112, 9110 (1990).

16. M. Sirois, M. George and J.L. Holmes, Submitted.

17. C. Wesdemiotis, A. Fura and F.W. McLafferty, ***J. Am. Soc. Mass Spectrom.*** 2, 459 (1991).

18. A.G.Harrison, ***Org. Mass Spectrom.*** 22, 637 (1987).

19. P.C. Burgers, J.L Holmes, A.A. Mommers, J.E. Szulejko, and J.K. Terlouw, ***Org. Mass Spectrom.*** 19, 442 (1984).

20. J.K. Terlouw, P.C. Burgers and J.L. Holmes ***Org. Mass Spectrom.*** 14, 387 (1979).

21. J. March, ***Advanced Organic Chemistry 3rd edition***, Wiley-Interscience, New-York (1985).

22. A. Streitwieser Jr. and C.H. Heathcock, ***Introduction to Organic Chemistry 3rd edition***, MacMillan Publishing Company, New-York (1985).

23. W. Wagner, H. Heimbach and K. Levsen, ***Int. J. Mass Spectrom. Ion Phys.*** 36, 125 (1980).

24. S.G. Lias, J.E. Bartmess, J.F. Liebman, J.L. Holmes, R.D. Levin and W.G. Mallard, ***J. Phys. Chem. Ref. Data,*** 17, Suppl. 1 (1988).

CHAPTER 8

HOMOLOGOUS HYDROGEN BRIDGED INTERMEDIATES $R_1R_2O\bullet\bullet\bullet H\bullet\bullet\bullet C(O)R_3^{+\bullet}$ FROM IONIZED β-HYDROXYETHERS

J. Am. Chem. Soc. 114, 2017, (1992)

J. Am. Chem. Soc. Submitted

8.1 Overview

This Chapter concerns the experimental investigation of the rearrangement of β-hydroxy alkyl ethers into potentially stable hydrogen bridged complexes. It was found that molecular ions of the form $R_1OCH(R_2)CH(OH)R_3$ yield protonated ethers $R_1O^+(H)R_2$ via intermediates of the type $R_1R_2O\bullet\bullet\bullet H\bullet\bullet\bullet C(O)R_3^{+\bullet}$. The metastable molecular ion of 1-methoxy-2-propanol provides a typical example, dissociating to produce protonated dimethyl ether and the acetyl radical, with a small kinetic energy release ($T_{0.5}$ = 6.5 meV). By varying the alkyl groups (R_1, R_2 and R_3) it was shown that this rearrangement process is general.

8.2 Introduction

The interpretation of mass spectra **[1]** has made great progress over the past decade, as experimental methods have been developed for assigning structures to organic ions in

the gas phase [2]. In parallel, and often in concert [3], developments in ab initio molecular orbital theory calculations have progressed from the accurate determination of relative ground state energies for ions [4] to a complete description of the potential surface for a small ion and its fragments (e.g. $CH_3OH^{+\bullet}$ [5]). Moreover, the use of ab initio calculations has revealed that ions of unconventional structure can exist as stable, isolated species in the gas phase. This Chapter addresses the fragmentation behavior of some ions which can be well described by the introduction of hydrogen bridged ions as intermediate species, in which a molecule and a free radical are formally bound by a proton lying between electronegative centres. That such hydrogen bridged ions may play an important role in the dissociation behavior of organic ions was clearly formulated by Morton [6] in 1982. In order to explain the production of protonated dimethyl ether from metastable ionized 2-methoxyethanol, the following mechanism was proposed:

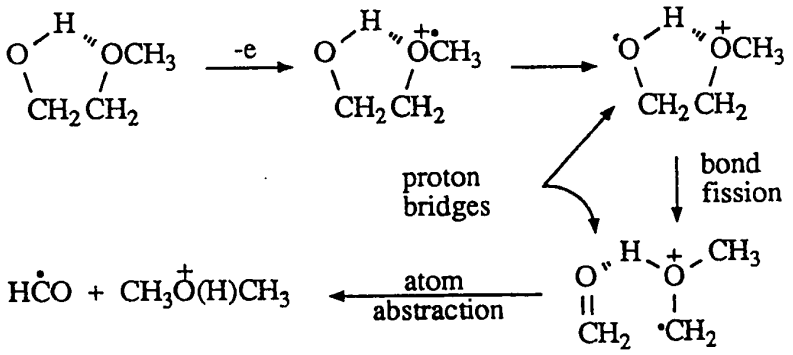

A key feature of the mechanism is the idea that the hydrogen bond in the neutral molecule plays a key role in the fragmentation of its molecular ion. Although this mechanism must now be substantially revised in light of recent observations [7] the results

of which are also considered in this Chapter, the original concept has been widely adopted.

It is appropriate briefly to review recent work in which H bridged odd electron ions have been proposed. In particular, emphasis will be given to cases where such a complex was a required feature of the analysis of experimental results and/or where it was only introduced as a result of theoretical calculations in order to provide an alternative mechanistic possibility.

In general, mechanisms for the rearrangement of molecular ions into hydrogen bridged intermediates prior to dissociation, can be described by two types of energy surfaces. (1) In which the energy barrier for the rearrangement of the molecular ion into the H-bridged complex is lower than the threshold energy level of products and (2) where the energy barrier giving rise to to the formation of the H-bridged species is that of the rate-determining transition state.

For (1), the evidence for the existence of the energetically stable hydrogen bridged intermediate could be obtained from mass spectrometry based experiments and energetic measurements.

For (2), the involvement of stable H-bridged intermediates is much more difficult to determine unambigously by experiments and so the ab initio theoretical calculations can provide particularly valuable information. For example, a theoretical investigation of the

metastable fragmentation of ionized methyl acetate **[8]** were required to show that the complex $CH_3C{=}O{\bullet\bullet\bullet}H{\bullet\bullet\bullet}OCH_2^{+\bullet}$ may be the key intermediate in the formation of CH_3CO^+ and $^{\bullet}CH_2OH$. A study **[9]** of the metastable dissociations of methyl carbamate radical cations, $H_2NCOOCH_3^{+\bullet}$, using the information obtained from mass spectrometry experiments in concert with ab initio molecular orbital theory calculations, showed that the hydrogen bridged radical cation $H_2NC{=}O{\bullet\bullet\bullet}H{\bullet\bullet\bullet}O{=}CH_2^{+\bullet}$ was a stable species and was the intermediate in the spontaneous unimolecular dissociations of methyl carbamate ions. From a combination of mass spectrometry based experiments and high level molecular orbital theory calculations, Burgers et al. **[10]** have proposed that the metastable generation of $CH_3OH_2^+$ from ionized 1,2-ethanediol proceeds via a series of O•••H•••O hydrogen bridged radical cations.

Due to the difficulty of providing direct evidence for the existence of stable H-bridged intermediates, their speculative introduction into fragmentation mechanisms must be treated with caution. Nevertheless, in this Chapter the experimental evidence for the existence of stable O•••H•••C complexes as important intermediates in the metastable dissociations of a series of β-hydroxyethers is reported.

8.3 Experimental

Metastable ion (MI), collision induced dissociation (CID) and collision induced dissociative ionization (CIDI) mass spectra were recorded using the VG Analytical ZAB-2F

mass spectrometer, modified as described elsewhere **[11]** (see also Chapter 2). For CID and CIDI experiments, helium was used as target gas. Appearance energy (AE) values were measured with energy-selected electrons using an apparatus comprising an electostatic electron monochromator and minicomputer data system **[12]**.

1-Methoxy-2-butanol, 1-methoxy-2-pentanol, 2-methoxy-3-butanol, 1-ethoxy-2-propanol and labeled compounds were synthesized by standard procedures. The OD labeled species were prepared in the inlet system and ion source of the mass spectrometer by exchange with excess D_2O.

8.4 Results and Discussion

Metastable dissociation of the molecular ions of β-hydroxyethers, of general formula $[R_1OCH(R_2)CH(OH)R_3]^{+\bullet}$ where $R_1 = CH_3$, C_2H_5, $R_2 = H$, CH_3, $R_3 = H$, CH_3, C_2H_5, C_3H_7, as well as some of their deuterium labeled isotopomers, have been studied through their mass spectra and energetic measurements. The above metastable species all fragmented to produce protonated ethers with small kinetic energy releases, results that can be rationalized by introducing hydrogen bridged intermediates of the type $[R_1R_2O\bullet\bullet\bullet H\bullet\bullet\bullet C(O)R_3]^{+\bullet}$. The experimental evidence supporting the existence of the latter complexes will now be discussed in detail.

8.4.1 1-Methoxy-2-Propanol

The metastable ion (MI) mass spectrum of ionized $CH_3OCH_2CH(OH)CH_3$, **1**, contains an intense peak at m/z 47, $C_2H_7O^+$, and two weak signals at m/z 71 and 72 (see Table 8.1). The kinetic energy release, calculated from the half height width of the major metastable peak, was small, $T_{0.5}$ = 6.5 meV. The intensity of the molecular ion of **1**, m/z 90, is only 0.8% of the base peak, m/z 45, but the metastable ion peak is relatively quite unusually intense, having an abundance 7% of m/z 90. The intensity of this metastable peak increases significantly when collision gas is admitted and m/z 45 becomes the only significant collision generated fragment ion. That the $C_2H_7O^+$ fragment ion is protonated dimethyl ether was confirmed by two types of experiment. First, the metastable ion mass spectrum of the $C_2H_7O^+$ ion showed a broad dished peak at m/z 31, CH_2OH^+, having a shape identical with that from the MI mass spectrum of protonated dimethyl ether **[13]**. The identity of the accompanying neutral $C_2H_3O^\bullet$ fragment was determined from its collision induced dissociative ionization (CIDI) mass spectrum (see Chapter 4) and was identical with that of the radical produced in the dissociation of ionized biacetyl, showing it to have the structure, $CH_3CO^\bullet$. **[14]**

The second experiment was to measure the appearance energy (AE) of the m/z 47 ion, 9.54 ± 0.05 eV, using energy selected electrons (see section 8.3), with $\Delta H_f(CH_3OCH_2CH(OH)CH_3)$ = -97 kcal mol^{-1} **[15]** and $\Delta H_f(CH_3CO^\bullet)$ = -6 kcal mol^{-1} **[16]**, the value for $\Delta H_f(C_2H_7O^+)$ = 129 kcal mol^{-1}, was thus in excellent agreement with the

literature value of 130 kcal mol^{-1}, derived from the proton affinity of dimethyl ether **[16]**.

A possible mechanism for this reaction leading to protonated dimethyl ether, involving hydrogen bridged intermediates is shown below.

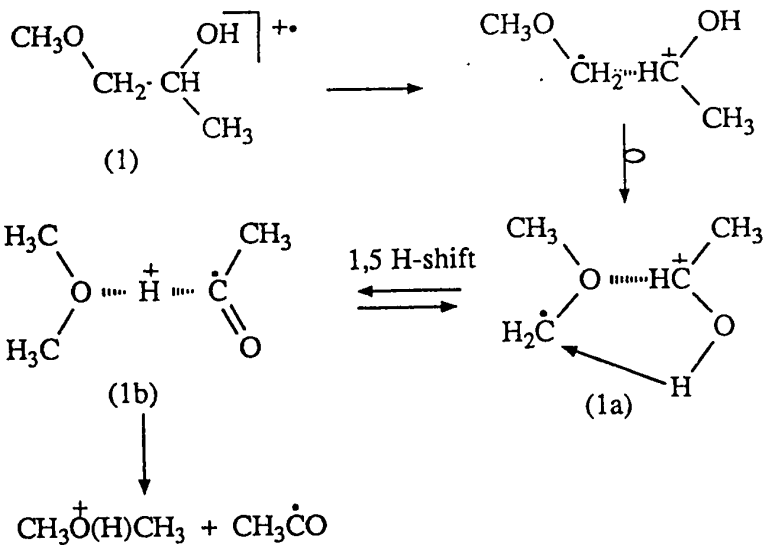

Scheme 8.1

The first step involves the formation of a complex between the CH_3CHOH^+ ion and a methoxymethyl radical which (by analogy with the proposed behavior of ionized neopentyl methyl ether **[17, 18]**), can form a more strongly bound intermediate involving the more electronegative O atom. A reversible 1,5-H shift in **1a** leads to a hydrogen bridged complex **1b** which can readily fragment to the products.

Table 8.1. Metastable ion (MI) mass spectra of β-hydroxyether radical cations.

Compound	Fragment ion abundance at m/z														
	47	48	50	58	59	61	62	63	71	72	73	75	76	77	100
$CH_3OCH_2CH(OH)CH_3$	91								5	4					
$CH_3OCH_2CH(OD)CH_3$		96								2	2				
$CH_3OCH_2CD(OH)CH_3$		98								1	1				
$CD_3OCH_2CH(OH)CH_3$			98									2			
$CH_3OCH_2CH_2OH$	56			44											
$CH_3OCH_2CH_2OD$		59		14	27										
$CH_3OCH_2CH(OH)C_2H_5$	34			22									44		
$CH_3OCH_2CH(OD)C_2H_5$		32		18	11									39	
$CH_3OCH_2CH(OH)C_3H_7$[a]	34														66
$CH_3OCH(CH_3)CH(OH)CH_3$				7		93									
$CH_3OCH(CH_3)CH(OD)CH_3$				3	9	88									
$CH_3CH_2OCH_2CH(OH)CH_3$				9		91									
$CH_3CH_2OCH_2CH(OD)CH_3$				3	10	87									
$CH_3OCH_2CH(OCH_3)CH_3$					100										
$CD_3OCH_2CH(OCD_3)CH_3$						54	41	5							

(a) Only the two major MI signals are given. See text for more detail.

To test the appropriatness of the above mechanism, some deuterium labeled compounds were examined. Ionized $CH_3OCH_2CH(OD)CH_3$, **1c**, showed only m/z 48 in its MI mass spectrum and this fragment ion in turn displayed m/z 31 (CH_3D loss) and m/z 32 (CH_4 loss), in a ratio of 63 : 37 in its MI mass spectrum. For these ions then, the label atom is on carbon, not attached to oxygen, because metastable $CH_3O^+(D)CH_3$ ions only lose CH_4 (see Table 8.4). In marked contrast, the m/z 48 ion derived from ionized $CH_3OCH_2CD(OH)CH_3$, **1d**, very largely loses CH_4 in its MI mass spectrum, the ratio m/z 32 : m/z 31 being ca. 93 : 7. Thus for this m/z 48 ion, the label atom must be on oxygen. In terms of the above mechanism then, the labeled intermediate ions for the C deuterated compound **1d** would be

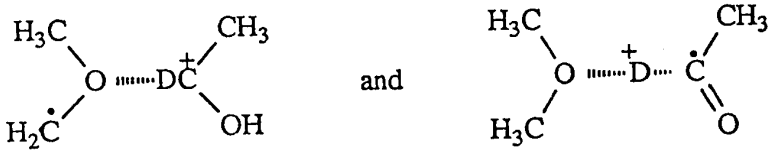

i.e. with the label atom in the bridging position.

In addition to the above, ionized $CD_3OCH_2CHOHCH_3$, **1e**, showed in its MI mass spectrum, an intense peak at m/z 50 corresponding to $CD_3O^+(H)CH_3$ which in turn displayed broad metastable peaks at m/z 31 and 33 in its MI mass spectrum, in a ratio of 42 : 58. Similarly to the above, we propose that the hydrogen bridged intermediates leading to the generation of $CD_3O^+(H)CH_3$ from **1e** are:

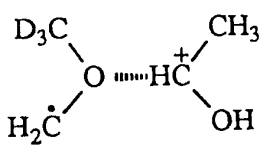

and

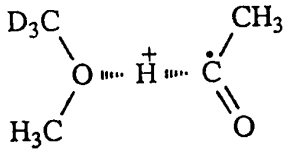

The evidence for the reversibility of the 1,5-H shift in the H-bridged complex **1a** (see Scheme 8.1) was obtained from the CID mass spectra of ions **1, 1c** and **1e**. The CID mass spectrum of ionized **1**, contains an intense peak at m/z 47, $CH_3O^+(H)CH_3$, together with a small m/z 45, $CH_3CHOH^{+\bullet}$, in a ratio of ca. 80 : 20. Note that the MI contribution of m/z 47 was subtracted and therefore the above ratio is a real indication that m/z 47 is four times more intense than m/z 45 in the CID mass spectrum of ionized **1**. In the CID mass spectra of ionized **1c** and **1e**, the peak at m/z 45 (which arises from the fragmentation of **1a**) was divided into m/z 45 and 46 signals of equal intensity. This observation clearly indicates that the 1,5-H shift in **1a** leading to **1b** is reversible. It also shows that the molecular ions have rearranged to either **1a** or **1b** prior to fragmentation. Note however, that because m/z 47 is relatively more intense than m/z 45, the H-bridged complex **1b** is likely to be more stable than **1a**.

In order for these intermediates to have validity in this mechanism, their energies must lie below the dissociation limit to the products. Moreover, at least one of them must have an energy appreciably below that of the molecular ion in order that the species may have a sufficient density of states for the fragmentation reaction to take place in the metastable ion (μs) time frame. The ΔH_f of ionized **1**, 118 kcal mol^{-1}, was determined from the ionization energy (IE), 9.32 ± 0.05 eV. There is no thoroughly reliable empirical

method for the estimation of ion-dipole complex energies but the relationship of McMahon and Larson **[19]** (see also section 3.4.1) can be used to estimate a fair ΔH_f value for a hydrogen bridged ion **[20]**. Using the following data **[16]**, $\Delta H_f(CH_3CHO^+)$ = 196 kcal mol^{-1}, $\Delta H_f(H^+)$ = 366 kcal mol^{-1} and $\Delta H_f(CH_3CO^{\bullet})$ = -6 kcal mol^{-1} one obtains $PA(CH_3CO^{\bullet})$ = 164 kcal mol^{-1}. Using the latter value with $PA(CH_3OCH_3)$ = 191 kcal mol^{-1}, $\Delta H_f(CH_3O^+(H)CH_3)$ = 130 kcal mol^{-1} and $\Delta H_f(CH_3CO^{\bullet})$ = -6 kcal mol^{-1}, the value for **1b** (see above) is 104 ± 2 kcal mol^{-1} using the equation of McMahon and Larson. Thus, see Figure 8.1, the proposed lowest energy species, **1b**, is attained after the initial ion-radical complex has undergone an internal rotation after which the specific 1,5-H transfer from oxygen to methylene takes place. Dissociation of the complex **1b**, requires 19 kcal mol^{-1} (see Figure 8.1).

The conclusions that have been described above for this compound do not represent an isolated example of ion fragmentation behavior, but can be taken as a general mechanism for β-hydroxyethers. Table 8.1 shows the MI mass spectra for a series of six other such ionized compounds in which the same type of fragmentation occurs also with small kinetic energy releases, to produce protonated ethers.

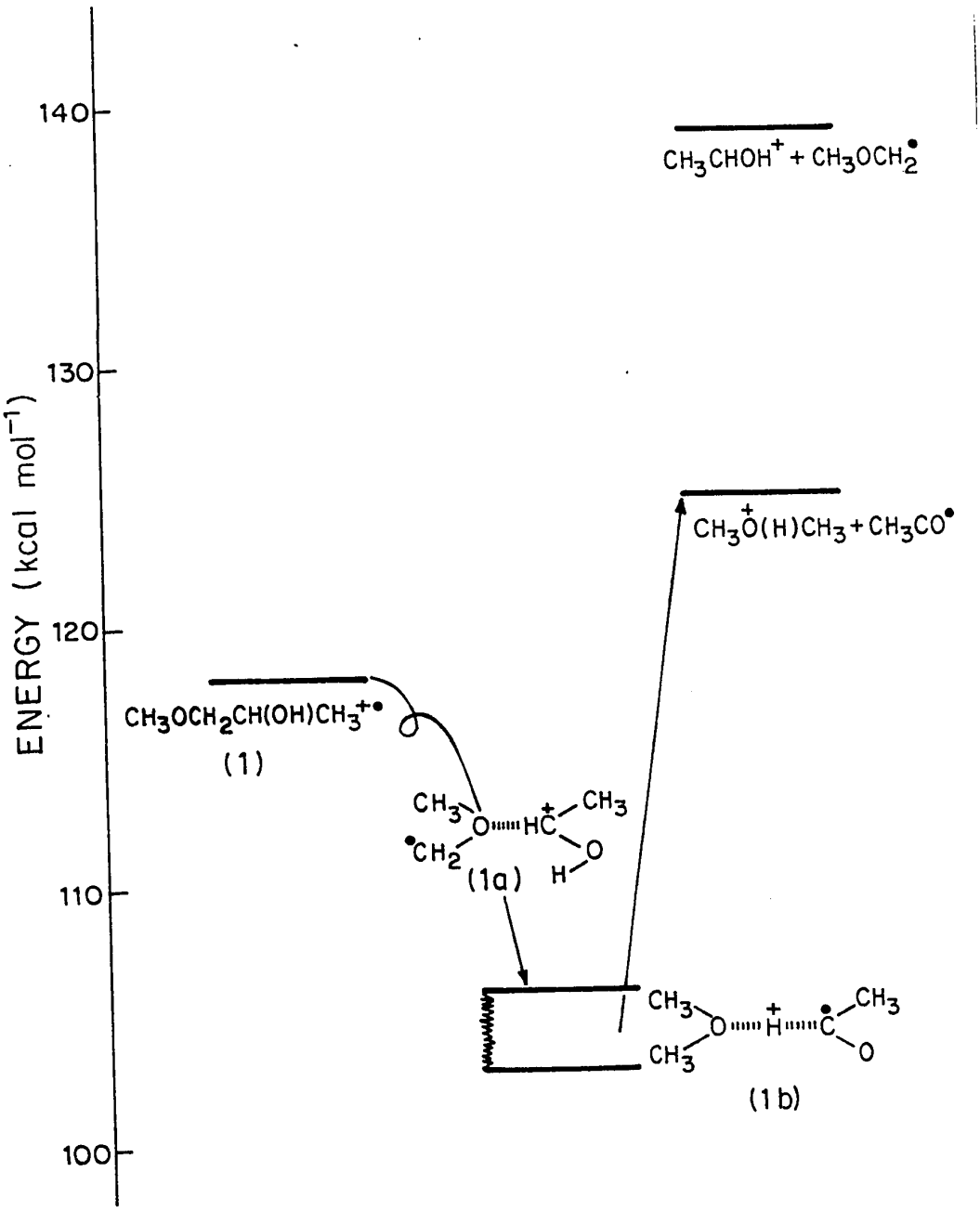

Figure 8.1. Energy diagram for the production of protonated dimethyl ether from metastable ionized 1-methoxy-2-propanol.

8.4.2 2-Methoxyethanol

For 2-methoxyethanol, the Morton mechanism (see section 8.2) predicts that the hydroxyl hydrogen becomes the proton in the product ion and that the second methyl group contains a hydrogen atom from the 1-methylene group and indeed, an indication that this mechanism may be incorrect was the report **[21]** that $CH_3O^+(D)CH_3$ was generated from $CH_3OCH_2CD_2OH^{+\bullet}$. However a mechanism explaining this marked difference was not specifically addressed.

Compound **2**, $CH_3OCH_2CH_2OH$, is the simplest β-hydroxyether and shows two intense peaks in its MI mass spectrum, corresponding to losses of $HCO^\bullet$ and H_2O. The kinetic energy releases were 16.5 and 18.7 meV respectively. It is necessary to describe the latter dissociation channel in some detail because it has a significant bearing on the discussion concerning the $HCO^\bullet$ loss which follows.

8.4.2.1 Loss of H_2O

The fragment ion m/z 58, $C_3H_6O^{+\bullet}$, produced by loss of H_2O, was shown to be a mixture of ionized oxetane (ΔH_f = 204 kcal mol^{-1} **[16]**) and methyloxirane (ΔH_f = 213 kcal mol^{-1} **[16]**), as described below.

The appearance energy (AE) values for the three dissociations of lowest energy

requirement, m/z 58, $C_3H_6O^{+\bullet}$ (H_2O loss), m/z 47, $CH_3O^+(H)CH_3$ ($HCO^\bullet$ loss) and m/z 45, $CH_3OCH_2^+$ ($CH_2OH^\bullet$ loss) were measured using energy selected electrons **[12]**. The AE values were 10.00, 9.96 and 10.42, all ± 0.05 eV, respectively. The respective calculated threshold AE values using established thermochemical data **[22]**, were 10.10 eV (assuming ionized oxetane as the product ion), 9.90 and 10.30 eV, all very close to the observed thresholds. Thus the three reactions take place close to their minimum required energies. The kinetic energy releases, $T_{0.5}$, for the first two (metastable) reactions, calculated from the half height width of the Gaussian type metastable peaks were 18.7 amd 16.5 meV respectively, in keeping with the reactions proceeding without a reverse energy barrier.

The m/z 58, $C_3H_6O^{+\bullet}$ ion displayed an MI mass spectrum with a broad, flat-topped peak at m/z 43 ($T_{0.5}$ = 710 meV) together with a Gaussian type peak at m/z 30 and an intense $H^\bullet$ loss peak. The broad peak is characteristic **[23]** only of either ionized methylvinyl ether (ΔH_f = 182 kcal mol^{-1} **[16]**) or methyloxirane, $CH_3\overline{CHCH_2O}$.

The CID mass spectrum of the $C_3H_6O^{+\bullet}$ daughter ions generated from 2-methoxyethanol are given in Table 8.2 together with those of reference ions from appropriate compounds. The metastably generated product ions from 2-methoxyethanol have a CID mass spectrum compatible with a mixture of ionized oxetane and methyloxirane, noting that oxetane is four times more collision sensitive than methyloxirane.

The proof that the second $C_3H_6O^{+\bullet}$ ion is methyloxirane comes from examination of deuterium labeled methoxyethanols. First, ionized metastable $CH_3OCH_2CD_2OH$ loses only H_2O showing that the 1-methylene hydrogens are not involved. Next the losses of H_2O, HDO and D_2O were examined for ionized metastable $CD_3OCH_2CH_2OH$, **2a**, $CH_3OCD_2CD_2OH$, **2b**, and $CH_3OCD_2CD_2OD$, **2c**. For the first isotopomer, the ratio 32 : 100 : 35 (for m/z 61, 60 and 59) is close to the ratio for randomisation of the three D and three H atoms, 33 : 100 : 33. However, complete atom scrambling is not taking place; the H_2O : HDO : D_2O losses for $CH_3OCD_2CD_2OH$ and $CH_3OCD_2CD_2OD$, 100 : 82 : 10 and 47 : 100 : 26 respectively, are significantly different from the appropriate random loss ratios, 100 : 33 : 16 and 33 : 100 : 33, respectively.

For the **2a** and **2b** isotopomers, the MI and CID mass spectra of the three water loss peaks were examined. For **2a**, the MI and CID mass spectra of the $[M - H_2O]^{+\bullet}$ ion, (ion source or metastably generated) were identical with those reported for $CD_3\overline{CHCH_2O}$ by Turecek and McLafferty **[24]** and the same result was obtained for $[M - HDO]^{+\bullet}$ ion from **2b**, which was identical with $CH_3\overline{CDCD_2O}$. The HDO loss ion, m/z 60, from **2a** showed no broad peak in its MI mass spectrum, whereas its CID mass spectra for ion source or metastably generated ions, displayed major peaks at m/z 30 and 32 which are compatible with ionized oxetane of the structure $\overline{CD_2CH_2CH_2O}$. If the H_2O loss involved randomization of the 6 H atoms, the m/z 60 ions would have been a mixture of $\overline{CD_2CH_2CH_2O}$ and $\overline{CHD\text{-}CH_2\text{-}CHDO}$. The D_2O loss peak, m/z 59, from **2a** could not be examined due to interference from artifact signals.

Table 8.2 *Collision Induced dissociation Mass Spectra of $C_3H_6O^{+\bullet}$ ions from $CH_3OCH_2CH_2OH$, methyl oxirane, methylvinyl ether and oxetane. Numbers in parentheses indicate peaks arising in part from metastable ions.*

	m/z											
$C_3H_6O^{+\bullet}$ ions from	13	14	15	26	27	28	29	30	31	41	42	43
$CH_3OCH_2CH_2OH$; ion source	-	1	2	8	15	43	19	(39)	9	-	3	(9)
$CH_3OCH_2CH_2OH$; metastable	-	1	1	7	13	49	17	(37)	8	-	2	2
$CH_3\overline{CHCH_2O}$; ion source	1	2	7	7	18	22	17	(14)	13	1	13	(59)
$CH_3OCH{=}CH_2$; ion source	1	2	8	5	18	15	15	(4)	15	2	2	(29)
$\overline{CH_2CH_2CH_2O}$; ion source	-	1	1	6	9	53	22	(31)	5	-	1	2

The relative cross section for methyl oxirane and oxetane are 1 : 4

Generation of $CH_3\overline{CHCH_2O}^{+\bullet}$ must take place via specific loss of water involving the OH group and a 2-methylene hydrogen atom but more significantly, the above results show that for this reaction channel, the $CH_3OCH_2CH_2OH^{+\bullet}$ do not undergo any significant loss of positional identity of H atoms prior to that fragmentation. Rather the apparent loss of positional identity of H atoms is due to two competing H_2O loss reactions of comparable importance.

8.4.2.2 Loss of HCO$^{\bullet}$

That the m/z 47 fragment ion from $CH_3OCH_2CH_2OH^{+\bullet}$ is protonated dimethyl ether is shown (i) by the AE of the ion and the small accompanying kinetic energy release (see above) and (ii) by its dissociation characteristics, namely the broad flat-topped metastable peak at m/z 31 (CH_4 loss), $T_{0.5}$ = 830 meV (800 meV **[25]**) and the CID mass spectrum (Table 8.3).

Various metastable isotopomeric ions were studied and they all show specific losses: $CD_3OCH_2CH_2OH^{+\bullet}$ and $CH_3OCH_2CH_2OD^{+\bullet}$, loses HCO$^{\bullet}$, whereas $CH_3OCD_2CD_2OH^{+\bullet}$, $CH_3OCD_2CD_2OD^{+\bullet}$ and $CH_3OCH_2CD_2OH^{+\bullet}$, eliminate DCO$^{\bullet}$. Thus for ions generated near threshold, complete mixing of all H and D atoms does not precede molecular ions' fragmentation and one H (or D) from the 1-methylene carbon is always lost.

Table 8.3 *Low mass (m/z 14-18) region of the Collision Induced Dissociation mass spectra of isotopomeric $CH_3O^+(H)CH_3$ ions.*

Ion	m/z 14	15	16	17	18
$CH_3O^+(H)CH_3$	8	90	2		
$CH_3O^+(D)CH_3$	7	91	2		
m/z 48 from $CH_3OCH_2CD_2OH$	10	85	5		
$CH_3O^+(H)CD_3$	6	20	12	9	44
m/z 50 from $CD_3OCH_2CH_2OH$	3	10	39	40	8.5
m/z 50 from $CH_3OCD_2CD_2OD$	3	8	39	41	8.5
m/z 50 from $CH_3OCD_2CD_2OH$	2.5	21	53	22	1
$CH_3O^+(H)CH_2D$	8	43	46	3	
m/z 48 from $CH_3OCH_2CH_2OD$	8	43	47	3	

The MI mass spectra of the protonated dimethyl ethers produced from labeled 2-methoxyethanols are shown in Table 8.4 from which it can be readily seen that the hydroxyl hydrogen atom in **2** becomes a methyl hydrogen in the $CH_3O^+(H)CH_3$ while the 1-methylene hydrogen is attached to oxygen in the product. It should also be noted that there is no loss of positional identity of H atoms prior to the loss of formyl radical e.g. the $[M - HCO]^+$ ion from $CD_3CH_2CH_2OH^{+\bullet}$ is exclusively $CD_3O^+(H)CH_3$ and not a mixture of $CD_2HO^+(H)CH_2D$ and $CD_3O^+(H)CH_3$.

The CID mass spectra of the metastably formed product ions from the above isotopomers are given in Table 8.3. Only the m/z 14-18 regions are presented; the more intense peaks at m/z 28-34 contain overlapping contributions from adjacent masses and so are much less informative than the low mass region, which in the unlabeled ion consists almost wholly of CH_3^+. It can immediatly be inferred from the first entry in Table 8.4 that $CH_3OCH_2CD_2OH^{+\bullet}$ produces $CH_3O^+(D)CH_3$ and not $CH_3O^+(H)CH_2D$. This is opposite to the original prediction of Morton, but it is in agreement with the earlier report **[21]**.

Considering the results from the MI mass spectra of the ion source generated [M - HCO]$^+$ ions, one would expect the CID mass spectrum of the metastably generated $CD_3O^+(H)CH_3$ ion to be the same as that of the reference ion prepared by protonation of CD_3OCH_3, but instead it is a mixture of $CD_3O^+(H)CH_3$ and $CD_2HO^+(H)CH_2D$. This observation indicates that the CH_3 hydrogen, the 2-methylene hydrogens and the O-H hydrogen lose positional identity (in the metastable 2-methoxyethanol ions only) prior to fragmentation (this is in keeping with a reversible H-shift in the scheme proposed below), unlike the H_2O loss channel. Hence the H_2O loss and HCO$^\bullet$ processes do not involve a common intermediate and any proposed mechanism for HCO$^\bullet$ from metastable ionized 2-methoxyethanol must take into account the following:

(i) the hydroxyl hydrogen atom becomes attached to the C-2 carbon atom;

(ii) one of the C-1 hydrogen atoms appears at the CH_3-O oxygen atom;

(iii) the CH_3-O, the 2-methylene and O-H hydrogen atoms become virtually positionally indistinguishable, but the 1-methylene hydrogens are not involved in the scrambling

processes.

Table 8.4. Metastable ion (MI) mass spectra of protonated dimethyl ethers.

Ion	m/z			
	31	32	33	34
$CH_3O^+(H)CH_3$	100			
$CH_3O^+(D)CH_3$	-	100		
m/z 48 from $CH_3CH_2CD_2OH$	-	100		
m/z 48 from $CH_3OCH_2CD(OH)CH_3$	7	93		
$CH_2DO^+(H)CH_3$	62	38		
m/z 48 from $CH_3OCH_2CH_2OD$[a]	~55	~45		
m/z 48 from $CH_3OCH_2CH(OD)CH_3$		63	37	
m/z 48 from $CH_3OCH_2CH(OD)C_2H_5$	40	60		
$CD_3O^+(H)CH_3$	42	-	58	
m/z 50 from $CD_3OCH_2CH_2OH$	43	-	57	
$CD_3O^+(D)CH_3$	-	42	-	58
m/z 51 from $CH_3OCD_2CD_2OD$	-	43	-	57

(a) Peak intensities uncertain due to artefact signals.

Therefore, considering these three points and because ionized 2-methoxyethanol displays parallel behavior to that of 1-methoxy-2-propanol (production of protonated dimethyl ether), we propose that the following Scheme (similarly to Scheme 1) is plausible, in order to explain the formation of the protonated dimethyl ether ions from ionized 2-methoxyethanol and its isotopomers.

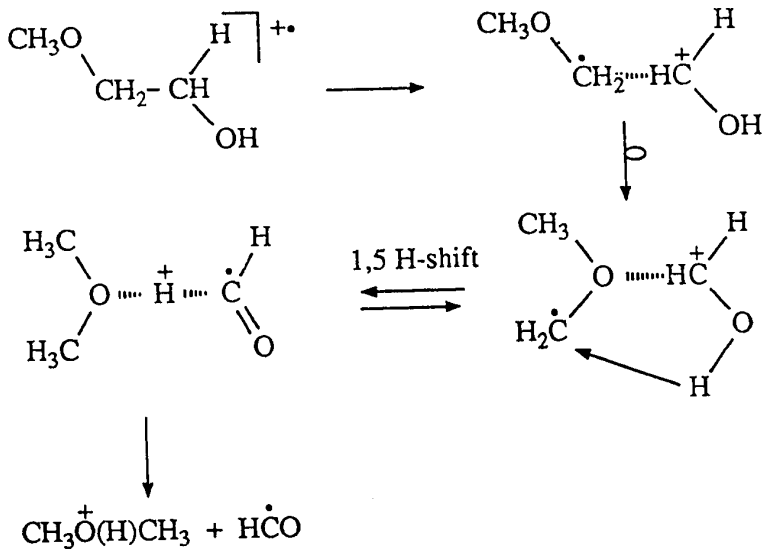

Scheme 8.2

8.4.3 1-Methoxy-2-Butanol

The MI mass spectrum of ionized $CH_3OCH_2CH(OH)CH_2CH_3$, **3**, showed three important metastable peaks (see Table 8.1) at m/z 47 (loss of $C_2H_5CO^{\bullet}$), m/z 58 (loss of CH_3OCH_3) and m/z 76 (loss of C_2H_4), with corresponding kinetic energy releases, $T_{0.5}$ = 4.1, 9.2 and 14.8 meV. The intensity of the molecular ion of **3**, m/z 104, is only 1% of the base peak, m/z 59, but again the metastable proceeses are quite unusually intense e.g m/z

47 has an abundance 3% of m/z 104. The structure of the m/z 47 ion, $CH_3O^+(H)CH_3$ was again confirmed by its AE value, 9.78 ± 0.05 eV leading to $\Delta H_f(C_2H_7O^+)$ = 133 kcal mol^{-1}, which was calculated using ΔH_f(**3**) = -102 kcal mol^{-1} **[15]** and $\Delta H_f(CH_3CH_2CO^{\bullet})$ = -10 kcal mol^{-1} **[16]**. The MI mass spectrum of the m/z 47 ion also showed the broad, dish-topped peak at m/z 31 characteristic of protonated dimethyl ether. Metastable $CH_3OCH_2CH(OD)CH_2CH_3^{+\bullet}$, **3a**, lost $C_2H_5CO^{\bullet}$ to produce an ion of m/z 48 which in turn metastably dissociates to give two peaks at m/z 31 and 32 in a ratio of 40 : 60, showing it to be $CH_2DO^+(H)CH_3$ (see Table 8.4). Once again, the general mechanism proposed above can be used to account for the production of protonated dimethyl ether (see Scheme 8.3).

The CID mass spectrum of the fragment ion m/z 58, $C_3H_6O^{+\bullet}$, produced by the loss of CH_3OCH_3 from ion **3**, was found to be in excellent agreement with that of ionized $CH_3CH{=}CHOH^{+\bullet}$ (see Table 8.5), an ion which can be obtained via a 1,5-H shift in and loss of propene from the molecular ion of 2-methylpentanal. However, the metastable $C_3H_6O^{+\bullet}$ ions produced from ionized 1-methoxy-2-butanol also displayed a weak (2% of the base peak m/z 57) broad peak at m/z 43, a signal which is absent in the MI mass spectrum of pure $CH_3CH{=}CHOH^{+\bullet}$ ions. It is therefore possible that, a small fraction of the $C_3H_6O^{+\bullet}$ ions produced from **3** have the structure $CH_3OCH{=}CH_2^{+\bullet}$ because the latter displayed an intense broad signal at m/z 43 in its MI mass spectrum **[23]**.

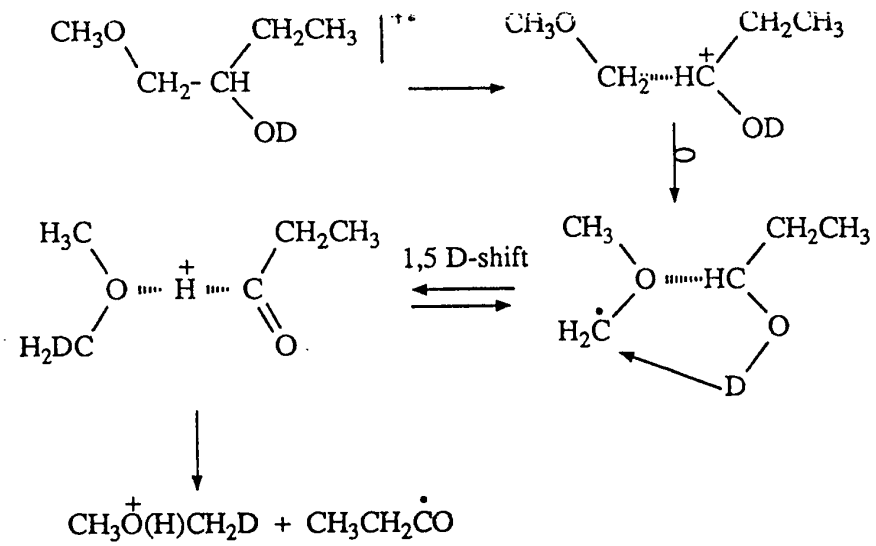

Scheme 8.3

Although the appearance energy measured for the process leading to the formation of $CH_3CH{=}CHOH^{+\bullet}$ was measured to be 9.78 ± 0.05 eV (identical with that measured for the formation of $CH_3O^+(H)CH_3$), it is very unlikely that $CH_3CH{=}CHOH^{+\bullet}$ was produced via the general mechanism discussed in this study (see Schemes above), since metastable ions **3b** displayed m/z 58 ($C_3H_6O^{+\bullet}$) and m/z 59 ($C_3H_5DO^{+\bullet}$) in a ratio of 64 : 36 whereas no peak at m/z 47 ($C_2H_7O^+$) was observed, showing that H/D mixing has occured only for the process giving rise to the formation of m/z 58, $CH_3CH{=}CHOH^{+\bullet}$.

8.4.4 1-Methoxy-2-Pentanol

Metastable $CH_3OCH_2CH(OH)C_3H_7^{+\bullet}$, **4**, showed major peaks at m/z 100, 90 and 47 and minor ones at m/z 72, 75 and 86. The generation of protonated dimethyl ether is proposed to have taken place via the general hydrogen bridged complex shown above.

Table 8.5. *Collision induced dissociaiton (CID) mass spectra of the $C_3H_6O^{+\bullet}$ ions generated from ionized 1-methoxy-2butanol and 2-methylpentanal.*

$C_3H_6O^{+\bullet}$ Ions from	Fragment ion abundance[a] at m/z												
	26	27	28	29	30	31	37	38	39	40	41	42	43
$CH_3OCH_2CH(OH)C_2H_5$	6	12	8	30	(6)	12	3	4	13	5	3	4	(6)
$CH_3CH_2CH_2CH(CH_3)CHO$[b]	5	12	8	29	(6)	13	2	3	12	4	3	4	7

(a) Abundances relative to the total ion abundance = 100 except for numbers in parentheses which contain contributions from unimolecular decompositions of metastable ions.

(b) m/z 58 was obtained as a 1,5-H shift in the molecular ion of 2-methylpentanal.

8.4.5 2-Methoxy-3-Butanol and 1-Ethoxy-2-Propanol

For both $CH_3OCH(CH_3)CH(OH)CH_3$, **5**, and $CH_3CH_2OCH_2CH(OH)CH_3$, **6**, two metastable channels were observed, the major giving rise to the formation of m/z 61 and the minor one yielding m/z 58 (see Table 8.1). The kinetic energy releases, $T_{0.5}$ values, accompanying the formation of the m/z 61 ions were measured to be 9.6 and 8.8 meV from ionized **5** and **6** respectively. By virtue of their MI and CID mass spectra, the m/z 61 ions produced from ionized **5** and **6** were found to be identical and were identified as protonated ethyl methyl ether. Metastable $CH_3O^+(H)C_2H_5$ ions, produced by direct protonation of ethyl

Table 8.6. Metastable ion (MI) mass spectra of protonated ethyl methyl ethers.

Ion	m/z	
	33	34
$CH_3O^+(H)CH_2CH_3$	100	-
$CH_3O^+(D)CH_2CH_3$	-	100
$CH_2DO^+(H)CH_2CH_3$	-	100
m/z 62 from $CH_3CH_2OCH_2CH(OD)CH_3$	-	100
m/z 62 from $CH_3OCH(CH_3)CH(OD)CH_3$	24	76

Table 8.7. *Partial collision induced dissociation (CID) mass spectra of protonated ethyl methyl ethers.*

Ion	m/z	
	33	34
m/z 62 from $CH_3OCH(CH_3)CH(OD)CH_3$, ion source	42	58
m/z 62 from $CH_3CH_2OCH_2CH(OD)CH_3$, ion source	8	92
m/z 62 from $CH_3OCH(CH_3)CH(OD)CH_3$, metastable	55	45
m/z 62 from $CH_3CH_2OCH_2CH(OD)CH_3$, metastable	54	46

methyl ether with CH_5^+, lose C_2H_4 to produce $CH_3OH_2^+$ with $T_{0.5}$ = 17 meV whereas the m/z 61 ions obtained from ionized **5** and **6** lose C_2H_4 with $T_{0.5}$ = 21 and 18 meV respectively, also indicating that the m/z 61 ions have the $CH_3O^+(H)CH_2CH_3$ structure.

With regard to metastable $CH_3OCH(CH_3)CH(OD)CH_3$,$^{+\bullet}$ **5a**, and $CH_3CH_2OCH_2CH(OD)CH_3$,$^{+\bullet}$ **6a** ions, they both displayed a major peak at m/z 62 and minor signals at m/z 58 and 59 (see Table 8.1). However, metastable m/z 62 ions, $CH_2DO^+(H)C_2H_5$, generated from **6a** (see Scheme 8.4) showed a single peak at m/z 34 (see Table 8.6), showing that no H/D mixing between the methyl and ethyl groups has occured, whereas metastable m/z 62 ions obtained from **5a**, produced m/z 33 and 34 in a ratio of 24 : 76 (see Table 8.6), showing it to be a mixture of $CH_3O^+(H)CHDCH_3$ and

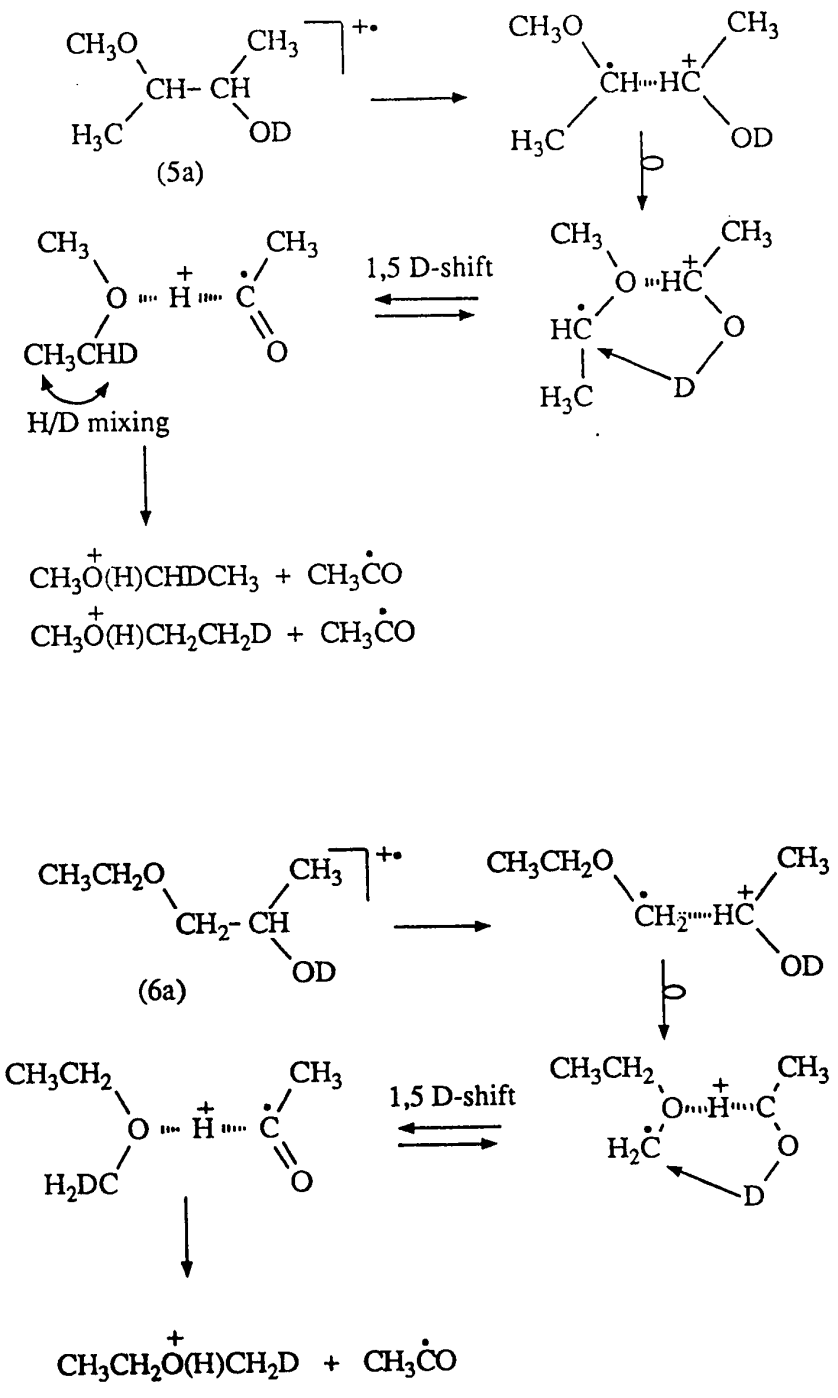

Scheme 8.4

$CH_3O^+(H)CH_2CH_2D$. Note however, that the CID mass spectra of the metastably generated m/z 62 ions were nearly identical and both showed peaks at m/z 33 and 34 (see Table 8.7). This observation indicates that the methyl hydrogen atoms and the ethyl hydrogen atoms together lose their positional identity (within the O•••H•••C complexes giving rise to the formation of m/z 62) prior to fragmentation.

8.4.6 1,2 Dimethoxypropane

1,2 Dimethoxypropane, **7**, is not a β-hydroxyether but can be viewed as an analogue of 1-methoxy-2-propanol, **1**, in which the hydroxyl hydrogen has been replaced by a methyl group, and so possesses the same chemical skeleton as the β-hydroxyethers discussed in the present study. It was readily observed that metastable $CH_3OCH_2CH(OCH_3)CH_3^{+\bullet}$ ions lose CH_3OCH_3 (whose structure was identified by its CIDI mass spectrum) to produce an ion at m/z 58. The AE of the latter was measured to be 9.94 ± 0,05 eV, which leads to an apparent heat of formation of 181 kcal mol^{-1}, when using $\Delta H_f(7)$ = -92.3 kcal mol^{-1} **[15]** and $\Delta H_f(CH_3OCH_3)$ = -44 kcal mol^{-1} **[16]**, showing that this $C_3H_6O^{+\bullet}$ has the methyl vinylether structure ($\Delta H_f(CH_3OCH{=}CH_2^{+\bullet})$ = 182 kcal mol^{-1} **[16]**).

As shown below (see Scheme 8.5) the general mechanism proposed in this paper can also be applied to ionized 1,2 dimethoxy propanol but instead of a 1,5 hydrogen shift of a hydroxyl hydrogen to the radical site, we propose a 1,5-H shift of a CH_3 hydrogen to the $^{\bullet}CH_2$ group.

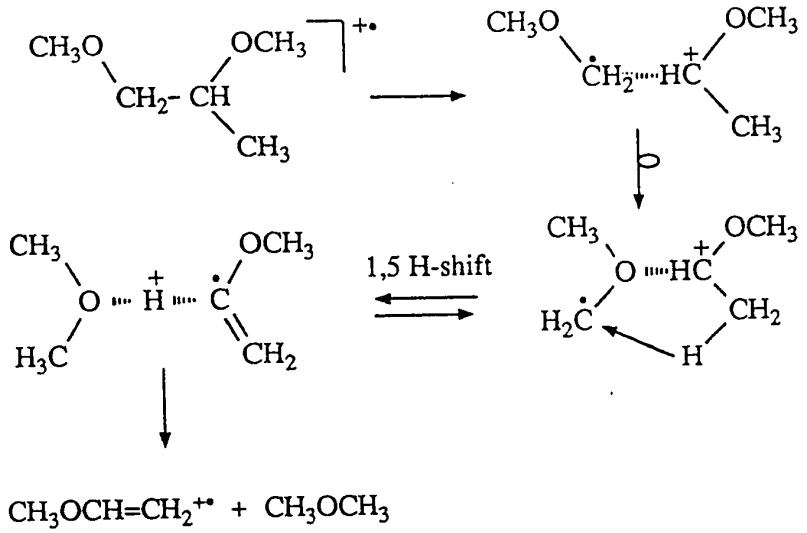

Scheme 8.5

The D_6 isotopomer $CD_3OCH_2CH(OCD_3)CH_3$, **7a**, was also studied. Its MI mass spectrum was recorded and it contained three peaks corresponding to m/z 61, 62 and 63, in a ratio of 54 : 41 : 5 (for statistical mixing of 5H and 3D atoms a ratio of 36 : 54 : 11 would be expected). The latter observation can be explained on the basis of a reversible 1.5-H shift as shown in Scheme 8.6. After the 1,5 H-shift has taken place to produce the intermediate **7b**, the six hydrogen (deuterium) atoms of the dimethyl ether moiety become equivalent and H/D mixing can occur, but with an isotope effect favoring H^+ transfer. Note that the m/z 61, 62, 63 ratio becomes 37 : 46 : 17 in the CID mass spectrum of ionized **7a**, a ratio which is now closer to statistical.

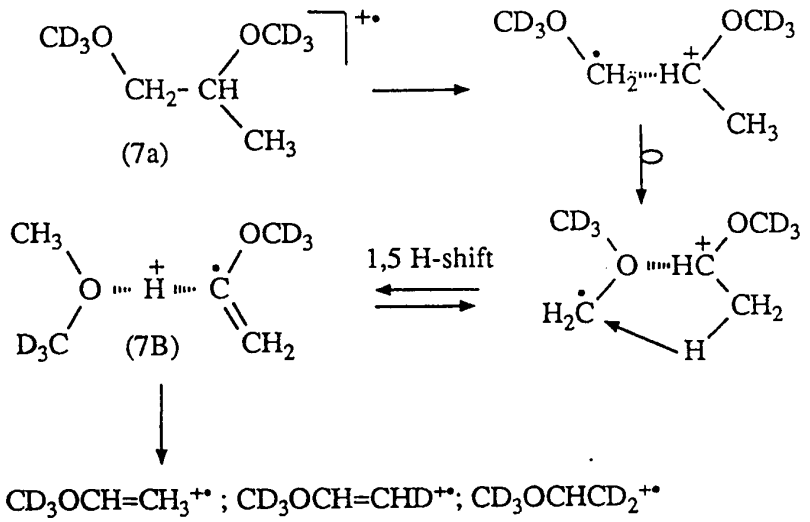

Scheme 8.6

8.5 Conclusions

We propose that metastable ionized β-hydroxyethers produce protonated ethers $R_1O^+(H)R_2$ via stable hydrogen bridged intermediates of the type $R_1R_2O\bullet\bullet\bullet H\bullet\bullet\bullet C(O)R_3^{\cdot\cdot}$. For the metastable molecular ion of 1-methoxy-2-propanol, deuterium labeling experiments have shown that the proton in m/z 47 is the methine H and that the hydroxyl H goes to form the second methyl group. Therefore we propose that the intermediate ions are

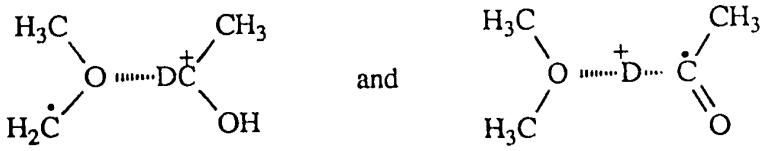

Note that species **1b** was estimated to have an energy appreciably below that of the molecular ion and that the above mechanism can be taken as a general mechanism for β-hydroxyethers.

Further support for the H-bridged structure was obtained from the MI mass spectrum of ionized 1,2-dimethoxypropane, which produced m/z 58, CH_2=CH-$OCH_3^{+\bullet}$ and CH_3OCH_3. Deuterium labeling experiments in this molecule showed that the H-bridged species, $(CH_3)_2O\bullet\bullet\bullet H\bullet\bullet\bullet C(OCH_3)=CH_2$, can perform reversible 1,5 H-shifts between the methyl groups of the dimethyl ether part and the $=CH_2$ group.

REFERENCES - CHAPTER 8

1. F.W. McLafferty, ***Interpretation of mass spectra***, University Science Books (Mill Valley California) (1980).
2. J.L. Holmes, ***Org. Mass Spectrom.*** 20, 169 (1985).
3. M.C. Blanchette, J.L. Holmes, C.E.C.A. Hop, F.P. Lossing, R. Postma, P.J. Ruttink and J.K. Terlouw, ***J. Am. Chem. Soc.*** 108, 7589 (1986).
4. W.J. Hehre, L. Radom, P.V.R. Schleyer and J.A. Pople, ***Ab initio molecular orbital theory***, Wiley-Interscience, New-York (1986).
5. N.L. Ma, B.J. Smith, J.A. Pople and L. Radom, ***J. Phys. Chem.*** 96, 5804 (1992).
6. T. Morton, ***Tetrahedron***, 38, 3195 (1982).
7. J.R. Cao, M. George, J.L. Holmes, M. Sirois, J.K. Terlouw and P.C. Burgers, ***J. Am. Chem. Soc.*** 114, 2017 (1992).
8. N. Heinrich, J. Schmidt, H. Schwarz and Y. Apeloig, ***J. Am. Chem. Soc.*** 109, 1317 (1987).
9. G. Schaftenaar, R. Postma, P.J.A. Ruttink, P.C. Burgers, G.A. McGibbon and J.K. Terlouw, ***Int. J. Mass Spectrom. Ion Processes***, 100, 521 (1990).
10. P.C. Burgers, J.L. Holmes, C.E.C.A. Hop, R. Postma, P.J.A. Ruttink and J.K. Terlouw, ***J. Am. Chem. Soc***. 109, 7315 (1987).
11. P.C. Burgers, J.L. Holmes, J.E. Szulejko and J.K. Terlouw, ***Org. Mass Spectrom***. 19, 442 (1984).
12. F.P. Lossing and J.C. Traeger, ***Int. J. Mass Spectrom. Ion Phys***. 19, 9 (1976).

REFERENCES - CHAPTER 8

13. J.L. Holmes and M. Sirois, ***Org. Mass Spectrom.*** 25, 481 (1990).

14. R. Clair, J.L. Holmes, A.A. Mommers and P.C. Burgers, ***Org. Mass Spectrom.*** 20, 207 (1985).

15. By group additivity; S.W. Benson, ***Thermochemical kinetics***, 2nd Ed. Wiley, New-York (1976).

16. S.G. Lias, J.E. Bartmess, J.F. Liebman, J.L. Holmes, R.D. Levin and W.G. Mallard, ***J. Phys. Chem. Ref. Data***, 17, suppl.1 (1988).

17. S. Hammerum, ***J. Chem. Soc. Chem. Commun.*** 858, (1988).

18. M.C. Bissonnette, M. George and J.L. Holmes, ***Int. J. Mass Spectrom. Ion Processes,*** 101, 309 (1990).

19. J.W. Larson and T.B. McMahon, ***J. Am. Chem. Soc.*** 104, 6255 (1982).

20. J.L. Holmes, ***Adv. Mass Spectrom.*** 11, 53 (1989).

21. P.C. Burgers, J.L. Holmes, J.K. Terlouw and B. Van Baar, ***Org. Mass Spectrom.*** 20, 202 (1985).

22. Using data from Ref. 16 and $\Delta H_f(CH_3OCH_2CH_2OH)$ = -87 kcal mol^{-1} **[15]**, IE $(CH_3OCH_2CH_2OH)$ = 9.58 ± 0.05 eV, measured in this study.

23. C. Lifshitz, ***Org. Mass Spectrom.*** 23, 303 (1988).

24. F. Turecek and F.W. McLafferty, ***J. Am. Chem. Soc.*** 106, 2528 (1984).

25. M.F. Jarrold, J. Krichner, S. Liu and M.T. Bowers, ***J. Phys. Chem*** 90, 78 (1986).

GENERAL CONCLUSION

This thesis reports the results obtained in a series of experiments aimed at probing ionic structures and fragmentation mechanisms in four systems, $[H_3,C,N,O_2]^{+\bullet}$ ions, $[C_2H_7O]^+$ ions and neutral counterparts, adducts of $[C_2H_5]^+$ ions with oxygen containing compounds and the intermediates involved in the fragmentation of $[R_1OCH(R_2)CH(OH)R_3]^{+\bullet}$ ions. A variety of mass spectrometric techniques have been used to reach the goals established for each experimental projects. The major part of the work concerns the study of newly found gaseous ions and neutrals and certainly makes a significant contribution to our knowledge of gas phase ion chemistry.